Development of Robust Control Schemes with New Estimation Algorithms for Shunt Active Power Filter

Rakhee Panigrahi

Department of Electrical Engineering
National Institute of Technology Rourkela
2015

Development of Robust Control Schemes with New Estimation Algorithms for Shunt Active Power Filter

Thesis submitted in partial fulfillment

of the requirement for the degree of

Doctor of Philosophy

in

Electrical Engineering

by

Rakhee Panigrahi

(Roll No:510EE111)

Under the Guidance of

Prof. Bidyadhar Subudhi
Prof. Prafulla Chandra Panda

Department of Electrical Engineering
National Institute of Technology Rourkela
2015

Department of Electrical Engineering
National Institute of Technology Rourkela

C E R T I F I C A T E

This is to certify that the thesis entitled "**Development of Robust Control Schemes with New Estimation Algorithms for Shunt Active Power Filter**," submitted by **Rakhee Panigrahi** to the National Institute of Technology, Rourkela for the award of Doctor of Philosophy in Electrical Engineering, is a record of bonafide research work carried out by her in the Department of Electrical Engineering, under our supervision. We believe that this thesis fulfills part of the requirements for the award of degree of Doctor of Philosophy. The results embodied in the thesis have not been submitted for the award of any other degree elsewhere.

Professor Prafulla Chandra Panda
Department of Electrical Engineering,
Ex-Prof., National Institute of Technology,
Rourkela

Professor Bidyadhar Subudhi
Department of Electrical Engineering,
National Institute of Technology,
Rourkela

Dedicated To

My Family Members

Acknowledgement

At the outset I express my sincere and heartfelt gratitude to my supervisors, Prof. B. Subudhi and Prof. P. C. Panda, who have acted constantly as my philosopher and guide in this Herculean job of thesis preparation and compilation. But for their spontaneous help and co-operation this thesis could not have seen the light of the day.

I am grateful to Director, Prof. S. K. Sarangi and Prof. A. K. Panda, Head of Electrical Engineering Department, NIT, Rourkela, for their kind support and concern regarding my academic requirements.

I would also like to thank the Doctoral Scrutiny Committee members, Prof. D. Patra, Prof. K.B. Mohanty, Prof. S. K. Patra and Prof. D. P. Mohapatra, for their helpful and stimulating comments and suggestions in the final stages of this thesis.

I thank all my friends for their unstinted help and co-operation.

I must acknowledge the academic infrastructure of NIT, Rourkela for offering me a soothing and active environment for pursuing my research freely and independently.

Last but not the least, I would like to record my warmest feelings of thanks to all my family members and particularly to my husband and my daughter 'Ritwika' who have endured a lot by tolerating my negligence of them during my research.

Rakhee Panigrahi

Abstract

The widespread use of power electronics in industrial, commercial and even residential electrical equipments causes deterioration of the quality of the electric power supply with distortion of the supply voltage. This has led to the development of more stringent requirements regarding harmonic current generation, as are found in standards such as IEEE-519. Power Quality is generally meant to measure of an ideal power supply system. Shunt active power filter (SAPF) is a viable solution for Power Quality enhancement, in order to comply with the standard recommendations. The dynamic performance of SAPF is mainly dependent on how quickly and how accurately the harmonic components are extracted from the load current. Therefore, a fast and accurate estimation algorithm for the detection of reference current signal along with an effective current control technique is needed in order for a SAPF to perform the harmonic elimination successfully. Several control strategies of SAPF have been proposed and implemented. But, still there is a lot of scope on designing new estimation algorithms to achieve fast and accurate generation of reference current signal in SAPF. Further, there is a need of development of efficient robust control algorithms that can be robust in face parametric uncertainties in the power system yielding improvement in power quality more effectively in terms of tracking error reduction and efficient current harmonics mitigation.

The work described in the thesis involves development of a number of new current control techniques along with new reference current generation schemes in SAPF. Two current control techniques namely a hysteresis current control (HCC) and sliding mode control (SMC) implemented with a new reference current generation scheme are proposed. This reference generation approach involves a Proportional Integral (PI) controller loop and exploits the estimation of the in phase fundamental components of distorted point of common coupling (PCC) voltages by using Kalman Filter (KF) algorithm. The KF-HCC based SAPF is found to be very simple in realization and performs well even under grid perturbations. But the slow convergence rate of KF leads towards an ineffective reference generation and hence harmonics cancellation is not perfect. Therefore, a SMC based SAPF is implemented with a faster reference scheme based on the proposed Robust Extended Complex Kalman Filter (RECKF) algorithm and the efficacy of this RECKF-SMC is compared with other variants of Kalman Filter such as KF, Extended Kalman Filter (EKF) and Extended Complex Kalman Filter (ECKF)

employing simulations as well as real-time simulations using an Opal-RT Real-Time digital Simulator. The RECKF-SMC based SAPF is found to be more effective as compared to the KF-HCC, KF-SMC, EKF-SMC and ECKF-SMC.

Subsequently, predictive control techniques namely Dead Beat Control (DBC) and Model Predictive Control (MPC) are proposed in SAPF along with an improved reference current generation scheme based on the proposed RECKF. This reference scheme is devoid of PI controller loop and can self-regulate the dc-link voltage. Both RECKF-DBC and RECKF-MPC approaches use a model of the SAPF system to predict its future behavior and select the most appropriate control action based on an optimality criterion. However, RECKF-DBC is more sensitive to load uncertainties. Also, a better compensation performance of RECKF-MPC is observed from the simulation as well as real-time simulation results. Moreover, to study the efficacy of this RECKF-MPC over PI-MPC, a comparative assessment has been performed using both steady state as well as transient state conditions. From the simulation and real-time simulation results, it is observed that the proposed RECKF-MPC outperforms PI-MPC. The thesis also proposed an optimal Linear Quadratic Regulator (LQR) with an advanced reference current generation strategy based on RECKF. This RECKF-LQR based SAPF has better tracking and disturbance rejection capability and hence RECKF-LQR is found to be more efficient as compared to RECKF-SMC, RECKF-DBC and RECKF-MPC approaches.

Subsequently, two robust control approaches namely Linear Quadratic Gaussian (LQG) servo control and H_∞ control are proposed in SAPF with highly improved reference generation schemes based on RECKF. These control strategies are designed with the purpose of achieving stability, high disturbance rejection and high level of harmonics cancellation. From simulation results, they are not only found to be robust against different load parameters, but also satisfactory THD results have been achieved in SAPF. A prototype experimental set up has been developed in the Laboratory with a dSPACE-1104 computing platform to verify their robustness. From both the simulation and experimentation, it is observed that the proposed RECKF-H_∞ control approach to design a SAPF is found to be more robust as compared to the RECKF-LQG servo control approach in face parametric uncertainties due to load perturbations yielding improvement in power quality in terms of tracking error reduction and efficient current harmonics mitigation. Further, there is no involvement of any voltage sensor in this realization of RECKF-H_∞ based SAPF resulting a more reliable and inexpensive SAPF system.

Therefore, superiority of proposed RECKF-H$_\infty$ is proved amongst all the proposed control strategies of SAPF.

Contents

List of Abbreviations

PQ	Power Quality
PCC	Point of Common Coupling
RMS	Root Mean Square
THD	Total Harmonic Distortion
TDD	Total Demand Distortion
RF	Ripple Factor
PF	Power Factor
SAPF	Shunt Active Power Filter
PWM	Pulse Width Modulation
GTO	Gate Turn-off Thyristor
PI	Proportional Integrator
IGBT	Insulated Gate Bipolar Transistor
NLS	Nonlinear Least Square
LQR	Linear Quadratic Regulator
LMS	Least Mean Square
VSC	Voltage Source Converter
DSP	Digital Signal Processor
SMC	Sliding Mode Controller
HCC	Hysteresis Current Controller
DBC	Dead Beat Control
MPC	Model Predictive Control
SVM	Space Vector Modulation
KF	Kalman Filter
EKF	Extended Kalman Filter
ECKF	Extended Complex Kalman Filter
RECKF	Robust Extended Complex Kalman Filter

PB	Power Balance
LQG	Linear Quadratic Gaussian
RT	Real Time
PLL	Phase Locked Loop
FACT	Flexible AC Transmission
ANN	Artificial Neural Network
VSI	Voltage Source Inverter
LPF	Low Pass Filter
DFT	Discrete Fourier Transform
DSO	Digital Storage Oscilloscope
FPGA	Field Programmable Gate Array
JTAG	Joint Test Action Group
CPLD	Complex Programmable Logic Device
I^{2}C	Inter-integrated Circuit
ISM	Integral Sliding Mode
ZOH	Zero Order Hold
ADC	Analog to Digital Converter
DAC	Digital to Analog Converter
RTI	Real Time Interface
RCP	Rapid Control prototyping

List of Figures

List of Tables

List of Symbols

i_{Sabc}, i_{Sabc}^*	Source and source reference Current
i_{Fabc}, i_{Fabc}^*	Compensating and reference Compensating Current
v_a, v_b, v_c	PCC voltages
v_{fa}, v_{fb}, v_{fc}	Inverter voltages
a_1, f_1, ϕ_1	Fundamental amplitude, frequency and phase angle
S_a, S_b, S_c	Switching states
i_α^p, i_β^p	Real and imaginary part of the predicted source current
i_α^*, i_β^*	Real and imaginary part of the future reference source current
S	Space vector of switching States
$S_{sliding}$	Sliding surface
v_s	Source voltage
v_{dc}^*	Reference DC capacitor voltage
u_{eq}	Equivalent switching function
T_s	Sampling time
f_{sw}	Switching frequency
f_s	Sampling frequency
i_{sm}	Peak value of source reference current
i_{Labc}	Load Current
ω	Angular Frequency
Φ_k	State transistion matrix
H_k	Observation matrix
K_k	Kalman gain

P_k	Estimated error covariance matrix
M_k	Predicted error covariance matrix
$\wedge$, $\sim$	Estimated and Predicted value
Q_k	Process error covariance matrix
R_k	Measurement error covariance matrix
w_k	Process Noise
v_k	Measurement Noise
R_f, L_f	Filter impedance
R_s, L_s	Source impedance
K_p, K_i	Proportional and Integral constants of PI controller
J_{LQR}	Cost function for LQR
J_{MPC}	Cost function for MPC
K_{LQR}	Linear Quadratic Regulator Gain
K_{LQI}	Linear Quadratic Integrator Gain
β	Gain of Feedback compensator
m_a	Amplitude Modulation Factor
m_F	Frequency Modulation of the PWM converter
v_{jl_k}	Inphase fundamental component of PCC voltage
$v_{jl_k}^{\perp}$	Inquadrature fundamental component of PCC voltage
$G_H(s)$	Transfer function of generalized SAPF system
$K_H(s)$	Transfer function of H_∞ controller
$S_H(s)$	Sensitivity transfer function
$T_H(s)$	Complementary sensitivity transfer function
W_l	Weighting function for tracking error performance

W_2	Weighting function for control effort
W_3	Weighting function for robust performance
w_h	Exogenous input
z_h	Controlled output
$\left\|T_{w_h z_h}\right\|_\infty$	H_∞ norm of the transfer function from w_h to z_h
e_s, e_u, e_t	Gains for low frequency control signal
M_s, M_u, M_t	Gains for high frequency disturbance
$i_{Sa_{1_k}}, i_{Sb_{1_k}}, i_{Sc_{1_k}}$	Inphase fundamental component of source current
$i_{Sa_{1_k}}^\perp, i_{Sb_{1_k}}^\perp, i_{Sc_{1_k}}^\perp$	Inquadrature fundamental component of source current
$i_{Sa_k}^+, i_{Sb_k}^+, i_{Sc_k}^+$	Positive Sequence components of source currents

CHAPTER 1

Introduction
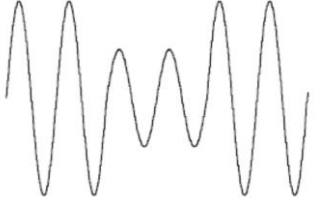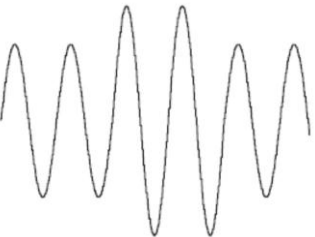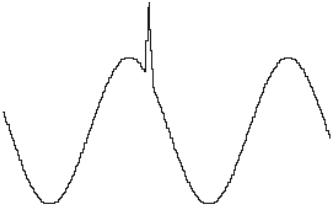
1.1   Background

1.1.1   Power Quality

The increased usage of power electronic devices in power system including renewable power generations led to a number of power quality (PQ) problems for the operation of machines, transformers, capacitors in power systems. PQ covers all aspects of power system engineering from transmission and distribution level analyses to end-user problems. Therefore, electric power quality has become a serious concern for both utilities and end users.

The PQ, at distribution level, broadly refers to maintaining a near sinusoidal power distribution bus voltage at a rated magnitude and frequency. In addition, the energy supplied to a customer must be uninterrupted. Therefore, the term PQ includes two aspects, namely voltage quality and supply reliability [1]. The voltage quality side comprises various disturbances, such as rapid changes, harmonics, interharmonics, flicker, imbalance and transients, whereas the reliability side involves phenomena with a longer duration, such as interruptions, voltage dips and sags, over and under voltages and frequency deviations. The above issues are significant in depicting the actual phenomena that may cause PQ problem. The possible causes and effects for some PQ disturbances are summarized in Table 1.1. One of the major issues namely harmonic distortion is not a new phenomenon in power system. It was discovered as early as the 1920s and 30s [2]. At that time, the major sources of harmonics were the transformers and the main problem was inductive interference telephone systems. Harmonics are qualitatively defined as sinusoidal waveforms having frequencies that are integer multiples of the power line frequency. In power system engineering, the term harmonics is extensively used to define the distortion for voltage or current waveforms. Primarily, the power electronic converters inject nonsinusoidal (i.e., harmonic) currents into the AC utility grid and the harmonics injected into the power system cause line voltage distortions at the Point of Common Coupling (PCC) where the linear and nonlinear loads

Table 1.1 PQ Disturbances

Disturbance	Origins	Effects
Sags	• Abrupt increase in load • Dropouts/outages • Lightning • Outdoor contact with transmission lines • Ground faults • Equipment failures	• Equipment shutdown • Power-down circuitry in power supply operates incorrectly • Computer lock-ups • Diminished speed of disk drives (data error)
Swells	• Shutdown of heavily loaded equipment • Abrupt power restoration • Utility switching	• Discomfort from flickering lights • Computer damages • Degradation of power Protection equipment
Harmonic distortion	• Nonlinear loads • Resonance phenomenon • Transformer saturation	• Extended heating • Failure of electronic equipment
Transients	• Switching load on and off • Utility switching • Lightning • Fault Clearing	• Insulation failure • Reduced lifetime of transformers and motors etc.
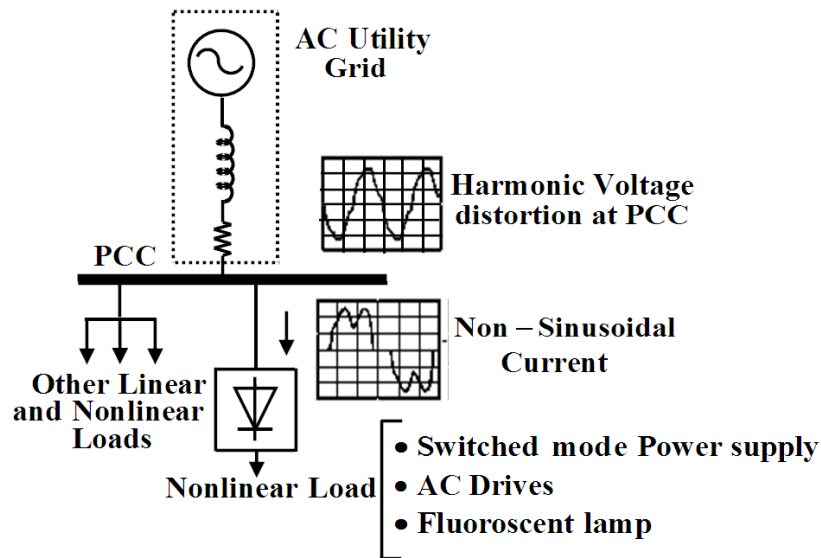
Figure 1.1: Harmonics distortion at PCC

are connected, as displayed in Fig. 1.1. As a consequence, harmonic distortion can have detrimental influences on electrical distribution systems. Identifying the problems associated with sources and impacts of harmonics as well as the methods to decrease the harmonic will increase the overall efficiency of the distribution system.

1.1.2   Sources of Harmonics

Fig. 1.2 shows the different sources of harmonics in power distribution system. The different sources of harmonics [3] namely from three major areas are listed below.

- Fast switching of power electronic devices

- The conventional sources such as electrical rotating machines and Transformers

- The modern electronic equipments

1.1.2.1   Types of Power System Harmonics

Different types of harmonics in power system are enlisted in Table 1.2.

1.1.2.2   Harmonics Measurement

Some definitions and formulations for harmonics measurement are described below:

Form factor (FF): It is a ratio between the Root Mean Square (RMS) value and the average value of a periodic waveform and is defined as
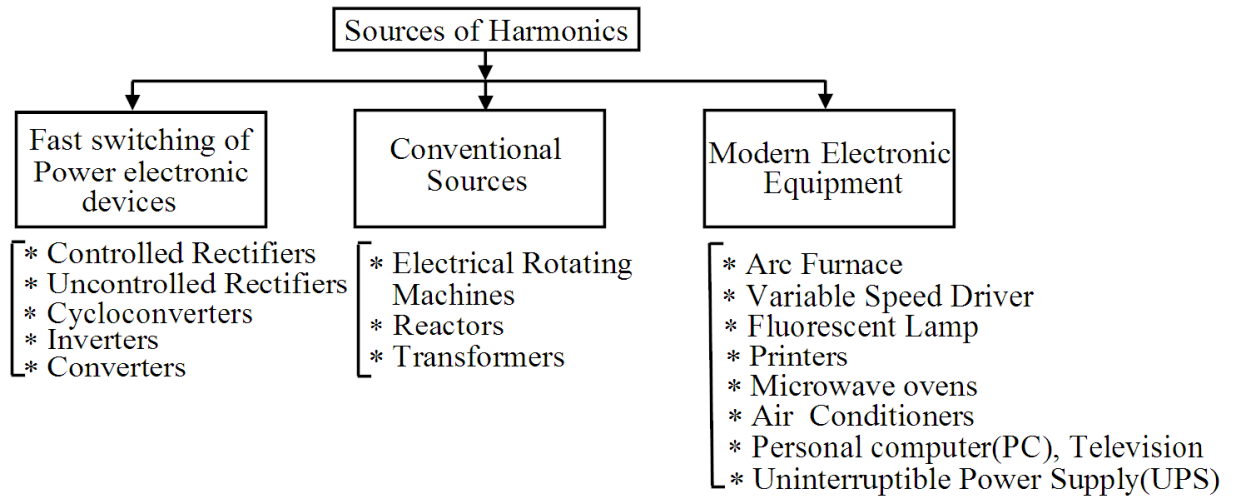
Figure 1.2: Sources of Harmonics in Power distribution Systems

Table 1.2 Types of Power System Harmonics

Types	Frequency (f_1= fundamental)
DC	0
Odd Harmonics	$h.f_1$(h=odd)
Even Harmonics	$h.f_1$(h=even)
Triplen Harmonics	$3h.f_1$ (h=1, 2, 3, 4,…..)
Positive-sequence Harmonics	$h.f_1$ (h=1, 4, 7, 10,…..)
Negative-sequence Harmonics	$h.f_1$ (h=2, 5, 8, 11,…..)
Zero-sequence Harmonics	$h.f_1$ (h=3, 6, 9, 12,…..)
Time Harmonics	$h.f_1$(h = an integer)
Spatial Harmonics	$h.f_1$(h = an integer)
Interharmonic	$h.f_1$(h = not an integer multiple of f_1)
Subharmonic	$h.f_1$(h<1 and not an integer multiple of f_1, e.g., h=15 Hz, 30 Hz)
Characteristic Harmonic	$(12k+1). f_1$(k=integer)
Uncharacteristic Harmonic	$(12k-1). f_1$(k=integer)

$$FF = \frac{I_{rms}}{I_{avg}} \tag{1.1}$$

where I_{rms} and I_{avg} are the RMS value and average value respectively.

Ripple Factor (RF): It is a measure of ripple content of the waveform and is defined as

$$RF = \frac{I_{ac}}{I_{dc}} \tag{1.2}$$

where I_{ac} and I_{dc} are the alternating current (ac) and direct current (dc) respectively and I_{ac} is given by

$$I_{ac} = \sqrt{\left(I_{rms}^2 - I_{dc}^2\right)}$$

Total Harmonic Distortion (THD): It is a measure of effective value of the harmonic components in a distorted waveform, which is defined as the RMS of the harmonics expressed as a percentage of the fundamental component.

$$THD = \frac{\sqrt{\sum_{h=2}^{\infty} (I^{(h)})^2}}{I^{(1)}} \tag{1.3}$$

where $I^{(1)}$ and $I^{(h)}$ are the fundamental and harmonic components of the waveform.

Total Demand Distortion (TDD): This is similar to THD except that the distortion is expressed as a percentage of some rated or maximum value, rather than as a percentage of the fundamental current.

$$TDD = \frac{\sqrt{\sum_{h=2}^{\infty} (I^{(h)})^2}}{I_{rated}} \tag{1.4}$$

where I_{rated} is the rated value of the current.

Displacement and True Power Factor (PF): Displacement power factor is the cosine of the angle between the fundamental voltage and current waveforms. But the presence of harmonics introduces additional phase shift between the voltage and the current. True

power factor is calculated as the total active power used in a circuit (including harmonics) and the total apparent power (including harmonics) supplied from the source.

$$\text{True PF} = \frac{P}{S} \tag{1.5}$$

P and Q are the total active power and total apparent power respectively, where $S = \sqrt{P^2 + Q^2}$ and Q is the reactive power.

1.1.2.3 Standard of Harmonics

The foremost purposes for setting guidelines, recommendations and standards in power systems with nonsinusoidal voltages or currents are to keep disturbances to user equipment within permissible limits, to provide uniform terminology and test procedures for power quality problems and to provide a common source on which a wide range of engineering is referenced. There are many standards and related documents [4][5][6][7][8] that deal with PQ issues. The mostly adopted standard is Institute of Electrical and Electronics Engineering (IEEE) 519-1992 standard.

1.1.2.3.1 IEEE 519-1992

This standard sets limits for harmonic voltage and currents at the PCC as shown in Table 1.3. It places concern on large commercial and industrial consumers.

1.1.2.3.2 Harmonic Effects

Harmonics (voltage or current) negatively affect a power system in several fronts. The classification of the effects of high harmonics [9][10][11] are summarized in Table 1.4.

1.1.2.3.3 Harmonics Reduction Techniques

The traditional techniques to eliminate the harmonic currents include: electrical equipment over dimensioning, three-phase transformer special connections to eliminate the third and its proportional harmonics and the connection of passive filters (PFs), but they have the following disadvantages:

- Fixed compensation or harmonic mitigation; large size and possible resonance with the supply system impedance at fundamental or other harmonic frequencies;
- Compensation is limited to a few orders of harmonics;

- Unsatisfactory performance may occur due to variation of filter parameters (caused by ageing, deterioration and temperature effects) and nonlinear load characteristics;

Table 1.3 Voltage and Current Distortion limits at PCC [9]

Voltage Distortion Limits		
Bus Voltage at PCC	Individual Voltage Distortion [%]*	Total Voltage Distortion [%]*
Below 69 kV	3.0	5.0
69kV to 138 kV	1.5	2.5
Above 138 kV	1.0	1.5

* Maximum for individual harmonic

Current Distortion Limits						
Maximum odd harmonic current distortion in percent of I_L for general distribution systems (1.120V – 69kV)						
I_{SC} / I_L	< 11	$11 \leq n < 17$	$17 \leq n < 23$	$23 \leq n < 35$	$35 \leq n$	TDD
< 20	4.0	2.0	1.5	0.6	0.3	5.0
20<50	7.0	3.5	2.5	1.0	0.5	8.0
50<100	10.0	4.5	4.0	1.5	0.7	12.0
100<1000	12.0	5.5	5.0	2.0	1.0	15.0
>1000	15.0	7.0	6.0	2.5	1.4	20.0

I_{SC} : Maximum short circuit current at the PCC

I_L : Fundamental of the average (over 12 months) maximum monthly demand load current at PCC

Table 1.4 Classifications of High Harmonic Effects

Classification Criterion	Type of Effect	Comment
Duration	Very Short Term Effects	These effects are linked with a failure, malfunction or defective state of apparatus exposed to high harmonics, such as control and instrumentation equipment, electronic equipment and IT equipment etc.
	Long Term Effects	Primarily of thermal nature. The thermal effect (producing accelerated ageing of insulation or rarely damage to equipment) is a function of many variables, of which the most significant are the values and order of harmonics.
Physical Nature of the distorted quantity	Current Effects	Related to the instantaneous or time-averaged current value (overheating of electric machines, capacitor fuses blowing, increased losses in transmission lines, unwanted operation of relays etc.). Harmonics in power supply systems are the major cause of temperature rise in the equipment and shortening of in-service time. This effect reaches extremely high values under conditions of resonant amplification of harmonic currents.
	Voltage Effects	Associated with the peak, average or RMS value of distorted voltage

The technical evolution in rated power and switching speed of electronic devices, allows now-a-days the application of the active power filters (APFs) [12][13][14] and they have many other advantages over traditional methods for harmonic compensation such as

- Adaptation with respect to the variation of the loads;
- Possibility of selective harmonics compensation;
- Limitations in the compensation power;
- Possibility of reactive power compensation;

1.1.3 Classification of Active Power Filters

A large number of APF circuit configurations have been proposed in the literature [15][16] to facilitate the compensation of harmonics in power systems. To classify these, it is desirable first to characterize the whole process of active filtering into its main building blocks.

A typical active filter configuration can be represented by the basic block diagram shown in Fig. 1.3. The block diagram shows five main constituents, namely nonlinear load, system variables feedback, reference current estimator, overall system controller and PWM switching strategy. The harmonic current generated by the nonlinear load is detected and fed back to the reference current estimator, in combination with the other system variables. The resulting reference signal drives the overall system controller, which, in turn, makes the control effort necessary for the PWM switching strategy to produce the switching pattern for the filter switches. The resulting filter current is also identified and fed back to the controller.
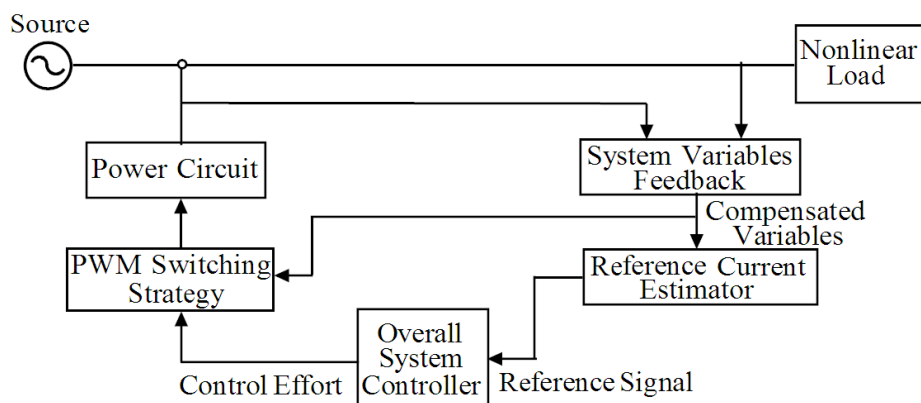
Figure 1.3: Generalized block diagram for active power filters

Power-circuit configurations play a crucial role in the selection of APFs, which are presented in the Table 1.5 and are briefly described in the following sections.

Table 1.5 Classifications of Active Power Filter according to the power circuit configurations and connections

Active Power Filter		
Shunt APF		
	Current Fed Inverter	
	Voltage Fed Inverter	
Series APF		
Filter Combinations	Shunt APF + Series APF	

10
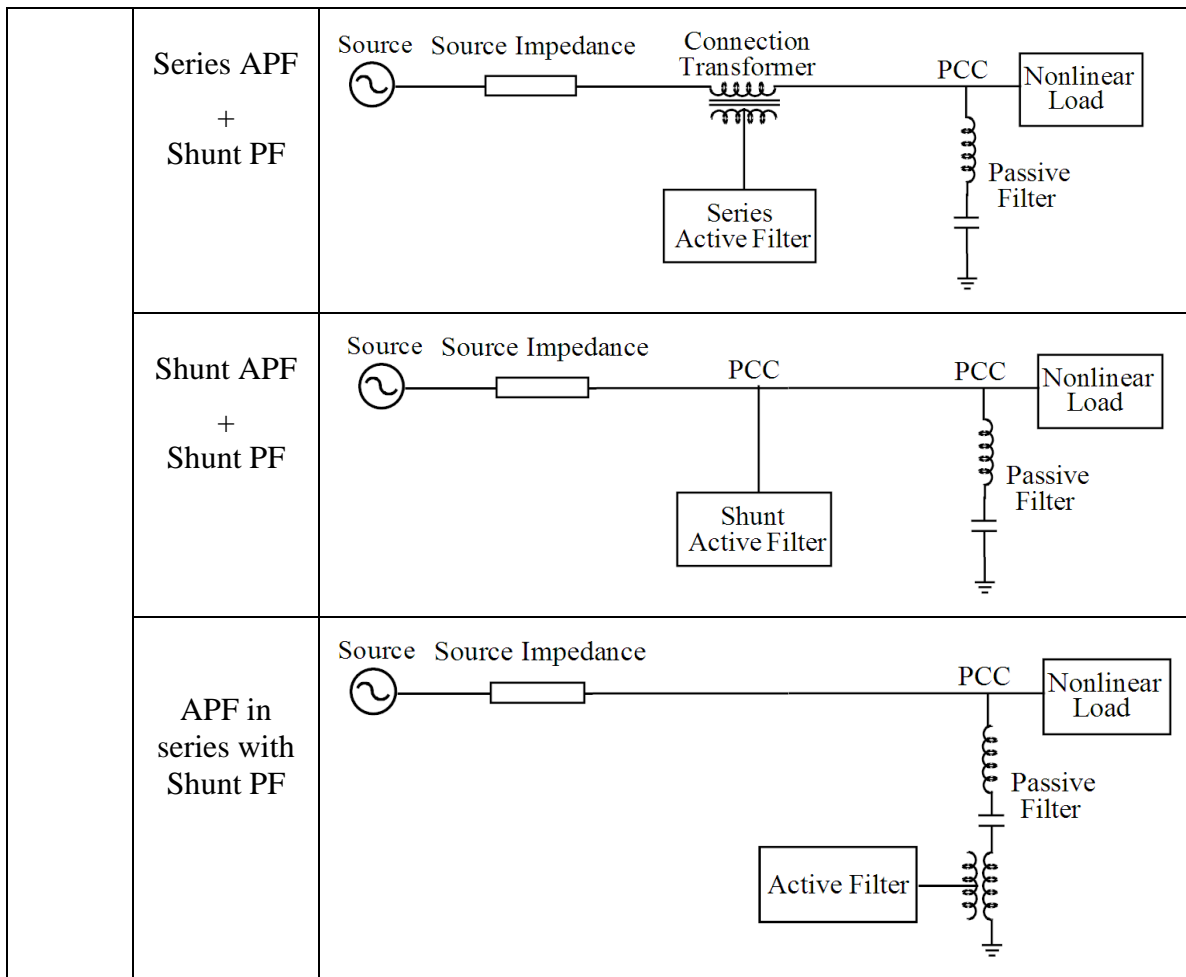
1.1.3.1 Shunt Active Power Filter

The shunt APF (displayed in Table 1.5) is based on injection of current harmonics of the same amplitude but opposite in phase to that of load current harmonics. Fig. 1.4 shows the shunt APF compensation principle, which is controlled in a closed loop manner to actively shape the source current into sinusoid.

Two main circuit configurations, namely, current and voltage fed inverters are used in the development of shunt APF.

- The current fed inverter is not popular in low power applications due to the complexity of the control strategy needed and sensitivity of the inverter circuit to current variations in the dc-link inductor. This configuration is mainly adequate for the case of medium power applications that matches the main requirement of lower switching frequencies and high power ratings of gate turn-off thyristor (GTO).
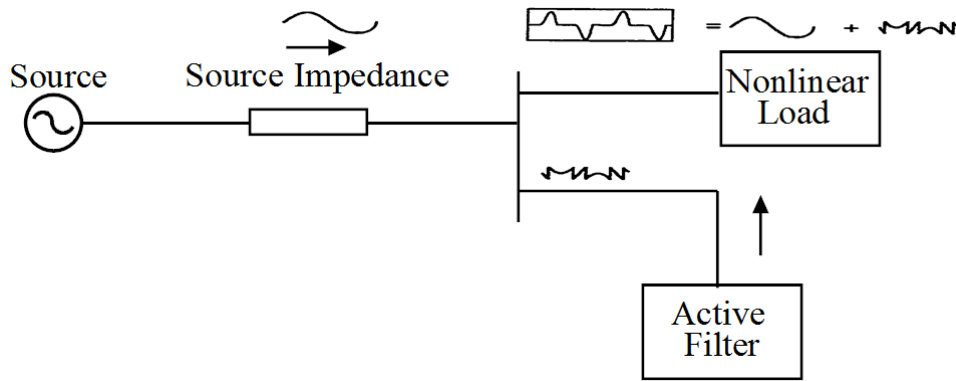
Figure 1.4: Principle of Shunt Active Filter

- The current controlled voltage fed inverter is common in most shunt APFs. It has a self-supporting dc voltage bus with a large dc capacitor. The main advantages of the current-controlled voltage-fed inverter type are the relatively simple control strategy needed for pulse width modulation (PWM) wave shaping and the standard availability of the inverter for power ratings that can cover the low and medium power application regions of active filters.

1.1.3.2 Series Active Power Filter

These series APFs are less common industrially than their rivals, the shunt active filters. Due to their position in the circuit, they have to tolerate high values of rated load current, which increases their current rating significantly; particularly the secondary side of the coupling transformer (increasing the copper losses and the physical size of the filter). Series filters have a main advantage over shunt ones is that they can be used much easier to eliminate voltage waveform harmonics and to balance three phase voltages.

1.1.3.3 Other Filter Combinations

The combination of several types of filters (shown in Table 1.5) achieves advantages for some applications. These are as follows.

- Combination of shunt and series APF has the control complexity due to dependency of the switching pattern of both shunt and series circuits. However, it is used for other purposes in power systems for flexible AC transmission systems (FACTS).

Table 1.6 Topology of Active Power Filter with compensation for different PQ Problems

Compensation for specific Application	Active Power filter Topology			
	Shunt APF	Series APF	Series APF + Shunt PF	Shunt APF + Series APF
Current Harmonics	Moderate		Fast	Low
Voltage Harmonics		Fast	Moderate	Low
Reactive Power	Fast		Moderate	Low
Load Balancing	Low			
Neutral Current	Moderate		Low	
Voltage Regulation	Low	Fast	Moderate	Low
Voltage Balancing		Fast	Moderate	Low
Voltage Flicker	Fast	Moderate		Low
Voltage Sags & Swells	Low	Fast	Moderate	Low

- Combination of series APF and shunt PF yields superior filtering performance over series APF used alone and the expansion of their abilities to include current harmonic reduction and voltage harmonic elimination.

- Combination of shunt APF and PF is intended, where the APF is designed to eliminate low order current harmonics while the PF is designed to eliminate bulk of load current harmonics.

- Series combination of APF with shunt PF is especially important for medium and high voltage applications where the passive filter reduces the voltage stress applied to the switches in the APF.

The compensation possible using each topology of APF is summarized in Table 1.6. With the advance of integrated circuit and the cost reduction of power semiconductor

devices, APFs are expected to be extensively used in common industrial or residential applications. A typical series APF, which functions in the cascade power path requires higher rated current and voltage devices and hence produces significant switching losses. Furthermore, the combinations of APFs provide an expensive and complicated filter system for the power distribution system. So far, the shunt type is much preferred and practical one as observed from Table 1.6. In this thesis, the shunt active power filter (SAPF) configuration is chosen.

1.2   Literature Review on Shunt Active Power Filter

To obtain efficient active filter performance, it is important to choose both a proper current reference and an adequate current control strategy. As far as control is concerned, two loops can be identified. The first one is used to calculate the current reference injected by the filter and the second one should guarantee that the filter follows that reference adequately. Several control strategies have been reported in literature for improving performance of SAPF and these are briefly reviewed below.

Instantaneous p-q method has been proposed in [17] for performance improvement of SAPF under unbalanced supply voltage condition, however performance under balanced and sinusoidal conditions is satisfactory. A hysteresis-band PWM current controller is employed for generation of switching pulses and proportional integrator (PI) controller supervises the dc capacitor voltages. The resulting source currents are found to be sinusoidal, but voltage regulation performance is not satisfactory. A simple modification is proposed in [18] to develop a generalized p-q theory in active power filtering under the condition of distorted supply condition. Addition of phase locked loop (PLL) with p-q approach helps in eliminating the adverse effect of the distorted supply voltage. The reference current signal is generated with help of direct and indirect current control technique and hysteresis current controller is used as a PWM generator. The SAPF system maintains a self-supporting DC bus voltage and it functions as a reactive power and harmonic compensator. The source current THD is reduced from 27.2 to 3.4% under a distorted supply voltage with a THD of 16.2%.

Yuan and Merk [19] reported a PI current controller using stationary-frame generalized integrators for current control of APFs. Instantaneous p-q theory is used for reference current generation and the sequence filter based on the positive sequence ideal

integrator resolves the problems of the p-q theory under distorted or unbalanced PCC voltage conditions. Extensive test results from a 10-kW prototype are demonstrated and the utility current is observed to be sinusoidal under both balanced and unbalanced loading conditions.

Synchronous - reference frame (SRF) method is proposed in [20] along with three independent two-level hysteresis comparators operating on a 3-leg VSC. Reference currents are derived directly from the load currents without considering the source voltages. Experimental results from a 2-kVA IGBT prototype showing the transient and steady-state system performance are presented, where the proposed method allows the operation of the SAPF in a large frequency range covering both 50 Hz and 60 Hz three-phase distribution systems and presents better harmonic compensation performance as compared to p-q based SAPF.

A new digital reference current estimation method for control of SAPF using a Kalman Filter (KF) is presented by Moreno [21]. Its capability of prediction avoids the effects of computational lags derived from the digital signal processing. The characteristics of the proposed technique are: the harmonic current compensation in a global or a selective way and the fast dynamical response. The dead beat current (DBC) control loop takes into account the SAPF model and ensures the correspondence of the injected current and its reference estimated by KF. Its immunity to harmonic distortion of the line voltage waveform has been confirmed for common levels of voltage THD (4.7%) and higher levels (11.4%) than those now present in the power system. Chudamani [22] has proposed nonlinear least square (NLS) based algorithm for reference current generation and hysteresis controller for generation of switching pulses in SAPF. The fundamental frequency of the grid is estimated by using NLS and the estimated frequency is then used in the signal model to compute the harmonic magnitudes resulting in reference compensation signals. The THD of the source current is found to be 4.6% in this proposed control strategy and also it performs well under sudden load changes as well as change in the wave shape of the load. A new control scheme based on KF and linear quadratic regulator (LQR) is proposed in [23] to improve the performance of SAPF under the effects of measurement noise, load currents and grid voltage transients. KF algorithm generates references for harmonics, unbalance and displacement power factor compensation and can also be responsible for LQR implementation. With increase of line impedance i.e., 0 mH, 2.8 mH and 5.8 mH, the THD of the proposed SAPF is found to be

6.37%, 5.78% and 4.85% respectively showing good tracking behavior even under high line impedance. Extensive tests and experimental results are presented in order to verify the performance of SAPF.

A fuzzy logic controller for a three level SAPF based on p–q theory to identify reference currents have been implemented in [24]. Fuzzy logic control algorithm is proposed for harmonic current and inverter dc voltage regulation to improve the performance of the SAPF. The proposed SAPF has produced a sinusoidal supply current of low harmonic distortion of 0.9% and is in phase with the line voltage as obtained from simulation results. Particle swarm optimization approach [25] and Takagi-Sugeno Fuzzy (TS-fuzzy) [26] have been developed to improve the performance of active power filter.

Tey and Chu [27] proposed artificial neural network (ANN) technique to design SAPF system. ANN algorithm computes harmonic contents and reactive power for the nonlinear load and these two signals are used as the reference signal for the hysteresis control of a three phase IGBT based VSI. The application of ANN makes extraction of harmonics faster resulting in faster adaptation of active filter to any variation in the operating conditions and it also has the capability to regulate the dc capacitor voltage. Referring simulation results, the THDs of the source current are found to be 2.14%, 2.00% and 2.25% for high-to-low, low-to-high and unbalanced nonlinear load current conditions respectively. An algorithm based on load conductance estimation using neural network (NN) is implemented on a three phase shunt compensation for mitigation of PQ problems such as load balancing, reactive power compensation, harmonics elimination and neutral current compensation in a four wire distribution system [28]. Its structure is reflected as Kohonen learning or Kohonen feature maps and is used for extraction of fundamental component of load currents in terms of conductance and susceptance, which finally helps in the source reference current estimation. This algorithm is found suitable for the conditions where the periodicity of loads is not fixed or load currents are frequently changing. It is based on the strong basic circuit theory compared to other traditional NN algorithms. The reference supply currents and sensed supply currents are compared and their current errors are amplified through PI current controllers. The output of PI current controller is fed to the PWM current controller to generate the gating pulses of IGBTs of the VSC. From experimental verification, THDs of the supply current and load current are observed to be 3.8% and 39.6%. In [29], SAPF is controlled using an adaptive-linear-element (Adaline) based current estimator to maintain sinusoidal and

unity power factor source currents. Three phase load currents are sensed and using least mean square (LMS) algorithm based Adaline, online calculation of weights are multiplied by the unit vector templates, which give the fundamental frequency real component of load currents. PI controller is used for maintaining dc bus voltage constant and the switching of VSC is performed using hysteresis based PWM indirect current control technique, which controls the source currents to follow the derived reference source currents. Moreover, a THD of as low as 2.5% is achieved in SAPF system. An adaline-based phase-locking scheme has been proposed in [30] to control three-phase SAPF. The proposed ANN-based synchronization scheme is done in two steps: 1) frequency estimation by modified NLS and 2) phase locking using adaline. Prefiltering of the supply voltage prior to the frequency estimation is suggested as it improves the estimation capability, regardless of the harmonic order present in the supply voltage and then reference current signal is generated utilizing synchronous unit templates. The hardware experimental results under different supply and load conditions are provided. In all cases, the source current THDs are achieved below 4% while maintaining unity-power-factor operation. In [31], Shyu proposed model reference adaptive control (MRAC) design for SAPF to improve line power factor and to reduce the line current harmonics. The MRAC approach improves many failures of the fixed gain PI controller, such as undesirable undershoots and overshoots at the transient and nonrobustness when changing loads. The proposed MRAC adaptive law is designed using Lyapunov's stability theory and Barbalat's lemma that guarantees asymptotic output tracking. Furthermore, a prototype system was built to show effectiveness and to verify the performance of the system. An integration of predictive and adaptive ANN-based controller for SAPF has been presented in [32] to improve the convergence and reduce the computational requirement. The predictive algorithm is derived from an ANN based PI controller used to regulate the dc-link voltage in the SAPF. This is followed by an adaline based THD minimization technique. Adaline is trained by conjugate gradient method to minimize THD. The system is extensively simulated and experimental prototype is produced in laboratory using dSPACE1104. The THDs for both the simulation and experimental results remain less than 5%.

An adaptive control strategy for SAPF for compensation of harmonic distortion, reactive power, and unbalanced load is proposed in [33]. In the proposed study, the amplitude of SAPF reference currents is generated by the dc-link voltage controller,

based on the active power balance of system. The current controller is implemented by an adaptive pole-placement control strategy integrated to a variable structure control scheme (VS-APPC) in which it introduced the internal model principle (IMP) of reference currents for achieving the zero steady-state tracking error. The main feature of this controller in comparison to the conventional resonance-based schemes is that VS-APPC controller gains are determined based on adaptive laws, which employs sliding-mode techniques. This hybrid structure leads to a robust adaptive control strategy with a good dynamic performance. After the use of compensation scheme, the harmonic distortion is reduced from 29% to 3.5%. Singh and Arya [34] proposed an adaptive theory-based improved linear sinusoidal tracer (ILST) control algorithm for three phase shunt compensation. The ILST control algorithm is used for the extraction of fundamental load currents and their active and reactive power components. These components are used for the estimation of reference source currents. These reference source currents and sensed source currents are compared for respective phases and each phase current error is amplified using PI current regulators and their outputs are compared with a triangular carrier signal of 10 kHz to generate the gating signals for IGBT switches of VSC. The phase 'a' source current and load current are observed to be 4.7% and 25.8% respectively. Also an adaptive filter is implemented for shunt compensation in three-phase distorted voltage ac mains [35].The proposed filter is based on adaptive synchronous extraction, which helps in estimation of reference supply currents. The main features of this control approach are high convergence speed and robustness with respect to input frequency and internal parameter variations and less sensitivity to voltage pollutions. The PWM current controller is employed for minimization of error between reference and actual source currents. The dc-link voltage of the APF has been also regulated to a desired value under time-varying load conditions. The compensation result for this proposed control strategy is analyzed to be 4.4% THD in the source current. Also, the power factor on the supply side is improved to near unity (0.99). A leaky LMS adaptive filter [36] is implemented in a shunt connected compensating device for the extraction of reference supply currents with a self-supporting dc bus. These extracted reference supply currents are used for the generation of switching pulses of VSC. An advantage of this adaptive filter algorithm is that it has improved dynamic response and fast convergence due to decreasing spread input eigenvalues. The value of the leaky factor should be higher to reduce the eigen spread for the simultaneously improved dynamic response. Based on the simulation and

implementation results, the proposed control system was able to shape the supply currents toward the sinusoidal and balanced at unit power factor.

In [37], a three phase shunt connected custom power device known as Distribution Static Compensator (DSTATCOM) is designed with back propagation (BP) algorithm for reference current generation and PWM current control technique for switching pulses generation. In this BP algorithm, the training of weights has three stages. It includes the feedforward of the input signal training, calculation and BP of the error signals and upgrading of training weights. In the training process, it is slow due to more number of learning steps, but after the training of weights, this algorithm produces very fast trained output response. Extensive tests are performed utilizing proposed control strategy of APF. The THDs of the phase 'a' source current and load current are observed to be 2.99% and 24.94% respectively specifying harmonic distortions of the source current within the IEEE-519 standard limit. Also a composite observer-based control algorithm along with PWM current control technique is implemented for three phase shunt compensation device [38]. This algorithm extracts load fundamental current components of polluted load current and these components of load currents are used for estimation of reference source currents. The advantages of this algorithm are that it is less sensitive with supply frequency variation, low distortion in the extracted signal without leakage of harmonics. The proposed control structure has been given a satisfactory performance according to IEEE-519–1992 guidelines. The dc bus voltage has also been regulated to desired level.

Rahmani and Mendalek [39] presented a nonlinear control technique for SAPF system. PI control law is derived through linearization of the inherently nonlinear SAPF model, so that tasks of the current control dynamics and dc capacitor voltage dynamics become decoupled. This decoupling allows controlling the SAPF output currents and dc bus voltage independently of each other and hence generates a delay. The computational control delay compensation method is proposed, which extracts the SAPF reference currents from nonlinear load currents by using SRF method in first step and then, reference currents are modified. SAPF performance is evaluated in real time using dSPACE1104 controller board. The THD of the current generated by nonlinear load is observed to be 25.8%, whereas the compensated supply current has a THD of 2.62%. Jorge [40] proposes a current controller based on the reduced order generalized integrator (ROGI) to control SAPF and this controller doesn't require accurate current references, nor the current references that must be updated quickly in presence of load transients or

grid voltage transients. The low computational burden of the whole control makes it ideal for its implementation in low-cost digital signal processor (DSP).

A single-step noniterative optimized control algorithm has been proposed in [41] for a three phase three wires SAPF to achieve an optimum performance between power factor and THD. The proposed optimized approach is simple to implement and does not require complex iterative optimization techniques such as Newton–Raphson and sequential quadratic programming to determine the conductance factors. It is shown mathematically that only three conductance factors (one for the fundamental harmonic and two other for odd and even harmonics) are sufficient to determine the desired reference source currents. These reference source currents are compared with the actual measured currents using the hysteresis current controller which determine the switching signals for the VSI.The performance of the proposed control strategy is validated by a real-time HIL experimental prototype and the compensation THD result is analyzed to be 1.7%. Trinh [42] proposes an advanced control strategy to enhance performance of SAPF. This scheme is implemented by using only supply current without detecting the load current and filter current. Hence this scheme comprises of only two loops. The outer voltage control loop is maintained by PI controller to generate the reference current and the inner current control loop is designed with PI and vector-PI controller to regulate the supply current. Experimental results demonstrate that the proposed control strategy achieves good performances under ideal sinusoidal as well as distorted supply conditions. The THD of the supply current is reduced to less than 2% for all cases. In [43], a novel source current detection control scheme is proposed in SAPF to generate reference current signal with power balance (PB) method. This PB method has good dc voltage regulation and has excellent stable filtering performance as compared to current source (CS) based method. A vector resonant controller is proposed, with which the SAPF performs as an equivalent multiband rejection filter that series between nonlinear loads and the grid source, blocking selected harmonics components from the load side flowing into the source side. The proposed SAPF is simple in structure and is needless of a harmonic extraction algorithm. In this SAPF system, THD of the source current is dropped from 28% to 2.9%. Lenwari [44] investigates an optimization procedure based on genetic algorithms (GA), which can automatically design a high-performance resonant-type current controller for SAPF application and SRF method is employed for generation of reference compensation signal. Even in the presence of power system

impedance variations , the SAPF can precisely regulate the 5th, 7th, 11th, and 13th harmonic currents by utilizing fitness function in GA, which is defined to be a compromise between speed of response, stability and robustness to supply impedance variations. The performance of the system is good; the THD of the supply current is reduced from 26.81% to 4.49%.

A robust control strategy is implemented in [45] to regulate the dc-link voltage by combining a standard PI controller and sliding mode controller (SMC), which helps in generation of reference current in SAPF. The SMC scheme continuously determines the gains of the PI controller based on the control loop error and its derivative. The chattering due to the SMC scheme is reduced by a transition rule that fixes the controller gains when steady state condition is reached. The phase currents of the power grid are indirectly regulated by double sequence controllers (DSC), where the internal model principle (IMP) is employed to avoid reference frame transformation. The proposed control strategy ensures zero steady-state error and after the compensation implemented by the SAPF, the THD obtained is 3.6%. Matas [46] proposed feedback linearization theory to SAPF system, where active filter is linearized by means of a nonlinear transformation of the system model, deduced from the application of Tellegen's theorem to the system. SMC is proposed to impose a desired dynamic behaviour on the system, giving robustness and insensitivity to parameter variations. Outer voltage controller loop is based on PI controller and also helps in reference current generation. The proposed SAPF ensures proper tracking of the reference signals and THD of the compensated source current is analysed to be 3.3%.

Odavic and Biagini [47] proposed an improved predictive current controller for SAPF. This algorithm is based on the conventional DBC method and introduces a modified approach to compensate for delays incurred through digital implementation of the control, by predicting a system behaviour one and two sample instants in advance with respect to the measurement instant. A polynomial type extrapolation predictor is considered to predict the SAPF reference currents and space vector modulation (SVM) scheme is employed for switching pulses generation in IGBT inverter. Compared to conventional DBC, the proposed SAPF is more suitable for practical implementations where measurement noise is very likely to appear. The THD of load current is reduced from 27% to 3.7%. The SAPF implemented with a four-leg VSI using a predictive control scheme is presented in [48]. This predictive algorithm is realized in three steps; current

reference generator, prediction model and cost function optimization. A SRF based current reference generator scheme is used to obtain the current reference signals and presents a fast and accurate signal tracking capability. The experimental results present that the THD of the line current is dropped from 27.09% to 4.54%. A new approach for harmonic distortion minimization in distributed power system has been proposed in [49] .

1.2.1 Remarks from Literature Review on SAPF

From the above discussions, the following remarks can be reported.

- Control strategies based on p-q method and conventional HCC technique are easier to realize in SAPF with higher accuracy and fast response. These approaches perform satisfactorily under balanced sinusoidal supply condition, but their performances deteriorate in unbalanced condition. However, variable switching frequency is one of the drawbacks related with HCC technique.

- SRF-HCC approach to improve SAPF performance is satisfied under unbalanced as well as distorted supply conditions and as a result, current harmonics can be effectively reduced in this approach as compared to p-q-HCC.

- SAPF performance employing reference current estimation using KF, NLS method is found to be effective under grid perturbations such as grid voltage transients and measurement noise.

- SAPF based on soft computing approaches such as fuzzy, ANN is very sensitive to system uncertainty and external disturbances.

- The source reference generation along with PWM current control realization in SAPF is the most established in the literature [36][37][38]. The extracted fundamental component of polluted load current helps in reference generation and PI controller is used for maintenance of dc-link voltage.

- Adaptive control based SAPF system improves many failures of fixed-gain PI controller in transient conditions of the load and makes THD less than 5%.

- PI-SMC based SAPF has main advantages including fast dynamic response, strong robustness of perturbation parameter and easier realization over other linear control methods. Moreover, a proper tracking of reference signal is achieved in SAPF.

- Predictive current control techniques employed in SAPF can handle multivariable characteristics as well as simplify the treatment of dead time compensation.

However this approach requires a high amount of calculations compared to a classic control based SAPF.

- SAPF with proper reference current generation as well as strong robust current controller approach is essential to reduce the THD of source current to a large extent.

1.3   Motivation of the Thesis

The motivations of the thesis are as follows.

- The information from the grid is used at different levels of the control system of a grid-connected converter. The internal reference signal generated by the control algorithm of a grid-connected power converter should be brought into line with a particular grid variable, usually the fundamental component of the grid voltage. This has motivated to generate the reference current signal in SAPF based upon the knowledge of fundamental component of the grid voltage such that a synchronization of the source current with the supply voltage can be achieved. Thus, an accurate estimation of this fundamental component is intended.

- Both linear and nonlinear Kalman filter (KF) [50][51][52][53][54] approaches have gained extensive attention as they accurately estimate the amplitude, phase and frequency of a signal buried under noise and harmonics. Further, most of the existing estimation approaches [55][56][57][58][59][60] have not considered the grid perturbations such as voltage distortion, measurement noise and harmonics. Hence in view of addressing these aforesaid issues (harmonics, voltage distortion, noise), a new estimation algorithm has to be developed, which can provide better improved estimations independent of all grid perturbations in SAPF with fast convergence.

- The dynamic performance of SAPF is mainly dependent upon the behavior of its current controller technique. From literature review, it is found that Predictive control concepts are intuitive and easy to understand, and can also be applied to a variety of systems. Constraints and nonlinearities can be easily included. Further, these types of controllers require a high amount of calculations compared to a classic control scheme; which is made possible through fast microprocessors available today. Therefore, new predictive control techniques need to be

developed in SAPF, which offer the potential for achieving fastest transient response, more precise current control and full compatibility with digital control platforms.

- It is not possible to supply quality power to special equipments such as converters with AC drives, distributed control system, programmable logic control (PLC) through conventional control schemes employed in SAPF. This results in malfunctioning of the above type of equipment, which demands pure power at all moments with fast changing disturbances occurring in power system. Hence, a fast and robust control action is necessary to deliver pure and distortion less power to above equipments considering all perturbations taken into account. Moreover, power line uncertainties such as unexpected failure of power system components, random variation of load, high disturbance conditions and sensor nonlinearities are the most challenging problems that might affect the dynamic performance of SAPF. Further, parameters of SAPF may vary owing to component aging, thermal drift and saturation effects caused by the operating environment. In view of aforementioned issues, it is necessary to design robust controllers that not only provide good disturbance rejection and robustness against uncertainties in the system dynamics, but also to achieve efficient current harmonics compensation through the SAPF.

1.4 Objectives of the Thesis

- To propose a robust estimation technique for estimation of fundamental amplitude and frequency in view of achieving accuracy and fast convergence considering all possible perturbations such as voltage distortion, measurement noise and harmonics.
- To develop a new reference current generation scheme that can self-regulate the dc-link voltage.
- To propose new current control techniques for improving the dynamic performance of SAPF system.
- To propose robust control technique such that it should provide robustness against parametric variations of load, reduce the current tracking error to zero, cancel the current harmonics effectively and achieve unity power factor in SAPF system.

- To develop a prototype experimental set up for verifying the robustness of the proposed robust control techniques in SAPF system.

1.5 Thesis Organization

The thesis consists of seven chapters that are organized as follows.

Chapter 1 provides an extensive review on SAPF based upon different reference current generation approaches as well as current controller techniques. Remarks on the review on different control strategies of SAPF are presented along with the discussion of their merits and demerits. Further, they are evaluated with respect to their benefits, drawbacks and appliances.

Chapter 2 proposed two current control techniques called HCC and SMC realized with a new reference current generation scheme for SAPF system. This reference generation scheme involves with exterior PI controller loop and the in phase fundamental components of distorted PCC voltages necessitated for this reference generation are estimated using the KF based algorithm. KF-HCC based SAPF performs under consideration of grid perturbations, but harmonics cancellation is not so fast and perfect owing to slower convergence rate of KF. Hence, the other controller called SMC is employed with a faster reference scheme based on proposed Robust Extended Complex Kalman Filter (RECKF). A new weighted exponential function is embedded into RECKF to estimate a fast and distortion less reference signal considering grid perturbations such as voltage distortion and measurement noise. The effectiveness of this proposed RECKF-SMC is assessed with other variants of KF such as KF, Extended Kalman Filter (EKF) and Extended Complex Kalman Filter (ECKF) using simulation results obtained from Matlab/Simulink and real-time simulation results obtained from Opal-RT. KF-SMC performs better than KF-HCC, but RECKF-SMC is analyzed to be more effective in harmonics cancellation as compared to KF-SMC, EKF-SMC and ECKF-SMC based control strategies in SAPF.

Chapter 3 proposed two predictive current control techniques called Dead beat control (DBC) and Model predictive control (MPC) with a new and improved reference generation scheme. The reference generation is comprised of two components: 1) estimation of in phase fundamental component of PCC voltage in p.u. value, and 2) estimation of fundamental amplitude of load current. The main advantage of this

reference scheme is the avoidance of PI controller loop to eliminate relatively large overshoots and undershoots associated with it, which may interrupt the stable operation of the inverter in protecting the switching devices. Further proposed RECKF is found to be excellent among KF, EKF and ECKF as investigated in Chapter 2. As a result, in this Chapter RECKF has been employed in reference generation scheme. Realization using proposed RECKF-DBC scheme is very simple and it needs a modulator to provide gate drive signals to IGBT inverter. In DBC, the optimal actuation is the one that makes the error equal to zero in the next sampling instant, whereas a more flexible criterion is employed in MPC, expressed as a cost function to be minimized. There is no need of any modulators and the gate drive signals are generated directly by this MPC scheme. RECKF-MPC performs better as compared to RECKF-DBC. Furthermore, to examine the efficiency of this proposed RECKF-MPC over PI-MPC, a comparative study has been done applying both steady state and transient state conditions.

Chapter 4 proposed an optimal Linear Quadratic Regulator (LQR) with a new reference current generation method in SAPF. LQR is chosen here due to its well-known features of tracking and disturbance rejection capability. A realistic representation of the SAPF system is achieved in LQR by using a resonant model of the PCC voltages instead of considering it as a disturbance. For LQR designing, the state space variables related to the PCC voltages, are accurately estimated using proposed RECKF based algorithm. Furthermore, stabilization of capacitor voltage is improved with a new reference generation scheme based on RECKF, adding an error between fundamental amplitudes of source and load current. Consequently, harmonics cancellation effect is more in case of RECKF-LQR approach. Thus, RECKF-LQR is analyzed to be more effective as compared to RECKF-SMC, RECKF-DBC and RECKF-MPC employing simulation as well as real-time simulation results.

Chapter 5 proposed a robust technique called Linear Quadratic Gaussian (LQG) Servo controller with higher disturbance rejection capability, which permits all perturbations such as PCC disturbances, parametric variations of load and tracking error variations so that compensation capability of the overall SAPF system can be enhanced (i.e., THD much less than 3%) with less consumption of time. From simulation results, LQG servo controller is not only analyzed to be robust against different load parameters, but also a satisfactory THD result has been achieved in SAPF. This has motivated to develop a prototype experimental set up in our Laboratory using dSPACE DS1104 R & D

controller board for verifying the robustness of LQG servo controller. Finally, it is found that the experimental results are in close agreement with the simulation results.

Chapter 6 proposed H_∞ controller with a mixed sensitivity approach with the purpose of achieving stability, high disturbance rejection and high level of harmonics cancellation. This mix sensitivity approach involves with the robustness performance, control effort performance as well as error tracking performance of SAPF system by selecting appropriate weighting functions. Further, a new current reference scheme is proposed in this Chapter, which deals with the measurement of source current only making whole SAPF a more reliable and cost efficient system. The effectiveness of the proposed RECKF-H_∞ based SAPF model is validated pursuing simulation and experimental studies. From the both simulation and experimental results, it is observed that the proposed RECKF-H_∞ control approach to design a SAPF is found to be more robust as compared to RECKF-LQG servo control approach in face parametric uncertainties due to load perturbations yielding improvement in power quality more effectively in terms of tracking error reduction, efficient current harmonics mitigation as well as reactive power compensation. Comparing with compensation performances of RECKF-SMC, RECKF-DBC, RECKF-MPC, RECKF-LQR and RECKF-LQG servo based SAPF; it is observed that overall performance of this robust RECKF-H_∞ is more.

Chapter 7 describes the concluding explanations and suggestions for some future research problems as extensions of the work described in the thesis.

CHAPTER 2

Hysteresis and Sliding Mode Controller with a New Reference Current Generation Strategy in SAPF

2.1   Introduction

Usually a signal can be constructed by using the estimation of its frequency, amplitude, and phase. This idea can be extended to identify the fundamental component from a distorted power system signal, which generates a reference signal for a SAPF. To obtain a high-quality estimate of this component is of particular interest. Most of the proposed methods to identify the fundamental component of voltage or current are based on the low-pass filter (LPF) method, conventional unit vector based method, discrete Fourier transform (DFT) method, and positive sequence calculation method. In the LPF method [61], the filter introduces a phase shift in the output, which requires a lead compensator to compensate this phase shift. Any change in the fundamental frequency introduces an error in the compensation network and causes a residual fundamental component to be added to the reference currents. This causes active power flow through the SAPF even under steady-state conditions. In the conventional unit vector method [29], the steady-state performance under balanced and sinusoidal conditions is satisfactory, but it produces inaccurate reference currents when the supply voltage contains distortions, resulting in incomplete harmonics compensation. In the DFT method [62], the estimation accuracy is inaccurate because of spectral leakage. This happens because grid frequency does not remain constant. In [63], the reference current is calculated by two steps: the first is related to the calculation of the positive-sequence component of unbalanced supply voltage and the second is deriving a simple fundamental extraction filter to extract the fundamental frequency component from the distorted positive-sequence voltage, hence increases computation time. Here additional measurement noise at the point of common coupling (PCC) does not seem to be taken into consideration in reference current generation. Once the current references have been determined with consideration of all grid perturbations such as voltage distortion and measurement noise, the SAPF must be able to track accurately such references with a suitable controller even in sudden slope variations of the reference.

Keeping these facts into consideration, two new control strategies namely Kalman filter-Hysteresis current control (KF-HCC) and Robust Extended Complex Kalman filter-Sliding Mode Control (RECKF-SMC) are proposed in this chapter, which are independent of all grid perturbations and make harmonic compensation effectively in SAPF system.

2.2   Chapter Objectives

1. To estimate the fundamental component of the distorted PCC voltage accurately under consideration of grid perturbations, which helps in the generation of reference current signal for SAPF system.

2. To track the reference current accurately employing suitable PWM current control techniques to enhance harmonic compensation performance of SAPF.

3. To simulate the proposed control techniques in MATLAB/Simulink and real-time simulation model in Opal-RT simulator.

2.3   Proposed KF-HCC based SAPF

Among several estimation techniques reported earlier such as least-square error technique [64], orthogonal component-filtered algorithm [65], Kalman filter (KF) [66][67][68][69][70][71] and recursive Newton-type algorithm [72], KF is found to be more optimal in noisy environments. Further a literature survey pursued on different control strategies of SAPF envisages that hysteresis current controller (HCC) is a simpler and it is easier to realize in SAPF. HCC is characterized by its unconditioned stability, fast response and good accuracy. This has motivated to design a KF-HCC based control strategy in SAPF, where KF is employed for generation of reference current and HCC for tracking of reference current in SAPF.

2.3.1   Description of Proposed KF-HCC based SAPF System

Fig. 2.1 depicts the proposed control structure adopted for the three phase SAPF using HCC and KF. The SAPF is composed of a DC-link capacitor v_{dc} and three-phase insulated-gate bipolar transistor (IGBT) inverter followed by an inductive output filter $\left(L_f, R_f\right)$. The SAPF is designed to inject a current i_{Fabc} at the PCC to cancel the harmonic content of the load current i_{Labc}, which results in a pure and sinusoidal current
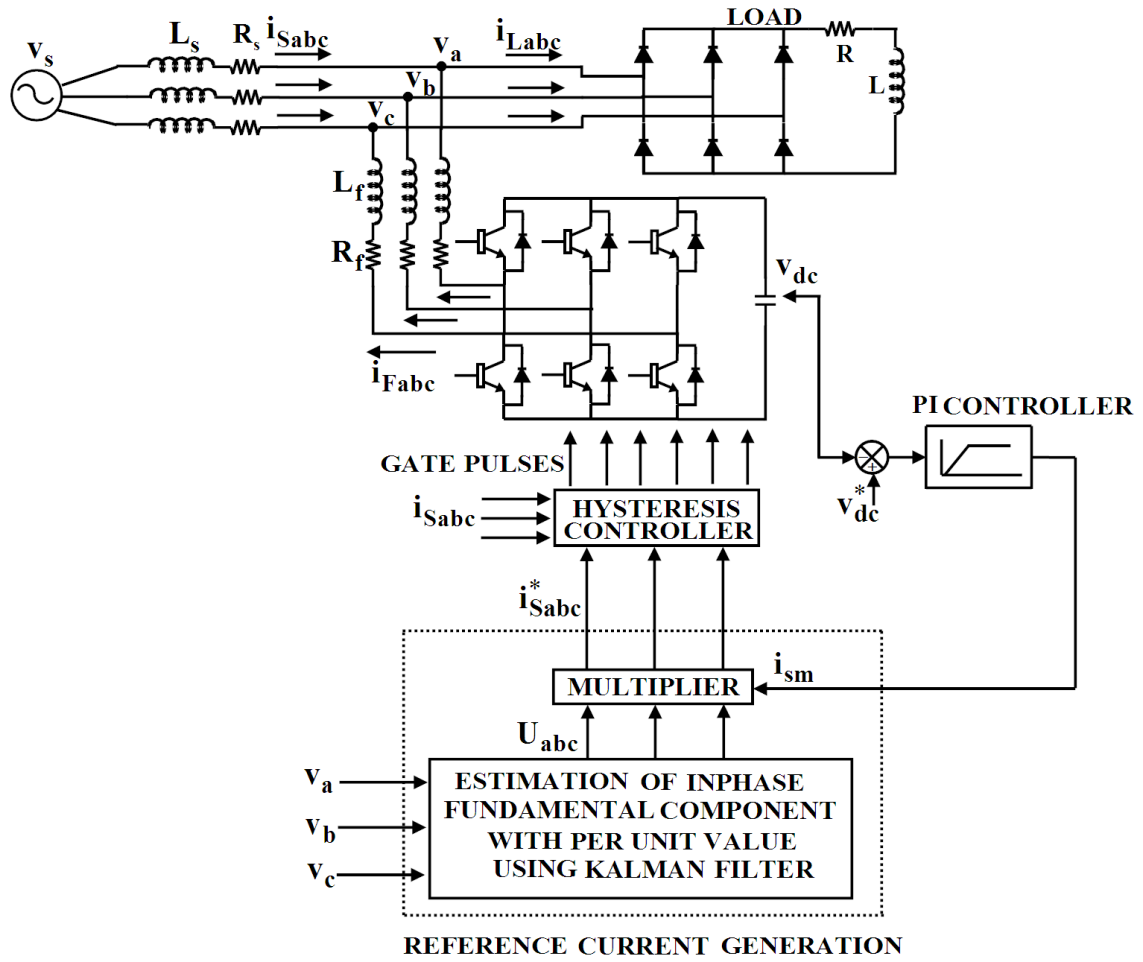
Figure 2.1: Proposed KF-HCC based SAPF

i_{Sabc} (where suffixes a, b and c represent different phases). To achieve the aforesaid objective, KF is employed to generate the reference current for the HCC.

The control system uses the measurement of the PCC voltages (v_a, v_b, v_c) and the KF estimation algorithm is used for identification of the in-phase fundamental component (U_{abc}) in per unit magnitude of PCC voltages. These are modulated with the output of PI controller i_{sm} to generate references (i^*_{Sabc}) for the current controller. HCC is used as a current controller and generates gate drive signals for the inverter (Fig. 2.1).

2.3.2 Proposed Reference Current Generation

Usually the performance of the SAPF depends upon the accuracy of the reference signal generator and for source reference generation, identification of the in phase fundamental component is the most critical item in determining SAPF behavior. The expression for source reference signal is given by

$$i_{Sabc}^{*} = i_{sm} \times U_{abc} \tag{2.1}$$

The estimation of the in phase fundamental component of PCC voltages using KF algorithm is presented below.

2.3.2.1 Signal Model and Formulation of KF Algorithm

A linear signal z_k of single sinusoid is represented by

$$z_k = a_1 \sin\left(k\omega_1 T_s + \phi_1\right), \qquad \text{k=1,....,N} \tag{2.2a}$$

N denotes an integer.

$$\omega_1 = 2\pi f_1 \tag{2.2b}$$

In eq (2.2a), T_s is the sampling time, parameters a_1 and f_1 are the fundamental amplitude and frequency respectively with initial phase ϕ_1. The signal z_{k+1} can be expressed as

$$z_{k+1} = x_{1_{k+1}} = x_{1_k} \cos\left(k\omega_1 T_s\right) + x_{2_k} \sin\left(k\omega_1 T_s\right) \tag{2.3}$$

Further,

$$x_{2_{k+1}} = -x_{1_k} \sin(k\omega_1 T_s) + x_{2_k} \cos(k\omega_1 T_s) \tag{2.4}$$

where x_{2_k} is known as the in quadrature component and is orthogonal to x_{1_k} and they are represented by

$$x_{1_k} = a_1 \sin(k\omega_1 T_s + \phi_1) \tag{2.5a}$$

$$x_{2_k} = a_1 \cos(k\omega_1 T_s + \phi_1) \tag{2.5b}$$

To model amplitude or phase variations in the signal, a perturbation vector $[\gamma_1 \quad \gamma_2]_k^T$ in the system states is considered. The state space representation of the signal then becomes

$$x_{k+1} = \Phi_k x_k + w_k \tag{2.6}$$

$$y_k = H_k x_k + v_k \tag{2.7}$$

where w_k and v_k are the process and measurement noises respectively. Φ_k and H_k are denoted as transition matrix and observation matrix respectively.

$$\Phi_k = \begin{bmatrix} \cos(\omega_1 T_s) & \sin(\omega_1 T_s) \\ -\sin(\omega_1 T_s) & \cos(\omega_1 T_s) \end{bmatrix} \tag{2.8}$$

$$H_k = [1 \quad 0] \tag{2.9}$$

Denoting the estimate of x_{k+1} as $\hat{x}_{k+1|k}$, the sequential recursive computation steps for fundamental component identification are given as follows.

$$\hat{x}_{k+1|k} = \Phi_k \hat{x}_{k|k-1} + K_k(y_k - H_k \hat{x}_{k|k-1}) \tag{2.10}$$

$$K_k = \Phi_k P_{k|k-1} H_k^T \left(H_k P_{k|k-1} H_k^T + R_k\right)^{-1} \tag{2.11}$$

$$P_{k+1|k} = \Phi_k P_{k|k-1} \Phi_k^T - K_k H_k P_{k|k-1} \Phi_k^T + Q_k \tag{2.12}$$

$$P_{k+1|k} = E\{(x_{k+1} - \hat{x}_{k+1|k})(x_{k+1} - \hat{x}_{k+1|k})^T\} \tag{2.13}$$

In eq (2.10), the innovation vector $y_k - H_k \hat{x}_{k|k-1}$ is used to refine the priori estimate $\hat{x}_{k|k-1}$ and K_k is the Kalman gain. In eq (2.11), it is intended to find the value of K_k that minimises the individual terms along the major diagonal of error covariance matrix P_k because these terms represent the estimation error variances for the elements of the state vector being estimated. Eq (2.12) is a general expression for the updated error covariance matrix for any gain K_k, where $P_{k+1|k}$ and $P_{k|k-1}$ represent a posteriori and a priori error covariance matrices respectively. Q_k and R_k are the process and measurement error covariance matrix respectively.

$$Q_k = E\{w_k w_k^T\} \tag{2.14}$$

$$R_k = E\{v_k v_k^T\} \tag{2.15}$$

Based on the above estimates ($\hat{x}_{1_{k|k-1}}$ and $\hat{x}_{2_{k|k-1}}$), the in phase fundamental component with per unit value can be expressed as

$$\sin\left(k\omega_1 T_s + \phi_1\right) = \frac{\hat{x}_{1_{k|k-1}}}{a_1} \tag{2.16}$$

where

$$a_1 = \sqrt{\left(\hat{x}_{1_{k|k-1}}^2 + \hat{x}_{2_{k|k-1}}^2\right)} \tag{2.17}$$

2.3.3 Hysteresis Current Control (HCC)

HCC is the most extensively used technique in APF because of its simpler implementation. Fig. 2.2 shows the basic idea behind HCC scheme. The principle of the HCC method for SAPF is implemented by presetting the upper and lower tolerance limits of hysteresis band (HB) which need to be compared to the error signal generated by the comparison of source reference current and actual source current. If the actual current exceeds the upper limit of the HB, the upper switch of the inverter arm is turned off and the lower switch is turned on. As a result, the current starts to decay. If the current crosses the lower limit of the HB, the lower switch of the inverter arm is turned off and the upper switch is turned on. As a result, the current gets back into the HB. Thus, the actual current is forced to track the reference current within the HB.
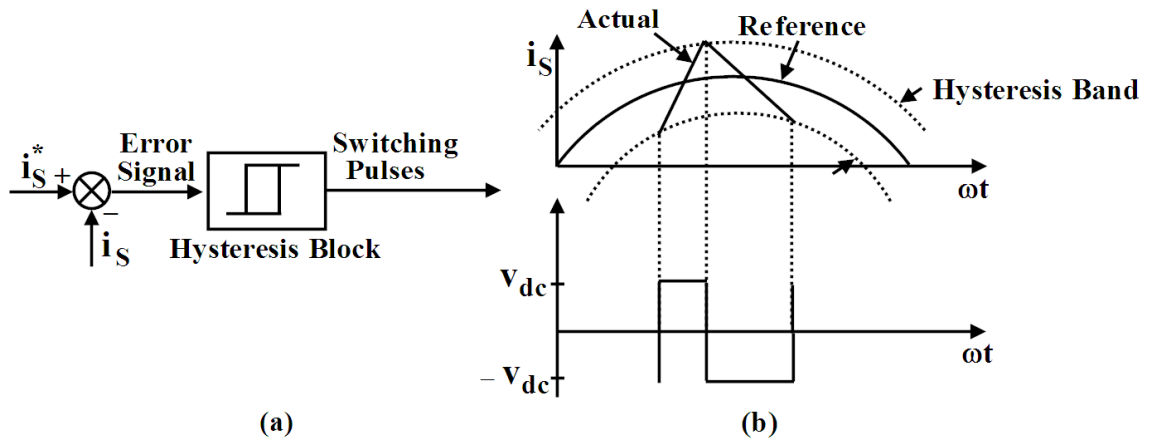
Figure 2.2: HCC Method, (a) Block Diagram of HCC, (b) Switching Pattern of HCC

The actual currents $\left(i_{Sa}, i_{Sb}, i_{Sc}\right)$ and reference currents $\left(i_{Sa}^*, i_{Sb}^*, i_{Sc}^*\right)$ are compared within the HB and the current controller decides the switching pattern of the devices in SAPF. The switching logic is formulated as follows:

if $i_{Sa} < (i_{Sa}^* - HB)$, then upper switch is OFF and lower switch is ON in leg 'a' of the SAPF;

if $i_{Sa} > (i_{Sa}^* - HB)$, then upper switch is ON and lower switch is OFF in leg 'a' of the SAPF;

Similarly, the switches in the legs 'b' and 'c' are activated.

A proper design of power circuit of SAPF is essential for implementation and hence a design procedure for parameters of SAPF is prescribed in the next Section.

2.3.4 Design of Power circuit of SAPF

The design of the power circuit includes three main parameters;

1. Selection of filter inductor, L_f

2. Selection of DC side capacitor, C

3. Selection of reference DC bus voltage, v_{dc}^*

2.3.4.1 Selection of L_f and v_{dc}^*

The design of these components is based on the following assumptions:

1. The AC source voltage is sinusoidal.

2. The AC side line current distortion is assumed to be 5% [34] for designing L_f. But when distortion is more than 5%, there would be an increase of interruption in injecting compensating current.

3. There is fixed capability of reactive power compensation of the active filter.

4. The PWM converter is assumed to operate in the linear modulation mode (i.e., $0 \le m_a \le 1$), where m_a is the amplitude modulation factor.

As per the compensation principle, the active filter corrects the current i_{Fl} to compensate the reactive power of the load. If the active filter compensates all the fundamental reactive power of the load, i_{Sl} will be in phase and i_{Fl} should be orthogonal to v_s as shown in Fig. 2.3, where one stands for the fundamental component.
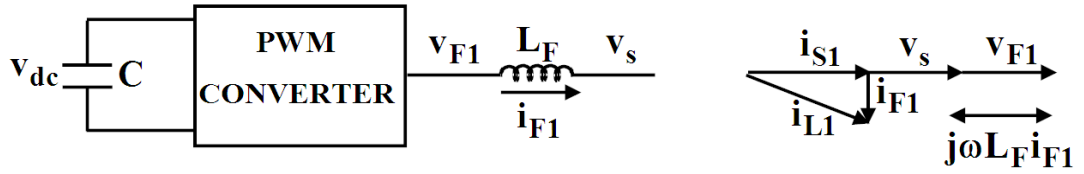
Figure 2.3: Vector Diagram representing reactive power flow

The 3-phase reactive power delivered from the active power filter can be calculated from a vector diagram, shown in Fig. 2.3.

$$Q_{c1} = 3v_s i_{s1} = 3v_s \frac{v_{F1}}{\omega L_F} \left(1 - \frac{v_s}{v_{F1}} \right) \qquad (2.18)$$

Hence, the active filter can compensate the reactive power from utility only when $v_{F1} > v_s$. The amplitude modulation factor m_a can be expressed as

$$m_a = \frac{v_M}{v_{dc}/2}, \qquad \text{where } v_M = \sqrt{2v_{F1}}$$

Therefore, v_{dc} can be presented as

$$v_{dc} = 2\sqrt{2v_{F1}} \quad \text{for } m_a = 1$$

The filter inductor L_F is also used to filter the ripples of the converter current and hence, the design of L_F is based on the principle of harmonic current reduction. The ripple current i_{Fh} of the PWM converter can be given in terms of maximum harmonic voltage v_{Fh} that occurs at the frequency $m_F\omega$.

$$i_{Fh}(m_F\omega) = \frac{v_{Fh}(m_F\omega)}{m_F\omega L_F} \qquad (2.19)$$

where m_F is the frequency modulation of the PWM converter. By solving eq (2.18) and eq (2.19) simultaneously, the value of L_F and v_{F1} can be calculated. v_{F1} and hence v_{dc}^* must be set according to the capacity requirement of the system (i.e., $v_s < v_{F1} < 2v_s$).

2.3.4.2 Selection of DC Capacitor C

Design of the dc side capacitor is based on the principle of instantaneous power flow. The selection of C can be governed by reducing the voltage ripple. As per the specification of peak-to-peak voltage ripple $v_{dr,p-p(max)}$ and rated filter current $i_{Fl,rated}$, the dc side capacitor C can be found from

$$C = \frac{\pi \times i_{Fl,rated}}{\sqrt{3}\omega v_{dr,p-p(max)}}$$ (2.20)

2.3.5 Results and Discussions

The structure of proposed KF-HCC control strategy is shown in Fig. 2.1. It is planned according to the design methodology described in Section 2.2.4. In order to verify its efficacy, a MATLAB/ SIMULINK simulation is pursued. A balanced three phase voltage supply has been applied to a typical non-linear load composed of a three phase diode rectifier bridge feeding a R-L load. Table 2.1 summarizes the simulation parameters, where L_s and R_s correspond to the source impedance, L_f and R_f correspond to the filter impedance, V_s is the supply voltage, C is the capacitance of the DC bus, v_{dc}^* is the reference DC bus voltage, K_p and K_i are the PI controller constants (Using Ziegler-Nichols tuning method), f is the supply frequency, f_s is the sampling frequency and f_{sw} is the switching frequency of SAPF.

Table 2.1 SAPF Parameters used for simulation

Parameters	Values	Parameters	Values
R_s , L_s	$1\,\Omega$, 0.1 mH	v_s	100V
R_f , L_f	$1\,\Omega$, 2.5 mH	K_p , K_i	0.248, 4.19
R , L	$20\,\Omega$,10 mH	v_{dc}^*	220V
f	50 Hz	C	2350 μF
f_s	25 kHz	f_{sw}	12.5 kHz

The performance of KF in estimation of reference current was analyzed using the following simulation results. For convenience, the initial state variables x_0 were chosen to be 0.0, and the filtered error covariance matrix P_0 was selected to be diagonal with the value of 10 p.u.^{2}. The measurement error covariance matrix R_0 was selected to be 1.0 p.u.^{2} to represent an inaccurate measurement and the process error covariance matrix Q_0 is fixed to be 0.001 p.u.^{2}. The covariance matrices P_0 and R_0 will be updated during the estimation process.

2.3.5.1 Simulation Results

Fig. 2.4 gives the details of PCC voltage with its in phase fundamental component, capacitor voltage, load current, compensating current, source current, THD (Total harmonic distortion) of source current before and after compensation with the proposed KF-HCC based SAPF system for phase 'a'. Referring to Fig. 2.4(a), it can be observed that in phase fundamental component estimated by KF takes about 0.045 sec to remain in the same track with PCC voltage. Before the compensating capabilities of the SAPF are tested, capacitor in DC link to be charged, this is displayed in Fig. 2.4(b). The instantaneous source current before compensation, which contains fundamental as well as harmonic components, is depicted in Fig. 2.4(c) and the harmonics compensation is achieved by the compensating current presented in Fig. 2.4(d). Fig. 2.4(e) displays the source current after compensation and indicates that they are sinusoidal, but large distortions are observed in the source current, which are measured on the basis of the amplitudes of different harmonic contents by a Fast Fourier Transform (FFT) analysis tool. From Fig. 2.4(f) and (g), it can be observed that THD of the source current is reduced from 25.6% to 4.87% with compensation of SAPF.

2.3.5.2 Real- time Simulation Results

For proper verification of the performance accuracy of SAPF system, the real-time response of the SAPF needs to be observed. Here the real time responses based on Opal-RT Platform are used to test the performance of the proposed SAPF system.

The Opal-RT Platform [73][74] enables the parallel simulation of power drives and electric circuits on clusters of PC running quick UNIX (QNX) or RT-Linux operating systems. Using standard SIMULINK models, RT–LAB builds computation and
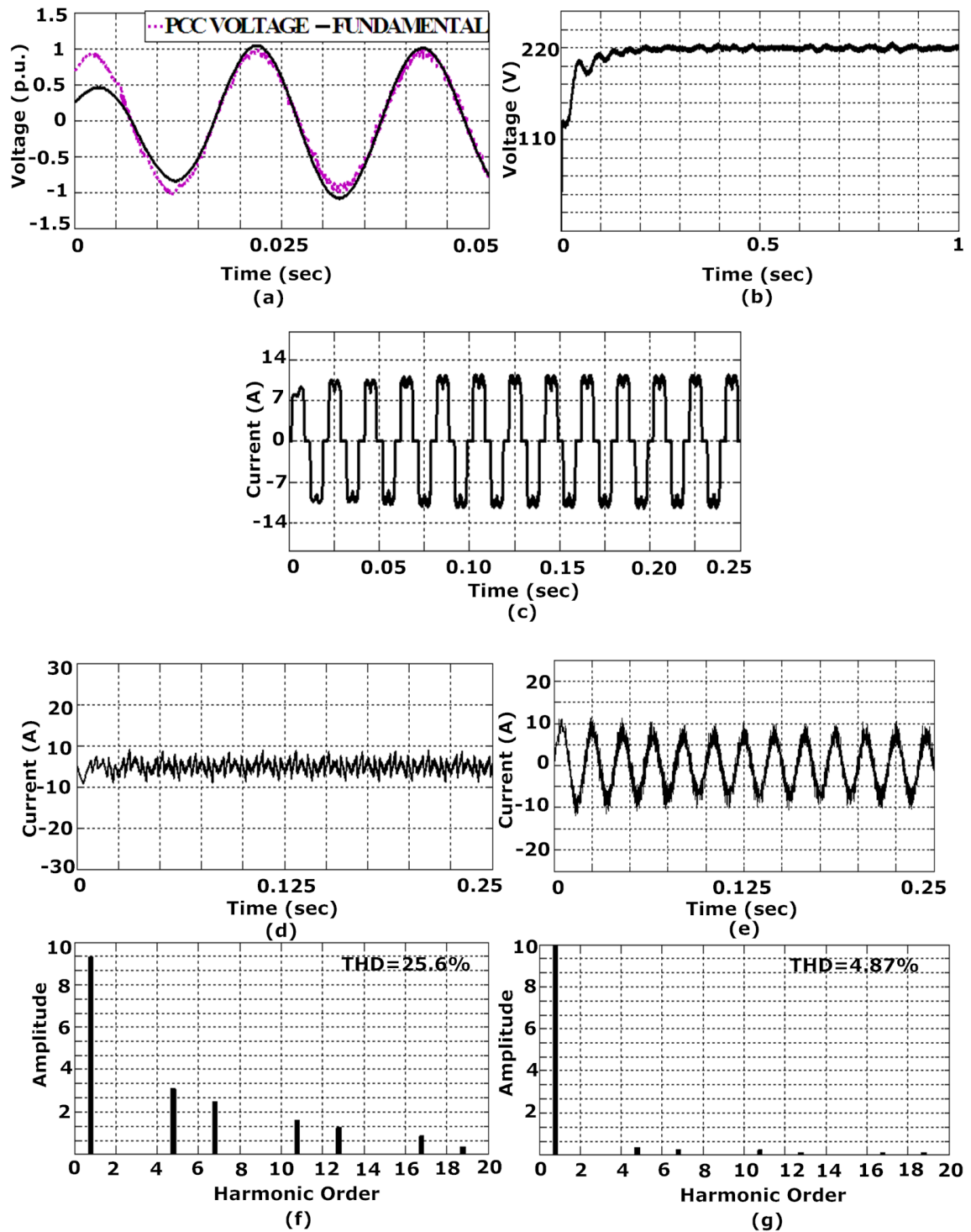
Figure 2.4: Response of KF-HCC based SAPF using MATLAB, (a) PCC voltage with its in phase fundamental, (b) Capacitor voltage, (c) Load current, (d) Compensating current, (e) Source current, (f) THD of load current, (g) THD of source current

communication tasks necessary to make parallel simulation of electrical systems with standard PCs and communication links. The Opal-RT allows developers to prove their

ideas, prototypes and final products in a realistic environment. It is an ideal tool for the design, development and testing of power system protection and control schemes.

The model of the SAPF system whose real-time response is required first constructed in MATLAB/SIMULINK. The model built in SIMULINK comprises of two subsystems such as master subsystem and console subsystem. In the master subsystem, the model to be simulated is kept whilst the console subsystem consists of scopes with outputs terminals for all the signals that are to be observed. The set up for real-time simulation using Opal-RT Lab is shown in Fig. 2.5(a). The results are observed in a digital storage oscilloscope (DSO), which is connected to RT-Lab simulator via connecting probes. The OP5142 displayed in Fig. 2.5(b) is one of the key building blocks in the modulator OP5000 I/O system from Opal-RT Technologies. The incorporation of field programmable gate array (FPGA) technologies in RT-Lab simulation clusters are allowed for distributed execution of hardware description language functions and high-speed digital I/O in real-time models. S1 is connected to master reset signal of OP5142 board and pressing this button sends a reset signal to all OP5142 subsystems. JTAG1 gives access to OP5142 JTAG (Joint test action group) chain and its use is to configure the flash memory with its default configuration file. Depending upon the presence of ''JUMP4'' jumper, this interface may give access to both FPGA and CPLD (Complex programmable logic device) configurations. If the ''JUMP4'' jumpers are set to independent mode, JTAG2 gives access to CPLD JTAG configuration interface. JTAG3 gives access to the PCIe (Peripheral component interconnect express) Bridge JTAG interface. JTAG4 gives access to the Texas Instrument Serializer–Deserializer (Ser-Des) JTAG interface. JP1 implements all data and power transfers needed with external world. J1, J2 and J3 exchange all I/O related data to I/O module, including identification data, serial communication with I^2C (Inter-integrated circuit) devices and user I/O dataflow. JUMP1 enables the write protection of the EEPROM (Electrically erasable programmable read-only memory) located on OP5142. JUMP2 enables the developer to select the way OP5142 FPGA should be configured that is (a) JTAG configuration, or (b) Slave parallel configuration (from the Flash memory). JUMP3 is to enable the developer to write some reserved sectors of the configuration flash memory.

Figure 2.5: Opal-RT Platform, (a) Set-up for Opal-RT Lab, (b) OP5142 layout and connectors

Fig. 2.6 (a), (b), (c), (d) and (e) show the real-time Opal-RT results such as capacitor voltage, load current, compensating current, source current and compensation effect of the proposed KF-HCC based SAPF system respectively. From the above results, THD of the source current is realized to be 4.91% after compensation with SAPF, whereas it is 26.4% before compensation. These Opal-RT results are quite matched with the simulation results obtained.
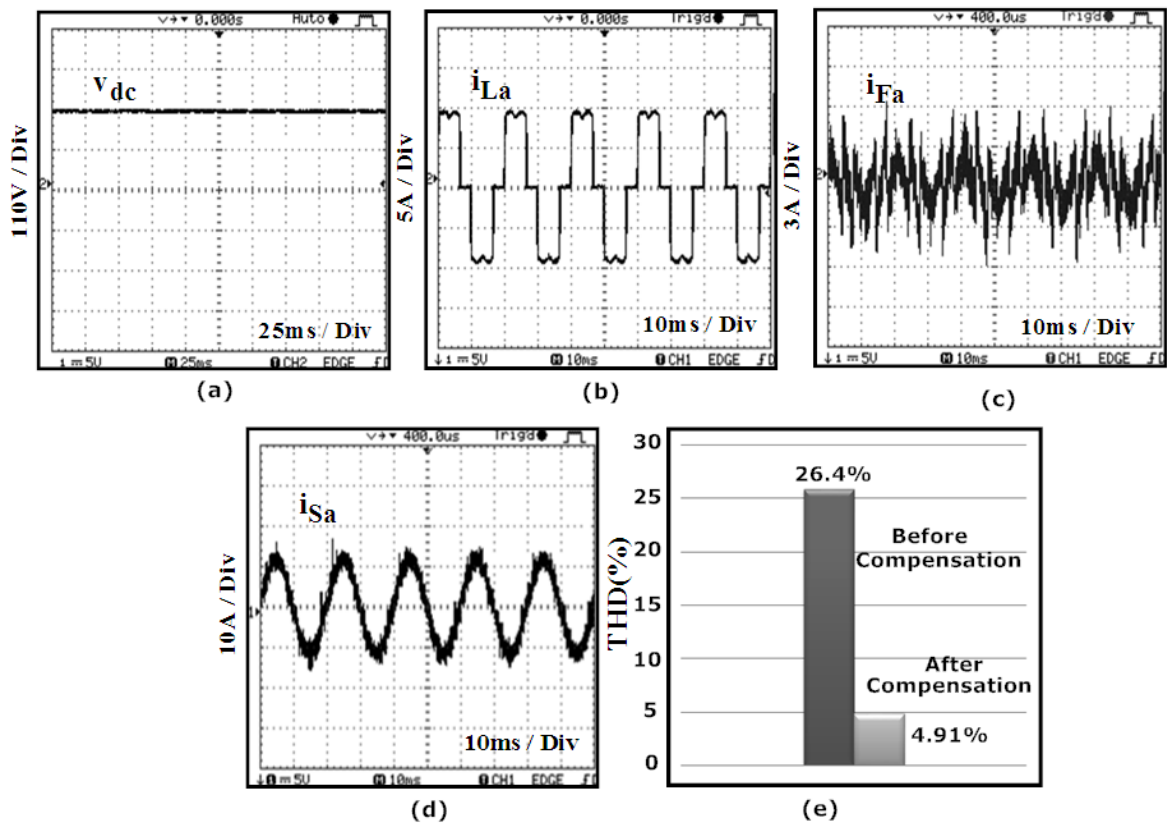
Figure 2.6: Response of KF-HCC based SAPF using Opal-RT, (a) Capacitor voltage, (b) Load current, (c) Compensating current, (d) Source current, (e) THD before and after compensation

2.3.5.3 Remarks on the Proposed KF-HCC based SAPF Method

Advantages:

- The main advantage of HCC method is the simplicity in calculus.
- KF acts as an important role in generation of reference signal, where it perfectly estimates the in phase fundamental component of PCC voltage with all grid perturbations taken into account.

Disadvantages:

Reference current generation is not so effective due to slower convergence rate of KF. Therefore, KF-HCC based SAPF method is not able to mitigate harmonics perfectly. The THD value for the source current is found to be 4.87% as verified by the simulation results (Fig. 2.3), which value is quite closer to the boundary of IEEE-519 standard.

From the above discussions, it is clear that a quick estimation method for the in phase fundamental component of PCC voltage is required to generate reference current, in which the rate of convergence should be very fast. As a result, mitigation of harmonics can be achieved at a faster rate. Among several estimation techniques [50][51][52][53][54][55], extended versions of KF such as EKF, ECKF have gained much attention, as they accurately estimate the amplitude, phase and frequency of a signal buried with noise and harmonics. EKF suffers from poor convergence because of higher order terms in solving Taylor's expansion. Even if the higher order terms in Taylor's expansion are reduced, the performance of ECKF fails in a highly distorted signal. Hence in view of addressing these above issues (harmonics, voltage distortion, noise, convergence rate), a new estimation algorithm "RECKF" has been proposed, in which a weighted exponential function $e^{-(y-h(x))^2}$ is incorporated considering all the above grid perturbations to estimate the reference current in SAPF. With arising abnormal condition, the value of "$y-h(x)$" increases faster because of inclusion of a 'square' term in the proposed function, as a result the influences of abnormality can be decreased at a faster rate as compared with the exponential function mentioned earlier in [54].

Once the current references have been determined after estimating the fundamental component described above, the SAPF must be able to track accurately such references even in sudden slope variations of the reference. Several current controller techniques [75][76][77][78][79][80] have been reported for tracking current references in the SAPF. Sliding mode control (SMC) is one of the most popular research fields of control strategies in power electronic circuit [81][82][83][84]. Devaraj [77] proposed a sliding surface that is a linear combination of the system state variables and the generated references in APF. This design results in the absence of integral terms in the controller, which makes the system sensitive to parameter variations and possibly affected by steady-state errors. Weibe and Duran [85] presented an efficient sliding-mode control law in APF without a proportional part using the d-q reference frame theory and once transformed to the abc reference frame, the integral sliding-mode (ISM) is used to get a practical control action. As a result, with time varying nature of the APF, SMC seems to be the most appropriate one because it is controlled by a variable structure approach. It has high degree of flexibility in its design choices and is relatively easy to implement as compared to other nonlinear control methods [86]. Hence, in this work an attempt has been made to exploit RECKF-SMC based control strategy in SAPF to improve THD of

the source current and the development of this proposed strategy is discussed in the following section.

2.4 Proposed RECKF-SMC based SAPF

Based on the discussions in the above section, the estimation accuracy of the proposed RECKF is more effective and hence can be employed for generation of reference current in SAPF. Further, sliding mode controller (SMC) technique is characterized by guaranteed stability, fast dynamic response and strong robustness against parameter uncertainties. Such properties make SMC suitable for applications in SAPF system, accounting for their wide utilization in industrial applications, e.g. electrical drivers, automotive control, furnace control, etc.

2.4.1 Description of Proposed RECKF-SMC based SAPF System

The control structure for proposed RECKF-SMC based SAPF system is developed by replacing HCC by SMC technique for generation of gate drive signals for IGBT inverter and KF by proposed RECKF for estimating in phase fundamental component of PCC voltage in Fig. 2.1, whereas the objective of this SAPF system is same as described for KF-HCC in Section 2.2.1. Hence a reduced block diagram for proposed RECKF-SMC based SAPF system is depicted in Fig. 2.7.
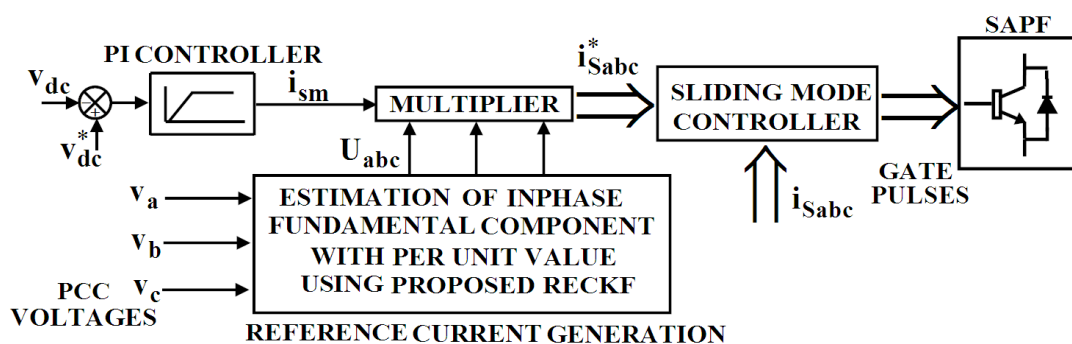
Figure 2.7: Proposed RECKF-SMC based SAPF

2.4.2 Proposed Reference Current Generation

The expression for reference signal is same as derived for KF-HCC in eq (2.1). In order to verify the estimation accuracy of the proposed RECKF based reference current generation, a comparative evaluation has to be performed using four variants of Kalman filtering algorithms (KF, EKF, ECKF and Proposed RECKF).Therefore the formulations for the above four Kalman algorithms are presented below. However, formulation for KF algorithm has already been described in Section 2.2.2.1.

2.4.2.1 Signal Model and Formulation of EKF Algorithm

As per simplicity in formulation, the signal in eq (2.2a) can be replaced by

$$z_k = a_1 \cos(k\omega_1 T_s + \phi_1) \tag{2.21}$$

It is noted that the three consecutive samples of this single sinusoid will satisfy the following relationship

$$z_k - 2\cos\omega_1 T_s z_{k-1} + z_{k-2} = 0 \tag{2.22}$$

The state space vector is given by

$$x_k = \begin{bmatrix} 2\cos\omega_1 T_s & z_{k-1} & z_{k-2} \end{bmatrix}^T \tag{2.23}$$

$$x_{k+1} = \begin{bmatrix} 1 & 0 & 0 \\ 0 & 2\cos\omega_1 T_s & -1 \\ 0 & 1 & 0 \end{bmatrix} x_k \tag{2.24}$$

The measurement equation can be expressed as

$$y_k = [0 \quad 2\cos\omega_1 T_s \quad -1]x_k + v_k \tag{2.25}$$

The nonlinear state space equations can be represented as

$$x_{k+1} = f(x_k) \tag{2.26}$$

$$y_k = g(x_k) + v_k \tag{2.27}$$

where

$$f(x_k) = [2\cos\omega_1 T_s \quad 2\cos\omega_1 T_s.x_{k-1} - x_{k-2} \quad x_{k-1}]^T \tag{2.28}$$

$$g(x_k) = 2\cos\omega_1 T_s.x_{k-1} - x_{k-2} \tag{2.29}$$

Linearizing the above system and applying EKF theory to first order system, a nonlinear recursive filter for estimating a single sinusoid is given as follows:

$$\hat{x}_{k|k} = \hat{x}_{k|k-1} + K_k (y_k - g(\hat{x}_{k|k-1})) \tag{2.30}$$

$$\hat{x}_{k+1|k} = f(\hat{x}_{k|k}) \tag{2.31}$$

$$K_k = P_{k|k-1} H_k^T \cdot \left[H_k P_{k|k-1} H_k^T + R_k \right]^{-1} \tag{2.32}$$

$$P_{k|k} = P_{k|k-1} - K_k H_k P_{k|k-1} \tag{2.33}$$

$$P_{k|k+1} = F_k P_{k|k} F_k^T \tag{2.34}$$

where

$$F_k = \frac{\partial f(\hat{x}_k)}{\partial \hat{x}_k} = \begin{bmatrix} 1 & 0 & 0 \\ \hat{x}_{2_k} & \hat{x}_{1_k} & -1 \\ 0 & 1 & 0 \end{bmatrix} \text{ and } H_k = \frac{\partial g(\hat{x}_k)}{\partial \hat{x}_k} = \begin{bmatrix} \hat{x}_{2_k} & \hat{x}_{1_k} & -1 \end{bmatrix}$$

To find in phase fundamental component $a_1 \sin(k\omega_1 T_s + \phi_1)$ as per eq (2.5a), we have to make 90 degree phase shift of the estimated signal $\hat{z}_k$. Then per unit representation of in phase fundamental component is same as prescribed in KF algorithm.

2.4.2.2 Signal Model and Formulation of ECKF Algorithm

The signal in eq (2.2a) can be represented in complex form as

$$z_k = (-0.5i) \left(a_1 e^{j(k\omega_1 T_s + \phi_1)} \right) + (0.5i) \left(a_1 e^{-j(k\omega_1 T_s + \phi_1)} \right) \tag{2.35}$$

The complex type state variable x_k can be given as

$$x_{1_k} = e^{i\omega_1 T_s} \tag{2.36}$$

$$x_{2_k} = a_1 e^{j(k\omega_1 T_s + \phi_1)} \tag{2.37}$$

$$x_{3_k} = a_1 e^{-j(k\omega_1 T_s + \phi_1)} \tag{2.38}$$

The nonlinear state space equations can be represented as

$$x_k = f(x_{k-1}) \tag{2.39}$$

$$y_k = g(x_k) + v_k \tag{2.40}$$

where

$$f(x_{k-1}) = \begin{bmatrix} x_{1_{(k-1)}} & x_{1_{(k-1)}} x_{2_{(k-1)}} & \dfrac{x_{3_{(k-1)}}}{x_{1_{(k-1)}}} \end{bmatrix}^T \tag{2.41}$$

The recursion process of the ECKF for estimating the signal parameters of sinusoid waves is given below.

$$\tilde{x}_k = f(\hat{x}_{k-1}) \tag{2.42}$$

$$M_k = F_k P_{k-1} F_k^T + Q_k \tag{2.43}$$

$$\hat{x}_k = \tilde{x}_k + K_k (y_k - H_k \tilde{x}_k) \tag{2.44}$$

$$K_k = M_k H_k^T \left[H_k M_k H_k^T + R_k \right]^{-1} \tag{2.45}$$

$$P_k = M_k (I - K_k H_k) \tag{2.46}$$

where the symbols $\sim$ and $\wedge$ stand for the predicted and estimated values respectively, M_k and P_k represent the predicted and estimated error covariance respectively. The values of F_k and H_k are given here.

$$F_k = \frac{\partial f(\hat{x}_{k-1})}{\partial \hat{x}_{k-1}} = \begin{bmatrix} 1 & 0 & 0 \\ \hat{x}_{2_{(k-1)}} & \hat{x}_{1_{(k-1)}} & 0 \\ -\hat{x}_{3_{(k-1)}} \Big/ \hat{x}_{1_{(k-1)}}^2 & 0 & 1 \Big/ \hat{x}_{1_{(k-1)}} \end{bmatrix} \tag{2.47}$$

$$H_k = \frac{\partial(g(x_k))}{\partial x_k} = \begin{bmatrix} 0 & -0.5i & 0.5i \end{bmatrix} \tag{2.48}$$

The parameters of frequency $\hat{f}_k$, amplitude $\hat{a}_k$ and phase angle $\hat{\phi}_k$ can be expressed as

$$\hat{f}_{1_k} = \frac{1}{2\pi T_s} \left[\text{Im } (\ln(\hat{x}_{1_k})) \right] \tag{2.49}$$

$$\hat{a}_{1_k} = \left| \hat{x}_{2_k} \right| \tag{2.50}$$

$$\hat{\phi}_{1_k} = \text{Im} \left[\ln \left(\frac{\hat{x}_{2_k}}{\left| \hat{x}_{2_k} \right| \times (\hat{x}_{1_k})^k} \right) \right] \tag{2.51}$$

Using the above parameters $\hat{f}_{1_k}$, $\hat{a}_{1_k}$ and $\hat{\phi}_{1_k}$, the in phase fundamental component can be identified and its per unit value can be expressed as

$$\sin\left(2\pi\hat{f}_{1_k} T_s + \hat{\phi}_{1_k}\right) = \frac{\hat{a}_{1_k} \sin\left(2\pi\hat{f}_{1_k} T_s + \hat{\phi}_{1_k}\right)}{\hat{a}_{1_k}} \tag{2.52}$$

2.4.2.3 Signal Model and Formulation of Proposed RECKF Algorithm

The signal model and filter formulations in proposed RECKF are same as in ECKF. The only difference is in the measurement error covariance " R_k ", which is the inverse of the weighting W_k , i.e.

$$R_k = W_k^{-1} \tag{2.53}$$

$$W_k = W_{k-1} e^{-(y_k - H_k \tilde{x}_k)^2} \tag{2.54}$$

where the exponential term $e^{-(y_k - H_k \tilde{x}_k)^2}$ is the proposed robust exponential function and the variable R_k is replaced in eq (2.41).When any grid disturbances occur at the PCC, the innovation vector $(y_k - H_k \tilde{x}_k)$ increases faster due to the inclusion of a 'square term' in the proposed exponential function. Consequently, the value of proposed robust exponential function decreases faster and finally a fast reduction of weighting and mitigation of error can be achieved.

2.4.3 Sliding Mode Control (SMC)

A single phase circuit of voltage source inverter is considered here in the design of an active power filter. Fig. 2.8 presents the equivalent circuit for a single phase voltage source inverter used for development of SMC law. If a switching function u is defined such that $u = 1$ when either S_1 or D_1 is conducting and $u = -1$ when either S_2 or D_2 is conducting, then the inductor current is given by

$$\frac{di_{F_x}}{dt} = \frac{v_{sxn}}{L_F} + u\frac{v_{dc}}{2L_F} \tag{2.55}$$

where x denotes the phase, v_{sxn} represents the phase to neutral voltage.
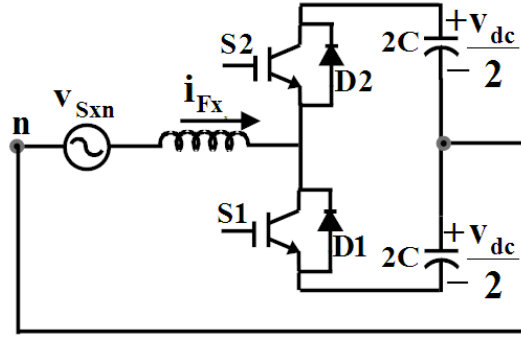
Figure 2.8: Equivalent circuit for a single-phase of voltage source inverter

An expression for capacitor voltage taking into account the ripple due to the compensating currents can be written as

$$\frac{dv_{dc}}{dx} = -\frac{1}{2}\left[u_a \frac{i_{Fa}}{C} + u_b \frac{i_{Fb}}{C} + u_c \frac{i_{Fc}}{C} \right] \qquad (2.56)$$

where u_a, u_b and u_c are the independent controls for phases a, b and c respectively. The SAPF circuit can be decomposed into three first order independent systems which can be expressed as

$$i_{source_x} = i_{load_x} + i_{comp_x} \qquad (2.57)$$

To apply SMC theory for designing SAPF, the sliding surfaces must be defined such that the source current i_{source_x} should follow the reference current i_{ref_x}. The sliding surfaces for source currents can be defined as

$$i_{ref_x} = i_{sm} * U_x \qquad (2.58)$$

where U is the in phase fundamental component with per unit magnitude at PCC. The sliding surface in a standard form can be written as

$$S_{sliding_x} = i_{source_x} - i_{ref_x} = 0 \qquad (2.59)$$

To ensure that the SAPF can be maintained on the sliding surface, it must be shown that there is a natural control which satisfies $S_{sliding}\dot{S}_{sliding} \leq 0$. For the SAPF, expression for $\dot{S}_{sliding}$ can be written as

$$\dot{S}_{sliding_x} = \dot{i}_{load_x} + \frac{v_{sxn}}{L_{Fx}} + (u_x)\left(\frac{v_{dc}}{2L_{Fx}}\right) - i_{sm} * \dot{U}_x \qquad (2.60)$$

The equivalent control u_{eq_x} can be found out by equating eq (2.60) to zero and the natural control limits of the circuit are $-1 \leq u_{eq_x} \leq 1$. The discontinuous control law can be written as follows.

If $S_{sliding} < 0$ then $u = 1$

If $S_{sliding} > 0$ then $u = -1$ \hfill (2.61)

For generating switching pulses, this control law can be applied to the SAPF.

2.4.4 Results and Discussions

Four control strategies namely KF-SMC, EKF-SMC, ECKF-SMC, and RECKF-SMC based SAPF were implemented and analyzed using the following simulation and Opal RT results.

2.4.4.1 Simulation Results

Fig. 2.9 depicts the simulation results for SAPF using KF-SMC, EKF-SMC, ECKF-SMC, and RECKF-SMC based control structure. The PCC voltage at phase a and its in phase fundamental component estimated with the help of above four Kalman algorithms is displayed in Fig. 2.9(a). It can be seen from Fig. 2.9(a) that in phase fundamental estimated by KF takes 0.005 sec to follow PCC voltage. But in case of EKF, the fundamental is initially not in phase with PCC, and it suffers a delay of 0.05 sec. However, the fundamental components are exactly matched with the PCC voltage in case of both ECKF and RECKF. The capacitor voltage waveforms presented in Fig. 2.9(b) are compared on the basis of above four filter algorithms. Generally, the harmonic compensating performance will be spoiled when large fluctuations of the voltage occur across the DC capacitor. As can be seen in Fig. 2.9(b), the fluctuation is more in the EKF-SMC as compared to the other three. Further comparison among the KF-SMC, ECKF-SMC and RECKF-SMC shows that the RECKF-SMC based SAPF system enables suppression of the voltage fluctuations across DC capacitor and is quickly set at around 220V indicating good harmonic compensating performance.

The compensating currents are compared in Fig. 2.9(c). It can be observed that the KF-SMC, ECKF-SMC and RECKF-SMC provide almost equal compensation with a fast response, while EKF-SMC exhibits a slow response. Fig. 2.9(d) gives the details of
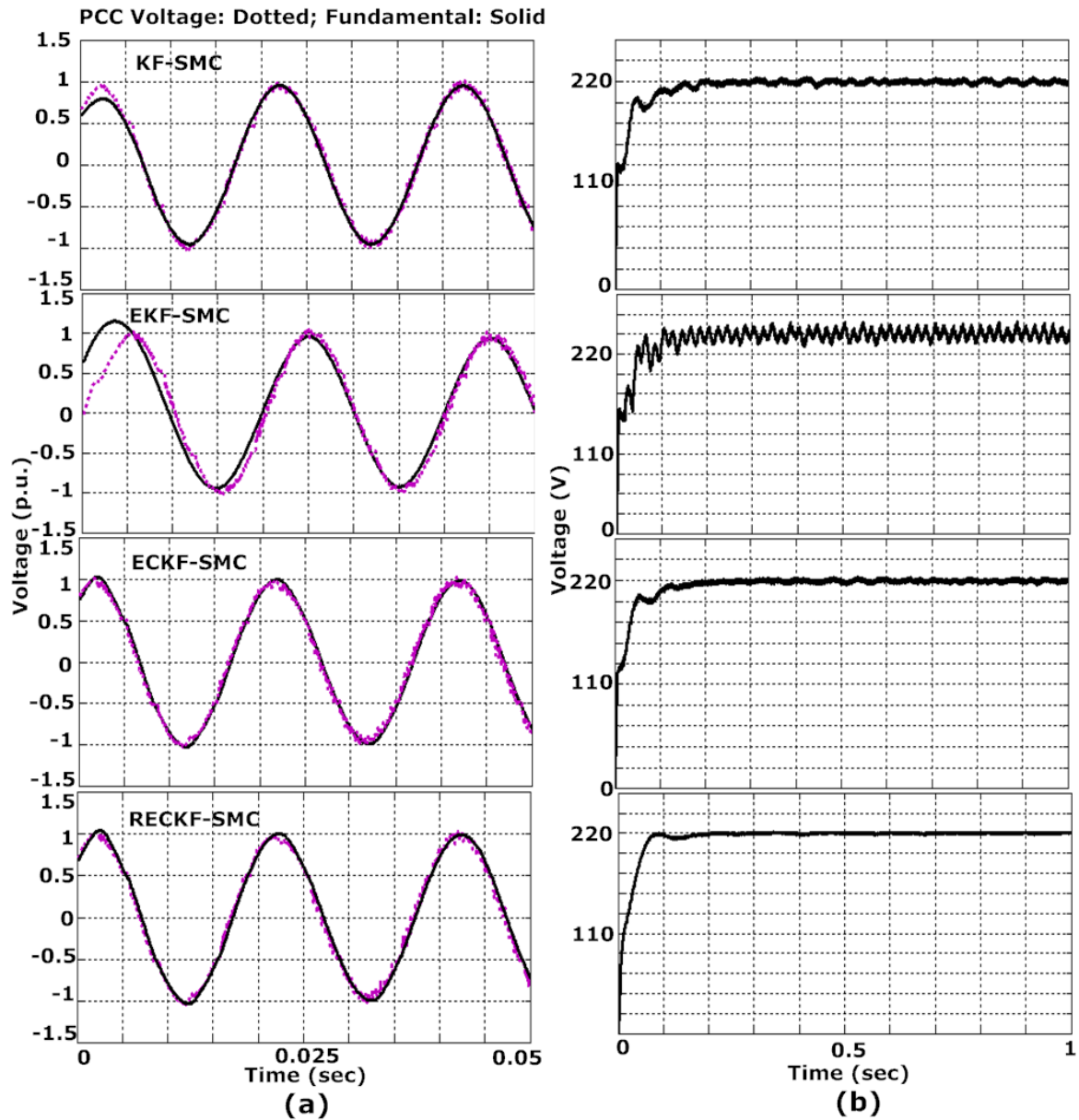
Figure 2.9: Response of SAPF using KF-SMC, EKF-SMC, ECKF-SMC and RECKF-SMC based control structure in MATLAB, (a) PCC voltage with its in phase fundamental, (b) Capacitor voltage, (c) Compensating current, (d) Source current, (e) THD of source current
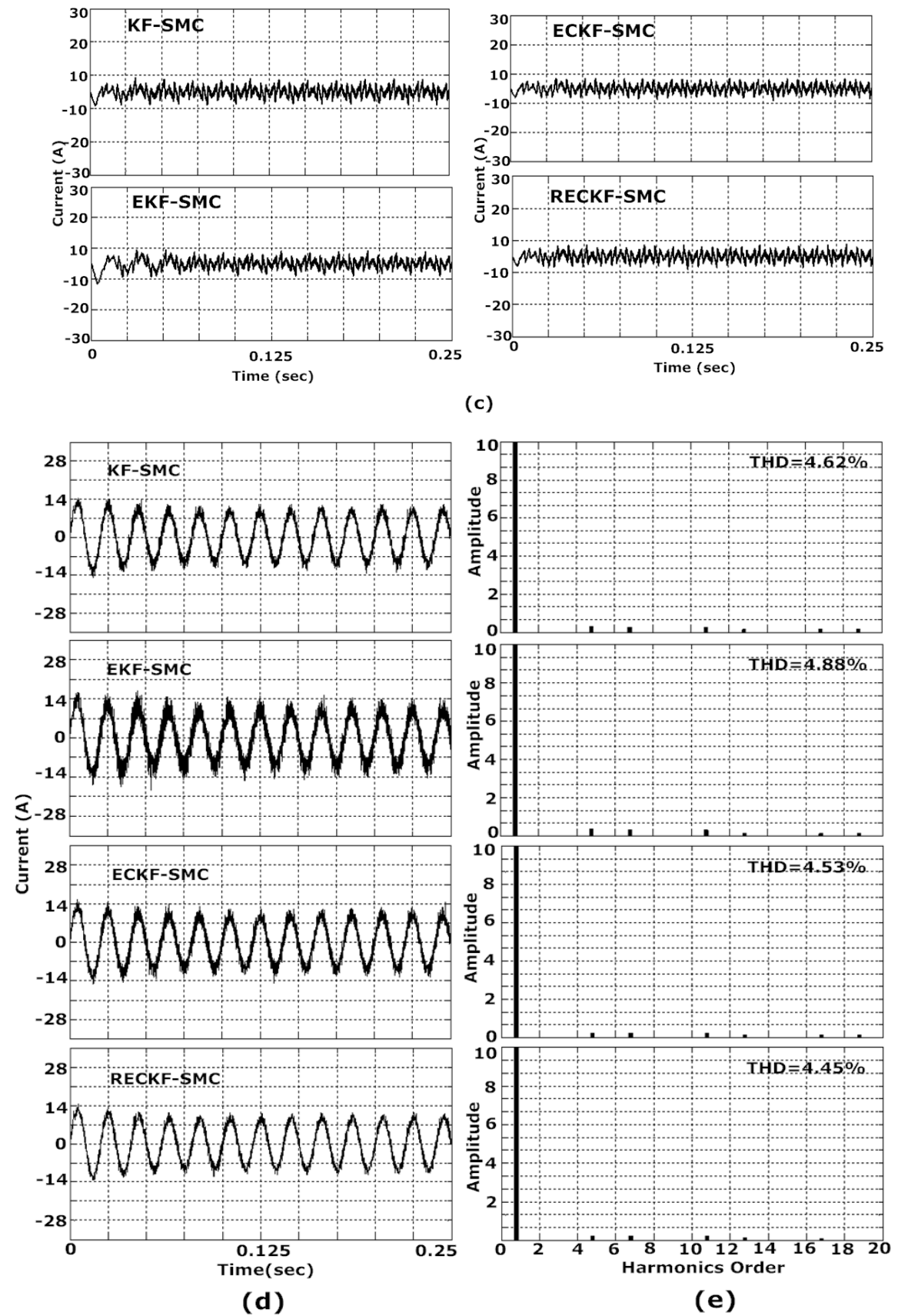
Figure 2.9: Response of SAPF using KF-SMC, EKF-SMC, ECKF-SMC and RECKF-SMC based control structure in MATLAB (Continued)

source current after compensation for above Kalman algorithms. They are observed to be sinusoidal, but they are compared on the basis of their amplitudes of different harmonic contents expressed in THD plot (Fig. 2.9(e)). It is noticed that the THD of the source current comparatively reduces to 4.62, 4.88, 4.53 and 4.45% after compensation with the KF-SMC, EKF-SMC, ECKF-SMC and RECKF-SMC based SAPF system respectively. A comparative reduction in amplitudes of harmonic contents envisages the superiority of the RECKF-SMC in harmonic compensation of the SAPF.

2.4.4.2 Real-time Simulation Results

This section presents the real-time results obtained from the implementation of the proposed SAPF algorithm on Opal-RT. Fig. 2.10(a), (b), (c) and (d) give the details of compensating current, DC link voltage, source current and compensation effect respectively, in the SMC-based SAPF system using the four variants of KF algorithms and they compare well with the detailed simulation results presented in Fig. 2.9. Referring Fig. 2.10(d), it is observed that THDs of the source current are 4.70, 4.96, 4.67 and 4.54% for the KF-SMC, EKF-SMC, ECKF-SMC and RECKF-SMC based SAPF system respectively. Hence a better performance of RECKF-SMC based SAPF can be realized through Opal-RT results.

2.4.4.3 Remarks on the Proposed RECKF-SMC based SAPF Method

- Reference current generation is effective due to faster convergence rate of proposed RECKF as compared to other three Kalman algorithms (KF, EKF and ECKF). Therefore, the proposed RECKF-SMC approach to design a SAPF responds faster to the grid perturbations arising at the PCC.

- RECKF-SMC based SAPF method is able to mitigate harmonics, where the THD value for the source current is found to be 4.45%, below the boundary of IEEE-519 standard.
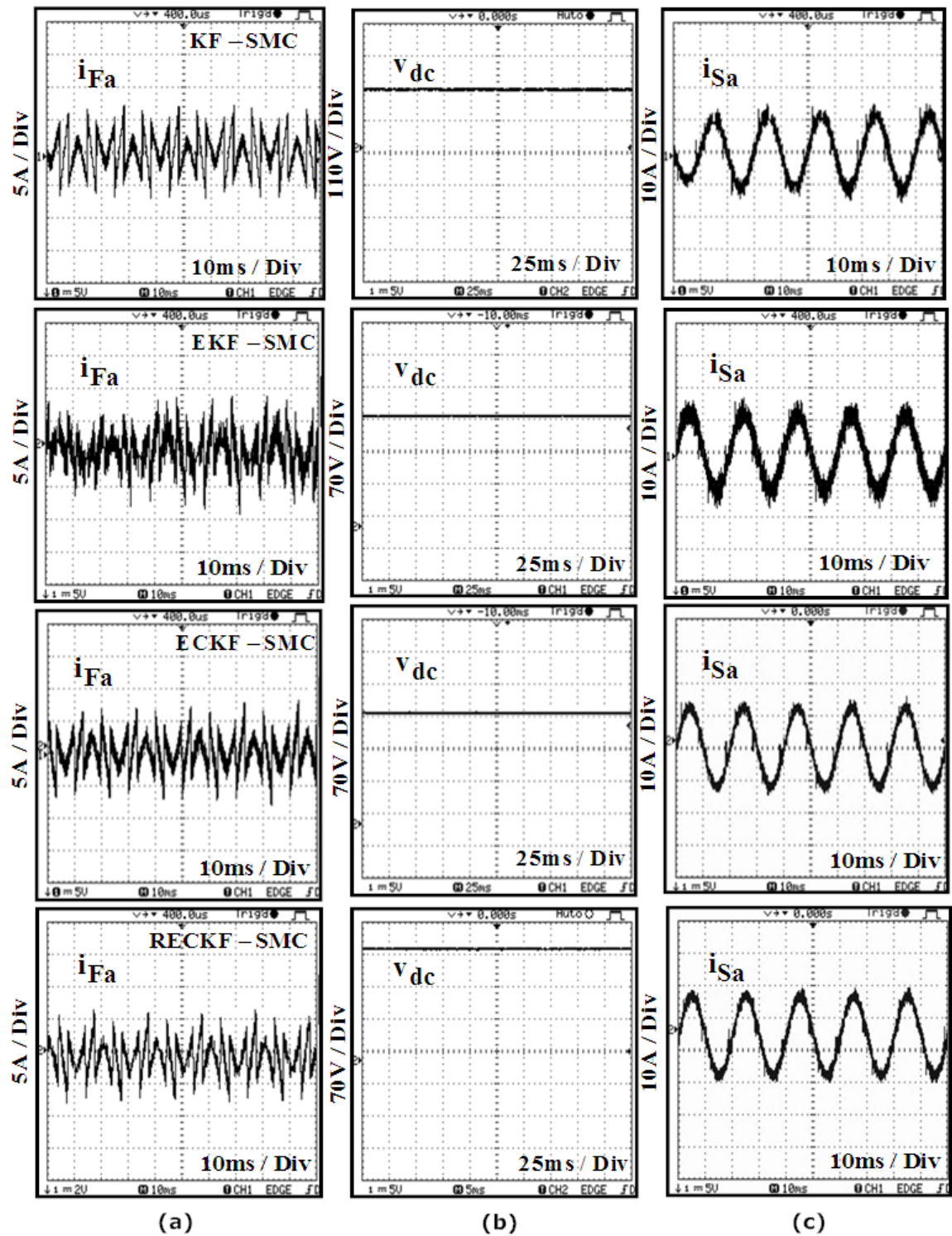
Figure 2.10: Response of SAPF using KF-SMC, EKF-SMC, ECKF-SMC and RECKF-SMC based control structure in Opal-RT, (a) Compensating current, (b) Capacitor voltage, (c) Source current, (d) THD before and after compensation
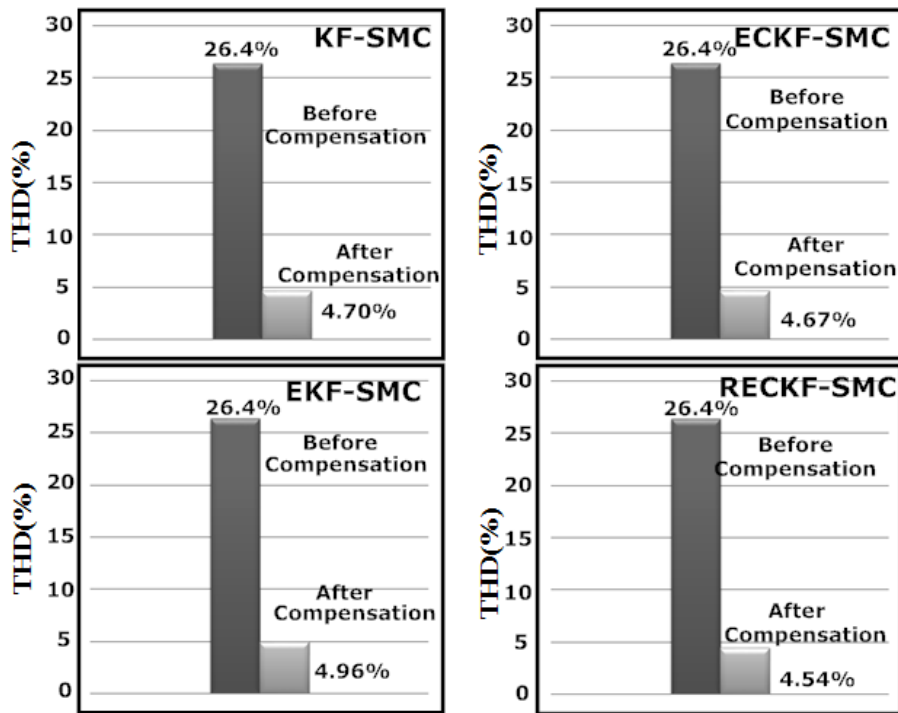
(d)

Figure 2.10: Response of SAPF using KF-SMC, EKF-SMC, ECKF-SMC and RECKF-SMC based control structure in Opal-RT (Continued)

Table 2.2 THD Factors of Control Structures of SAPF

(KF-HCC, KF-SMC, EKF-SMC, RECKF-SMC)

Control Structure of SAPF	THD% of Source Current After Compensation	
	Simulation Results	Real-Time Simulation Results
KF-HCC	4.87	4.91
KF-SMC	4.62	4.70
EKF-SMC	4.88	4.96
ECKF-SMC	4.53	4.67
RECKF-SMC	4.45	4.54

Table 2.2 shows the THD factors of different control structures of SAPF employing both simulation and real-time simulation results and the outperformance of RECKF-SMC (4.54%) over KF-HCC (4.91%), KF-SMC (4.70%), EKF-SMC (4.96%) and ECKF-SMC (4.67%) has been verified.

2.5   Chapter Summary

HCC and SMC based SAPF implemented with a new reference current generation scheme are proposed. This scheme exploits the estimation of the in phase fundamental components of distorted PCC voltages using the KF, EKF, ECKF and proposed RECKF algorithms. KF-HCC based SAPF is found to be very simple in realization and can be able to perform under consideration of grid perturbations. But the slower convergence rate of KF leads towards an ineffective reference generation. Hence, harmonic mitigation is not so fast and perfect. Also the THD obtained from simulation as well as Opal-RT results, is just touching the boundary line of IEEE-519 standard. Therefore, a SMC based SAPF is implemented with a faster reference scheme based on proposed RECKF and the efficacy of this proposed RECKF-SMC is compared with other variants of KF. As observed from both simulation and real-time simulation results, KF-SMC performs better as compared to KF-HCC and the proposed RECKF-SMC approach to design a SAPF is found to be quite effective and reacts faster to grid disturbances at PCC as compared to other control structures such as KF-SMC, EKF-SMC and ECKF-SMC.

CHAPTER 3

Robust Extended Complex Kalman Filter and Model Predictive based SAPF

3.1 Introduction

Chapter 2 discusses the harmonics compensation performance of HCC and SMC based SAPF together with reference generation scheme through different variants of KF algorithms such as KF, EKF, ECKF and RECKF. The harmonics compensation performances of these control strategies are very poor as THD obtained (i.e., 4.91%, 4.70%, 4.96%, 4.67% and 4.54%) are very close to 5%. In order to obtain accurate current harmonics compensation, predictive current control techniques with improved reference generation scheme are proposed in this chapter. The motivation for developing these predictive controllers has emerged because of obvious advantages of digital control techniques [87][88][89][90][91][92][93][94][95] over the analog ones. The proposed predictive current controller comprises of a deadbeat controller (DBC) and model predictive controller (MPC) in designing a SAPF. Since implementation of a predictive current control requires a fast and accurate reference current estimator, the proposed RECKF algorithm is more effective owing to its fastest convergence rate as observed in Chapter 2 and hence it can be employed for the reference generation scheme.

In order to regulate dc bus voltage, a PI controller is needed in the external loop using conventional unit vector approach [29]. Fryze theory [96] necessitates a measurement of both load current and source voltage for reference generation without PI controller loop. However, more computations are involved in this approach for calculating reference source current. In the operation of the SAPF system, the ac mains supplies real power needed to the load and meets some losses e.g. switching losses of devices, losses in the reactor and dielectric losses of dc capacitor. Therefore, the proposed reference source currents that are used to decide the switching of the SAPF have two parts: one is the real fundamental-frequency component of the load current, which is estimated using the proposed RECKF and another component, which corresponds to the losses in the SAPF, is also estimated using the proposed RECKF. The advantage of this method is the simpler computations and avoiding tuning and thus less number of voltage

sensors are necessary to obtain the reference current. This proposed approach is chosen to eliminate large overshoots and undershoots associated with conventional PI control, causing unstable operation of the inverter in protecting the switching devices. Furthermore, recent applications need faster response, minimum power dissipation and robustness, which are not achieved by using the PI controller. It is expected that by using the proposed reference generation the above demerits of PI control can be resolved and the dc-link capacitor voltage can be kept constant at the set point.

With the evolution of powerful, fast and inexpensive microcomputers, research is progressing faster on designing and subsequent real-time implementation of predictive controller for several systems including power electronic systems. In predictive control, a model of the system is used to predict its future behavior and the most appropriate control action based on an optimality criterion is generated. Dead Beat Control (DBC) is a popular predictive controller applied to power converters. DBC can eliminate the classic linear controller by using a predictive model of the system. This model is used to calculate the required reference voltage in order to reach the desired reference value for a certain variable (usually the current). The predicted reference voltage is later generated by the converter via a modulation stage. Malesani [88] considered a control strategy combining dead-beat control of inverter currents and space vector modulation in SAPF. A generalized discrete-time state-space representation of the controlled converter and its load is presented and this reveals the stability margins of the deadbeat algorithm in the case of a conventional load model and line voltage estimation technique, giving the possibility of predicting the occurrence of oscillations in the current loop by mapping the closed loop SAPF's eigenvalues. In [89] an improved deadbeat current control scheme with a novel adaptive self-tuning load model for a three phase PWM VSI was introduced. First, an improved deadbeat current controller with delay compensation has been developed for a fully digital platform with a relatively small control period (150 μs). The compensation method forces the delay elements, which are caused by voltage calculation, PWM and synchronous frame rotation, to be equivalently placed outside the closed-loop control system. Hence, their effect on the closed-loop stability is eliminated and the current controller can be designed with high-bandwidth characteristics. A robust deadbeat current control technique [90] is derived based on the average current tracking scheme in hybrid APF, where the grid current feedback and load current feed forward strategies are used to achieve precise current tracking and fast dynamic response.

In MPC, there is an advantage of using less number of switching states of voltage source inverter for solving optimization problem. A discrete model is used to predict the behavior of the SAPF system for every admissible actuation sequence up to the prediction horizon. The switching action that minimizes a predefined cost function is finally selected to be applied in the next sampling instant. The main advantage of MPC lies in the direct application of the control action to the inverter, without requiring a modulation stage. MPC technique has been successfully applied to wide range of power converters [91][92][93][94][95].

It is demonstrated that predictive control is a very powerful and flexible concept for designing controllers. Furthermore, application of above predictive approaches towards a SAPF system is not very popular. With abovementioned views, the two approaches namely RECKF-DBC and RECKF-MPC have been considered for improvement of the performance of SAPF and are described in the subsequent sections.

3.2 Chapter Objectives

1. To avoid external PI controller loop for dc voltage regulation.

2. To design a faster reference current scheme necessitating the implementation of predictive current control strategy.

3. To improve the current harmonics compensation effect of SAPF.

4. To simulate the proposed control techniques in MATLAB/Simulink and real-time simulation model in Opal-RT simulator.

3.3 Proposed RECKF-DBC based SAPF

3.3.1 Description of proposed RECKF-DBC based SAPF system

The SAPF (Fig. 3.1(a)) can be controlled to compensate the ac line current harmonics introduced by non-linear load. The SAPF consists of a VSI, whose dc side is connected to a capacitor bank C, whereas its ac side is connected to the mains through series impedance and the schematic of VSI power circuit is provided in Fig. 3.1(b). A predictive controller based on DBC scheme with a new reference current generation approach is presented here. The reference generation scheme exploits the estimation of in phase fundamental component of distorted PCC voltage along with the estimation of

fundamental amplitude of load current using proposed RECKF algorithm with all grid perturbations taken into account. Moreover, DBC technique uses triangular carrier based PWM generation of gate signals and a typical DBC scheme is shown in Fig. 3.2(a).
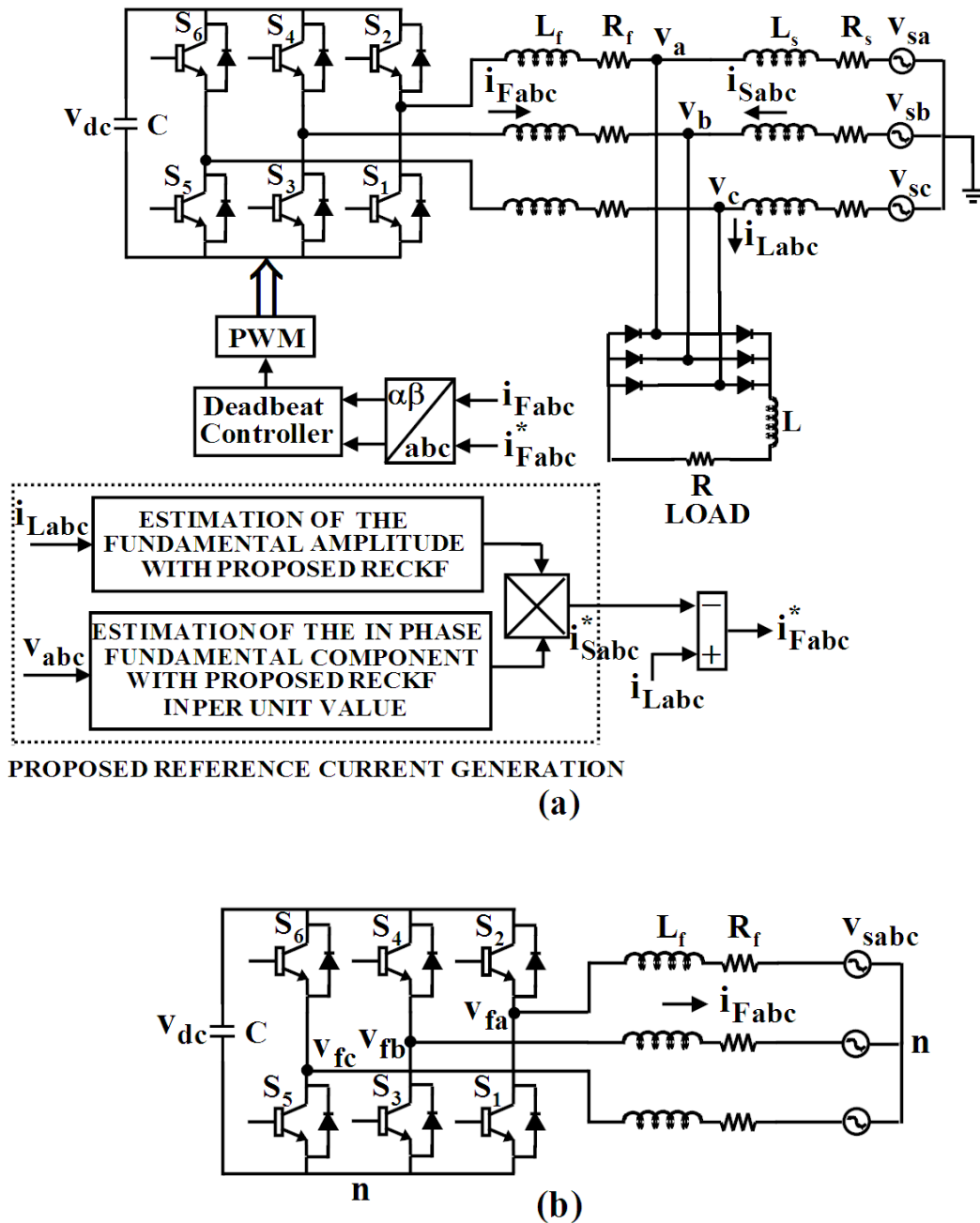
Figure 3.1: Proposed RECKF-DBC based SAPF; (a) Block Diagram of Proposed RECKF- DBC based SAPF, (b) Schematic of VSI power circuit
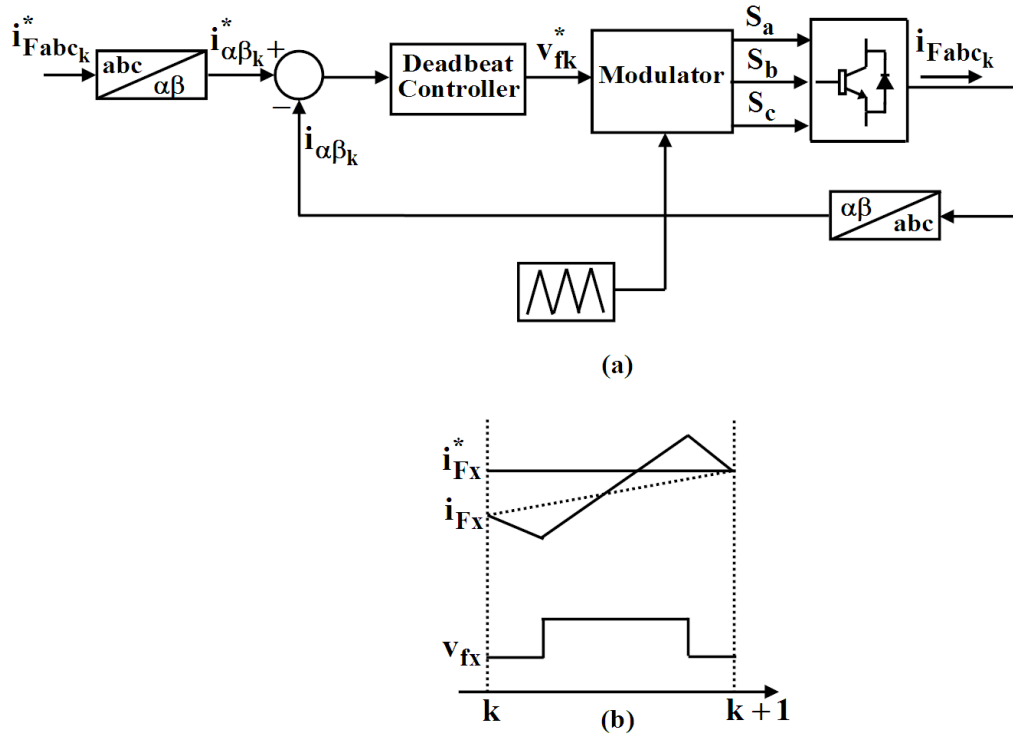
Figure 3.2: DBC Method, (a) DBC with PWM block diagram, (b) Illustration of DBC Operation

3.3.2 Proposed Reference Current Generation

The proposed reference current generation approach is simply modulation of the estimated fundamental amplitude of the load current with the estimated in phase fundamental component of PCC voltage in p.u. value. By using this reference current generation approach, there is no requirement of an external PI controller, hence it becomes cost effective. The proposed RECKF is applied for estimation of the in phase fundamental component along with its magnitude from the observed signal. The signal model and formulations for proposed RECKF were presented in Chapter 2.

3.3.3 Dead Beat Control (DBC)

The three phase inverter shown in Fig. 3.1(b) is considered here for the description of dynamic behavior of the current i_x. Applying Kirchoff's voltage law to the ac side of voltage source inverter shown in Fig. 3.1(b), one obtains

$$v_{fx} = R_f i_{Fx} + L_f \frac{di_{Fx}}{dt} + v_{sx} \tag{3.1}$$

61

where x represents the phases a, b, c and v_f is the voltage generated by inverter. The source EMF is denoted by v_s.

The following discrete time equation can be obtained from eq. (3.1) for a sampling time T_s, under the assumption that the variables are constant between sampling instants.

$$\frac{1}{\chi} i_{Fx}(k+1) - \frac{\sigma}{\chi} i_{Fx}(k) = v_{fx}(k) - v_{sx}(k) \tag{3.2}$$

where $\sigma = e^{-T_s R_f / L_f}$ and $\chi = 1 / R_f (1 - e^{-T_s R_f / L_f})$

Based on the discrete-time model (eq. (3.2)), the reference voltage vector can be obtained as follows,

$$v_{fx}^*(k) = \frac{1}{\chi}(i_{Fx}^*(k+1) - \sigma i_{Fx}(k)) + v_{sx}(k) \tag{3.3}$$

Reference voltage v_{fx}^* is applied to VSI using a modulator. The basic operating principle of DBC technique is shown in Fig. 3.2(b). Here, the current i_{Fx} at time k is different to the reference current i_{Fx}^*. This error is used for calculation of the reference voltage v_{fx}^*, which is applied at time k. Ideally, at time (k+1), the current i_{Fx} becomes equal to the reference current i_{Fx}^*.

3.3.4 Results and Discussions

3.3.4.1 Simulation Results

The performance of the proposed RECKF-DBC control strategy shown in Fig. 3.1(a) has been verified using MATLAB/SIMULINK and the simulation results are shown in Fig. 3.3. A supply voltage is 100V peak to peak as shown (Fig. 3.3(a)). The tracking performance of the proposed SAPF system is depicted in Fig. 3.3(b), where the compensating current is able to track the reference current. The behavior of capacitor voltage is presented in Fig. 3.3 (c) and the capacitor voltage takes about 0.2 sec to attain a reference point of 220V. As observed from Fig. 3.3 (d), the source current is found to be sinusoidal. Moreover, the THD of the source current after compensation is obtained to be 4.26%, as shown in Fig. 3.3(e).
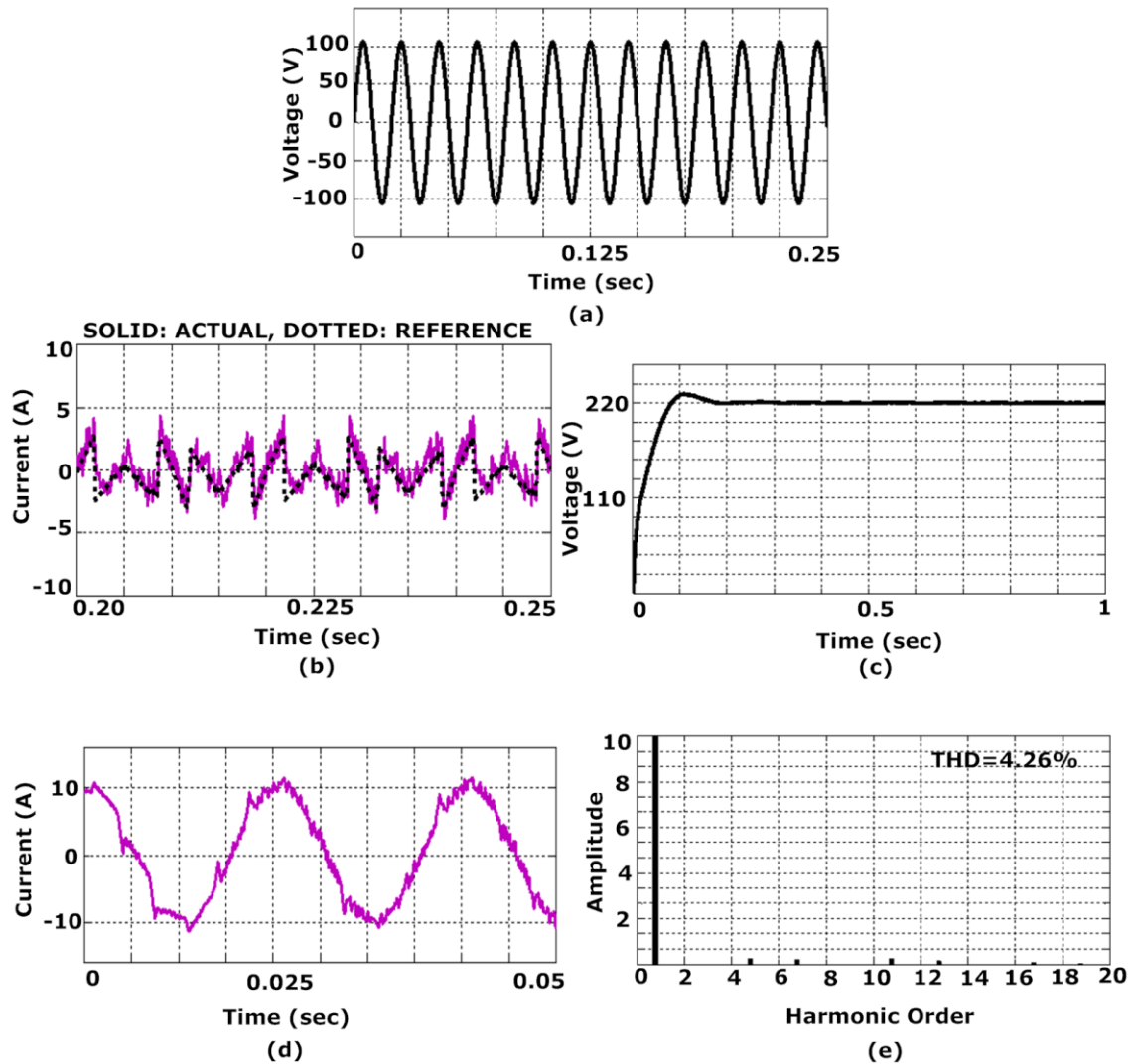
Figure 3.3: Response of RECKF-DBC based SAPF using MATLAB, (a) Source voltage, (b) Compensating and Reference Compensating current, (c) Capacitor voltage, (d) Source current, (e) THD of source current

3.3.4.2   Real-time Simulation Results

The real-time results obtained from the implementation of the proposed SAPF algorithm on Opal-RT are presented in this section. Fig.3.4 shows the real-time results displaying capacitor voltage, tracking of compensating and reference compensating currents, source voltage and source current after compensation, and the THD effects with the proposed RECKF-DBC based SAPF system respectively. It is observed from Fig. 3.4 that the response for capacitor voltage and reference tracking are the same as obtained from

MATLAB simulations (Fig. 3.3). From Fig. 3.4(c), it is observed that the source current is sinusoidal and in phase with the source voltage. Furthermore, the source current THD after compensation is achieved as 4.31% (closer to simulation result).
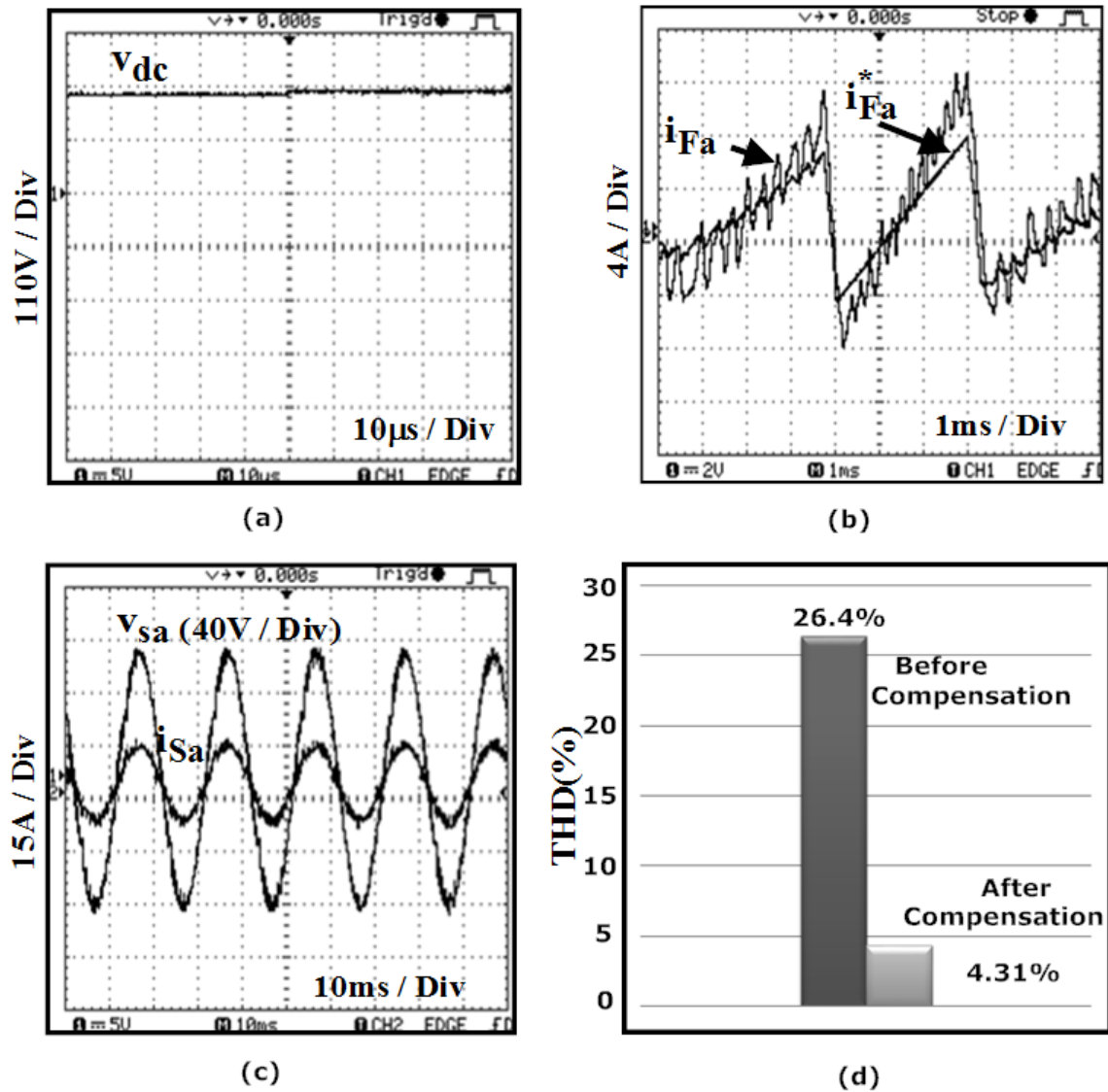
Figure 3.4: Response of RECKF-DBC based SAPF using Opal-RT, (a) Capacitor voltage, (b) Compensating and reference compensating current, (d) Source voltage and source current after compensation, (e) THD before and after compensation

3.3.4.3 Remarks on the Performance exhibited by the Proposed RECKF-DBC based SAPF

Advantages:

- Implementation using proposed RECKF-DBC scheme is very simple.
- Using DBC technique, it is possible to avoid the cascaded structure, which is typically used in the linear control scheme, ensuring a very fast transient response.
- This proposed SAPF system has full compatibility with digital control platforms.

Disadvantages:
- DBC scheme needs a modulator to provide gate drive signals to IGBT inverter.
- Irrespective of fixed switching frequency, DBC method is incapable of achieving a satisfactory performance level and distortions are present in the source current after compensation (i.e., THD%=4.26).

Nonlinearities of the system can be included in the model, avoiding the need of linearizing the model for a given operating point and improving the operation of the system for all conditions. It is also possible to include restrictions to some variables when designing the controller. These advantages can be easily implemented in an advanced predictive scheme known as MPC, but it is very difficult to implement in DBC scheme. In DBC, the optimal actuation is the one that makes the error equal to zero in the next sampling instant, whereas a more flexible criterion is used in MPC, expressed as a cost function to be minimized. Internal current control loops and modulators are not needed and the gate drive signals are generated directly by this MPC scheme.

Hence, there is a scope of improvement of the proposed RECKF-DBC based SAPF system by designing an advanced predictive control scheme based on MPC and the design of the proposed RECKF-MPC based SAPF is presented in next section.

3.4 Proposed RECKF-MPC based SAPF

3.4.1 Description of proposed RECKF-MPC based SAPF system

The control structure for the proposed RECKF-MPC is similar as mentioned in Fig. 3.1(a) except that the current controller is replaced by MPC without any PWM scheme. The reference generation approach with RECKF is same as prescribed in Section 3.2.2.

3.4.2 Model Predictive Control (MPC)

MPC is based on the fact that only a finite number of possible switching states can be generated by VSI and that models of the system can be used to predict the behavior of the variables for each switching state. For the selection of the appropriate switching state to be applied, a selection criterion must be defined. This selection criterion is expressed as a quality function that will be evaluated for the predicted values of the variables to be controlled. The switching state that minimizes the quality function is selected. A block diagram of the MPC applied to the current control for a three phase inverter is shown in Fig. 3.5. The current control is performed in the following steps.

1. The value of the reference source current $\left(i^*_{Sabc_k}\right)$ is obtained from outer control loop and the source current $\left(i_{Sabc_k}\right)$ is measured.

2. The model of the system (block 1) is used to predict the value of the source current in the next sampling interval $(k+1)$ for each of the different voltage vectors.

3. In this case, the quality function J_{MPC} evaluates the error between the reference and predicted currents in the next sampling interval. The voltage that minimizes the current error is selected and applied to the (block 2).
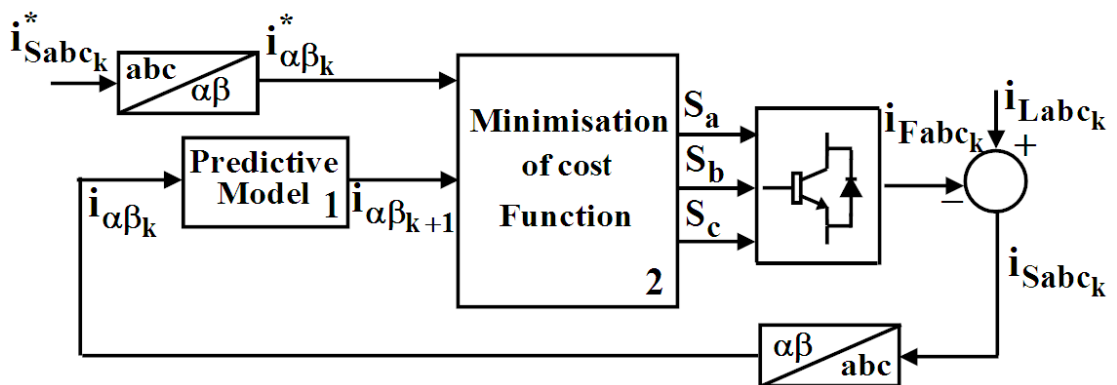
Figure 3.5: Structure of MPC for SAPF

The current error for the next sampling instant can be expressed in orthogonal coordinates as follows:

$$J_{MPC} = \left| i_\alpha^* - i_\alpha^p \right| + \left| i_\beta^* - i_\beta^p \right| \tag{3.4}$$

where i_α^p and i_β^p are the real and imaginary part of the predicted source current, i_α^* and i_β^* are the real and imaginary part of future reference current.

3.4.2.1 Inverter Model

From the power circuit of VSI shown in Fig. 3.1(b), the switching state of the inverter can be described by variables S_a, S_b and S_c, which can take values of 1 (ON state) or 0 (OFF STATE). Since there are three phases with two possible switching states each, there are a total of $2^3 = 8$ different switching states. The space vector of switching state and the inverter voltage are defined by eq. (3.5) and eq. (3.6) respectively,

$$S = \frac{2}{3}(S_a + aS_b + a^2 S_c) \tag{3.5}$$

$$v_f = \frac{2}{3}(v_{fan} + av_{fbn} + a^2 v_{fcn}) \tag{3.6}$$

where $a = e^{j(2\pi/3)}$ and $v_{fan}, v_{fbn}, v_{fcn}$ are the phase to neutral (n) voltages. Thus, the inverter voltage vector can be related with switching state vector by the equation,

$$v_f = v_{dc} S \tag{3.7}$$

By evaluating each of the switching states in eq. (3.7), eight voltage vectors $(v_0 - v_7)$ can be generated by the inverter, as shown in Fig. 3.6.
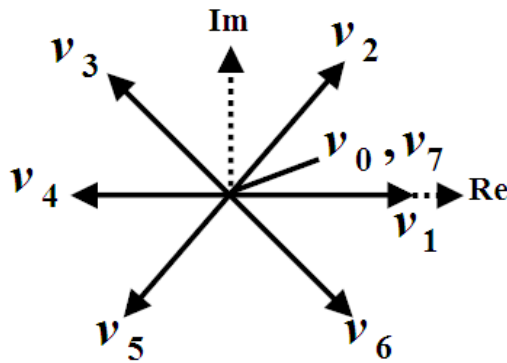
Figure 3.6: Voltage Space Vector Diagram

3.4.2.2 Discrete Time Model

The predictive model used for calculating the predicted currents is obtained by discretization (using the Euler Method) of eq. (3.1) and is expressed as

$$i_{Fx}(k+1) = \left(1 - \frac{R_f T_s}{L_f}\right) i_{Fx}(k) + \frac{T_s}{L_f}(v_{fx}(k) - v_{sx}(k)) \tag{3.8}$$

Further, the source current $i_{Sx}(k)$ is obtained from the load current $i_{Lx}(k)$ and filter current $i_{Fx}(k)$.

$$i_{Sx}(k) = i_{Lx}(k) - i_{Fx}(k) \tag{3.9}$$

3.4.3 Results and Discussions

3.4.3.1 Simulation Results

The steady state response of proposed RECKF-MPC based SAPF system is depicted in Fig. 3.7 using MATLAB. From the Fig. 3.7, it is observed that the response of compensating current is quite effective than RECKF-DBC. Further, the dc link voltage is quickly set at 220V without any overshoot. The source current tracks the reference more effectively so that tracking error can be reduced to a large extent and the source current THD is found to be 3.82%, very much less than that yielded with RECKF-DBC. Hence it is clear that the proposed RECKF-MPC approach exhibits superior performance. To further assess the performance of proposed RECKF-MPC with conventional PI-MPC, the transient test analyses are performed in the SAPF system.

   Fig. 3.8 shows the transient responses of load current, compensating current, capacitor voltage, source current and THD of source current after compensation respectively for a comparative study between proposed RECKF-MPC and PI-MPC based SAPF system with MATLAB. For transient state (sudden change in load from $R = 20\Omega$, $L = 10\text{mH}$ to $R = 12\Omega$, $L = 5\text{mH}$) condition, the step time is applied between 0.05 sec to 1 sec as shown in Fig. 3.8(a). The compensating current is smoother in case of RECKF-MPC as compared to PI-MPC as specified in Fig. 3.8(b). From Fig. 3.8(c), it can be observed that the capacitor voltage suddenly settles (≈ 0.08sec) to set point even in transient condition in case of proposed RECKF-MPC, whereas it takes (≈ 0.2sec) to reach the set point in case of PI-MPC. As depicted in Fig. 3.8(d), although the source current waveforms of both RECKF-MPC and PI-MPC are sinusoidal even when subjected to a
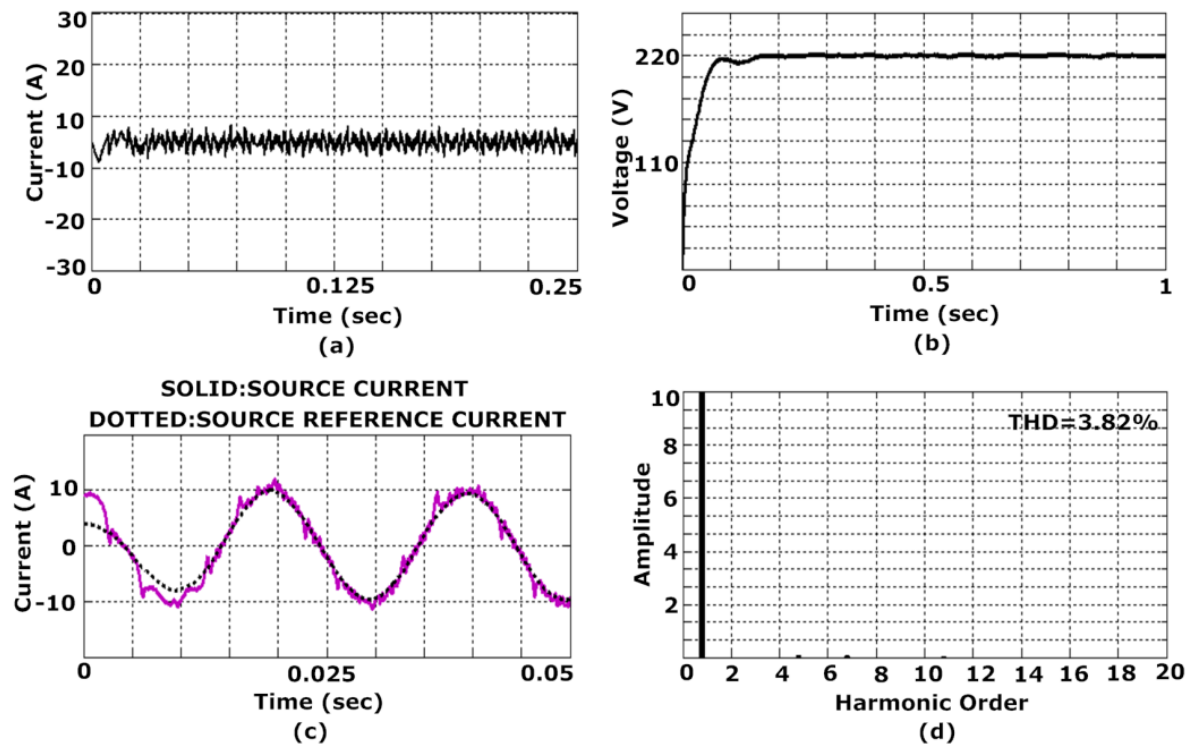
Figure 3.7: Steady State Response of RECKF-MPC based SAPF using MATLAB, (a) Compensating current, (b) Capacitor voltage, (c) Source and Source reference current, (e) THD of source current

changing nonlinear load, the source current waveform of the proposed RECKF-MPC is smoother and less distorted than that of PI-MPC. Fig. 3.8 (e) and (f) show the comparison of the compensation effects for both the PI-MPC and RECKF-MPC based SAPF system in steady state and transient state respectively. For PI-MPC based SAPF, the source current THD is realized as 3.93% (steady state) and 4.59% (transient state). However, the system performance becomes worse if load changes. On the other hand, the same tests were performed, except that the proposed RECKF approach is used instead of the PI one. The source current THD is dropped to about 3.82% (steady state) and 3.97% (transient state) in case of RECKF-MPC. PI control gains are tuned for steady state condition to get the best response. When the transient state occurs, the gains of the PI controller cannot ensure that the system has same response due to the lack of adaptability. However, in RECKF-MPC based SAPF systems, a considerable flexibility is achieved to the designer to alter the goals by quickly modifying the weighted exponential function under abnormal condition (i.e., change from steady to transient condition). Hence, RECKF-MPC approach can assure the system stability.
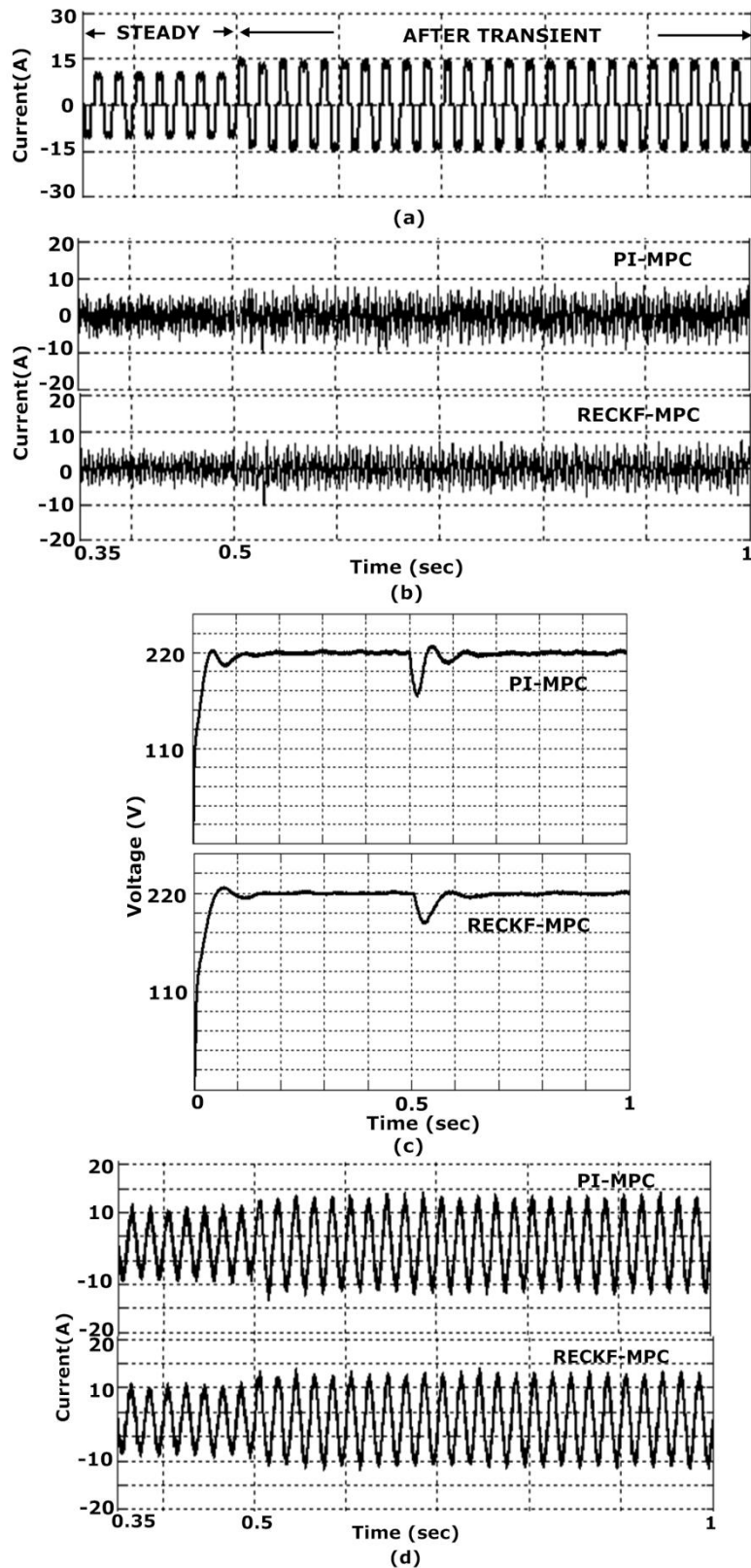
Figure 3.8: Transient State Response of RECKF-MPC and PI-MPC based SAPF using MATLAB, (a) Load current, (b) Compensating current, (c) Capacitor voltage, (d) Source current, (e) THD of source current in steady state, (f) THD of source current in transient state
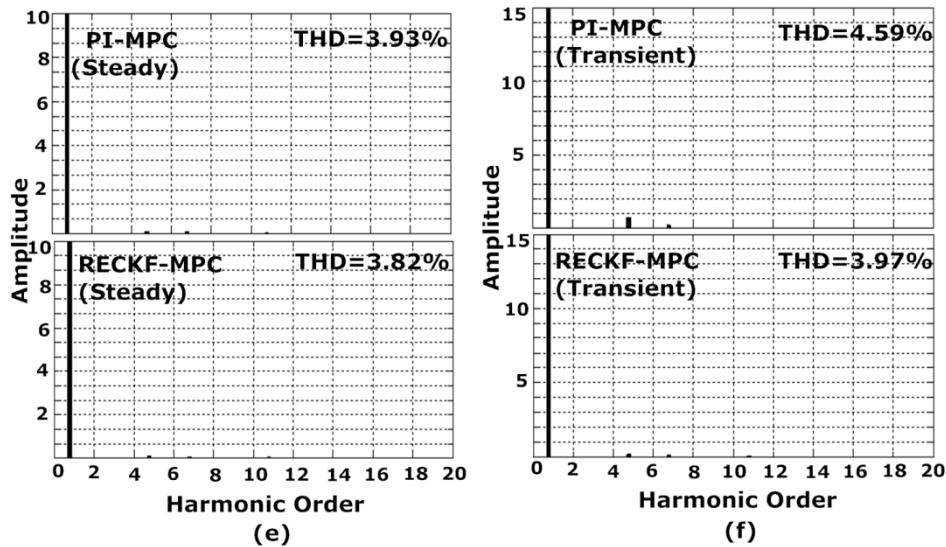
Figure 3.8: Continued

3.4.3.2 Real-time Simulation Results

Fig. 3.9 presents the transient responses of load current, capacitor voltage, compensating current, source current and THD of source current after compensation respectively for a comparative analysis between proposed RECKF-MPC and PI-MPC based SAPF system using Opal-RT. It is observed from the Fig. 3.9(a), (b) and (c) that the response for load current, capacitor voltage and compensating current are in close agreement with the simulation results shown in Fig. 3.8. From Fig. 3.9(d), it can be seen that the source current after compensation is in phase with the source voltage but it has larger number of distortions during steady as well as transient conditions in case of PI-MPC as compared to RECKF-MPC. Analyzing THD results (Fig. 3.9 (e)), it can be found that the THD in steady state case is 4.03% for PI-MPC, but largely increased to 4.62% in transient case. However, THD level is nearly same (i.e., 3.89% (steady) and 3.99% (transient)) for RECKF-MPC. Hence, the effectiveness of the proposed RECKF-MPC based SAPF can be successfully verified.
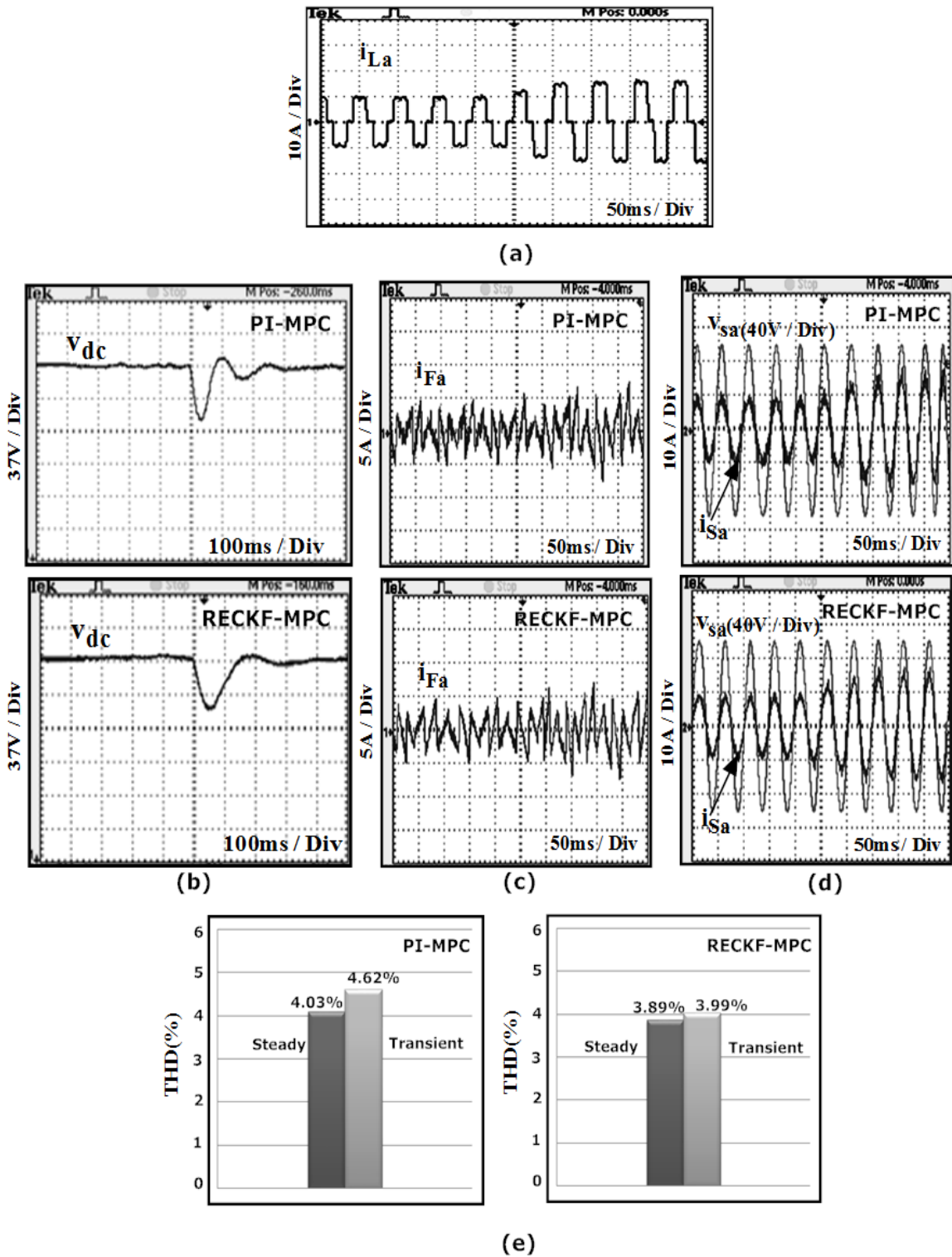
Figure 3.9: Transient State Response of RECKF-MPC and PI-MPC based SAPF using Opal-RT, (a) Load current, (b) Capacitor voltage, (c) Compensating current, (d) Source voltage and source current, (e) THD of source current in steady and transient state

3.4.3.3 Remarks on the Proposed RECKF-MPC based SAPF Method

- It is not necessary to include any type of modulator in MPC approach.
- RECKF-MPC based SAPF method is able to mitigate harmonics successfully both in steady state and transient state conditions. It can overcome the difficulties encountered with the fixed-gain PI controller, such as flexibility and robustness over stabilization of capacitor voltage when changing loads.

Table 3.1 shows the superiority of RECKF-MPC both in steady state and transient state conditions, when a comparative investigation has been performed on the basis of THD factors employing simulation and real-time simulation results.

Table 3.1 THD Factor of Control Structures of SAPF

(RECKF-DBC, RECKF-MPC, PI-MPC)

Cases	Control Structure of SAPF	THD% of Source Current After Compensation	
		Simulation Results	Real-Time Simulation Results
	RECKF-DBC	4.26	4.31
Steady State	RECKF-MPC	3.82	3.89
	PI-MPC	3.93	4.03
Transient State	RECKF-MPC	3.97	3.99
	PI-MPC	4.59	4.62

3.5 Chapter Summary

A RECKF-DBC and RECKF-MPC based SAPF are proposed in this chapter. These two approaches have been developed with less number of voltage sensors and resolve the

difficulty of gain tuning of PI controller. In the first proposed RECKF-DBC method, harmonics cancellation is not perfect (THD is above 4%) in spite of having fixed switching frequency in SAPF. Therefore, a MPC based SAPF is implemented with the main advantage of direct application of switching pulses to the IGBT inverter, without necessitating a modulation stage. Moreover, to study the efficacy of this proposed RECKF-MPC over PI-MPC, a comparative assessment has been performed using both steady state as well as transient state conditions. From the simulation and real-time simulation results, it is observed that the proposed RECKF-MPC outperforms over PI-MPC and exhibits an excellent control approach to SAPF design in steady as well as transient condition which improves PQ more effectively in terms of efficient harmonics mitigation.

CHAPTER 4

Robust Extended Complex Kalman Filter and Linear Quadratic Regulator based SAPF

4.1 Introduction

This chapter proposed LQR controller approach that is developed using the estimation techniques based on proposed RECKF for SAPF system. Chapter 3 presented predictive current controllers such as DBC and MPC with a new reference generation scheme based on RECKF avoiding the need of a PI controller in the external loop. DC voltage regulation is found to be better in case of RECKF-MPC as compared to PI-MPC from a comparative study in steady state as well as transient state conditions in SAPF system. Large settling time in dc voltage leads to poor tracking performance of RECKF-MPC controlled SAPF and thus compensation of current harmonics is not effective. Moreover, MPC is very sensitive to model mismatch and noise. It is quite sluggish in rejecting large drifting grid disturbances. Hence, a suitable control strategy needs to be developed in SAPF to improve tracking performance as well as grid disturbance rejection capability.

The LQR based on the optimal control [97][98][99][100] of three-phase ac–dc converters with unity power factor was applied for sinusoidal current PWM rectifiers and the neutral point clamped PWM rectifier in [101] and [102]. An optimal servo-controller was also applied in [103] to the current inner loop of the SAPF in the cascade strategy where an outer loop used a simple PI regulator for the dc bus voltage.

In this Chapter, the LQR is designed for SAPF due to its obvious advantage for controlling multi-input–multi-output systems such as the SAPF in addition to insensitivity to small parameter variations [104].Taking advantage of the LQR robustness [105], it is used for the signal model describing the SAPF dynamics to keep the power factor at PCC close to unity. Using this approach, it becomes easier to find the optimal gains of the controller with the acceptable tracking of the SAPF's current components for the entire operating range. The advantage of LQR over other controllers such as DBC, SMC, and HCC is that by minimizing a performance index as a function of u (control effort) and states, one can reduce the control effort needed or the energy of some state variable can

be reduced. Moreover, if the SAPF is accurately modeled, the LQR may be considered a robust controller, minimizing satisfactorily the considered states.

It may be noted that in order to achieve a superior compensation of harmonics beside the controller, the reference current generation should be made appropriately [106]. For implementation of LQR, generation of reference compensating current is essential. Hence, harmonic contents of the load current should be identified in SAPF. It can be determined by (a) directly determining each of the parameters of the harmonic components, or (b) indirectly subtracting the fundamental component from the load current. The indirect method is commonly used in view of ease in its implementation. However, if the fundamental component is not estimated accurately, then the active filter may source or sink the active power. Several methods have been reported in literature [17][18][27][61][62] for the extraction of harmonic components such as LPF method, pq method, dq method, ANN approach and DFT approach. In this Chapter, an approach based on RECKF is described for estimating the in phase fundamental of PCC as well as peak value of source current. It is shown that by using this approach, capacitor voltage stabilization is improved with lessening settling time.

This Chapter focuses on the minimizing the effects of the PCC voltage by considering it as a part of the SAPF model and designing LQR with the help of RECKF based estimation approach.

4.2 Chapter Objectives

1. To improve current tracking and disturbance rejection capability of SAPF system considering dynamic information of distorted voltage signal at the PCC.

2. To design an improved reference current scheme without necessitating PI controller loop.

3. To self-regulate dc-link voltage.

4. To improve the current harmonics compensation capability of SAPF.

5. To simulate the proposed control structure in MATLAB/Simulink and real-time simulation model in Opal-RT simulator.

4.3 Proposed RECKF-LQR based SAPF

4.3.1 Description of proposed RECKF-LQR based SAPF system

The SAPF shown in Fig. 4.1(a) is controlled by the proposed RECKF and LQR method. RECKF is employed for estimation of in phase and in quadrature components of PCC voltages v_{abc} and these are used to estimate the PCC voltages and their derivatives. Also, the fundamental amplitudes of load current as well as source current are estimated by RECKF, which are utilized for generation of reference current. Then the LQR is designed along with the information of the above state space variables and gate pulses are given to the IGBT inverter through triangular carrier based PWM method.

4.3.2 Development of SAPF

4.3.2.1 Mathematical Model of SAPF

The SAPF model in the dq frame according to [107] can be expressed by eq (4.1) and (4.2), where PCC voltage is considered as a disturbance. i_{Fdq}, u_{dq} and v_{dq} denote the dq frame model for filter current i_{Fabc}, switching function u_{abc} and PCC voltage v_{abc} respectively.

$$\dot{i}_{Fdq} = Ai_{Fdq} + Bu_{dq} + Ev_{dq} \tag{4.1}$$

$$y_{dq} = Ci_{Fdq} \tag{4.2}$$

where

$$A = \begin{bmatrix} -\dfrac{R_f}{L_f} & \omega \\ -\omega & -\dfrac{R_f}{L_f} \end{bmatrix}, \quad B = \begin{bmatrix} -\dfrac{v_{dc}}{L_f} & 0 \\ 0 & -\dfrac{v_{dc}}{L_f} \end{bmatrix},$$

$$E = \begin{bmatrix} \dfrac{1}{L_f} & 0 \\ 0 & \dfrac{1}{L_f} \end{bmatrix}, \quad C = \begin{bmatrix} 1 & 0 \\ 0 & 1 \end{bmatrix}$$
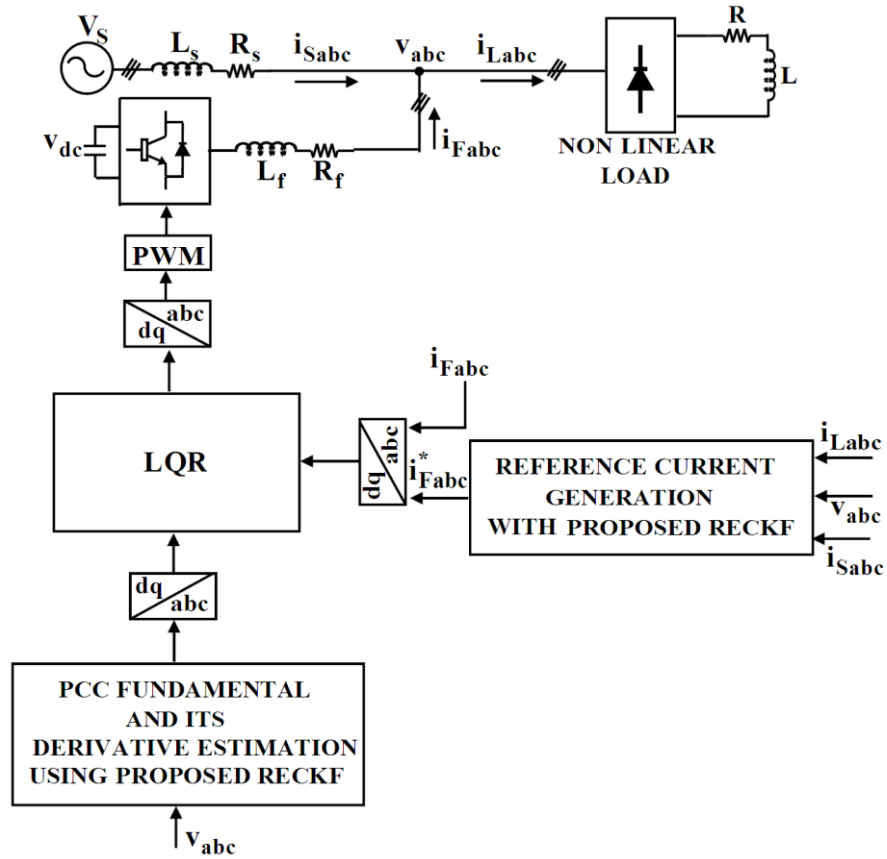
(a)
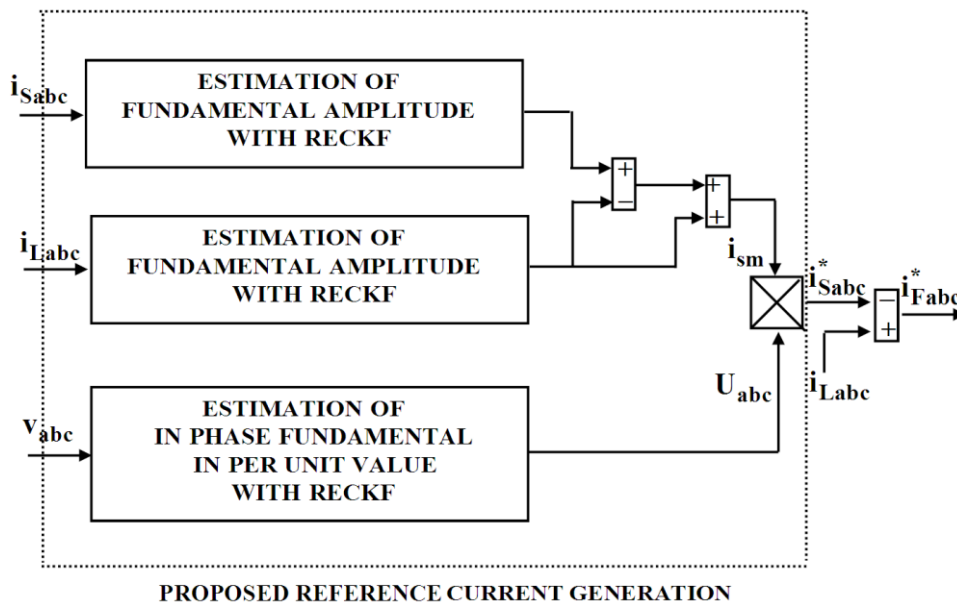
(b)

Figure 4.1: Proposed RECKF- LQR based SAPF, (a) Block Diagram of Proposed RECKF- LQR based SAPF, (b) Proposed Reference Current Generation

In this Chapter PCC voltage dynamics are included in the model. Considering the PCC voltages as sinusoidal, balanced and each phase is delayed by ϕ radians, the following equations can be written to describe the SAPF system.

$$v_a = V\sin(\omega t)$$
$$v_b = V\sin(\omega t + \theta)$$
$$v_c = V\sin(\omega t - \theta)$$

(4.3)

where V is the magnitude of the voltage, $\omega = 2\pi f$ is the angular frequency of the grid and $\theta = \dfrac{2\pi}{3}$ rad. The first derivatives of these waveforms are shown in eq (4.4).

$$\frac{dv_a}{dt} = V\omega\cos(\omega t)$$
$$\frac{dv_b}{dt} = V\omega\cos(\omega t + \theta)$$
$$\frac{dv_c}{dt} = V\omega\cos(\omega t - \theta)$$

(4.4)

The second derivatives of eq (4.3) are obtained as follows.

$$\frac{d^2 v_a}{dt^2} = -V\omega^2\sin(\omega t)$$
$$\frac{d^2 v_b}{dt^2} = -V\omega^2\sin(\omega t + \theta)$$
$$\frac{d^2 v_c}{dt^2} = -V\omega^2\sin(\omega t - \theta)$$

(4.5)

From eq (4.3), eq (4.4) and eq (4.5), it is verified that $\dfrac{d^2 v_{abc}}{dt^2} = -V\omega^2 v_{abc}$, thus the complete model that represents the behavior of the voltages at PCC in the 'abc' frame is given in eq (4.6).

$$
\begin{bmatrix} \dot{v}_a \\ \dot{v}_b \\ \dot{v}_c \\ \dot{v}_a \\ \dot{v}_b \\ \dot{v}_c \end{bmatrix} =
\begin{bmatrix}
0 & 0 & 0 & 1 & 0 & 0 \\
0 & 0 & 0 & 0 & 1 & 0 \\
0 & 0 & 0 & 0 & 0 & 1 \\
-\omega^2 & 0 & 0 & 0 & 0 & 0 \\
0 & -\omega^2 & 0 & 0 & 0 & 0 \\
0 & 0 & -\omega^2 & 0 & 0 & 0
\end{bmatrix}
\begin{bmatrix} v_a \\ v_b \\ v_c \\ \dot{v}_a \\ \dot{v}_b \\ \dot{v}_c \end{bmatrix}
$$

(4.6)

Using the matrix differentiation property as below

$$\frac{d}{dt}\left[\left(C_{abc}^{dq0}\right)^{-1} i_{Fdq0}\right] = i_{Fdq0}\frac{d}{dt}\left(C_{abc}^{dq0}\right)^{-1} + \left(C_{abc}^{dq0}\right)^{-1}\frac{d}{dt}i_{Fdq0} \tag{4.7}$$

where C_{abc}^{dq0} is the Park transform, it is possible to derive the following dq frame model for fundamental voltages at the PCC,

$$\begin{bmatrix} \dot{v}_d \\ v_q \\ \dot{v}_d \\ \dot{v}_q \end{bmatrix} = \begin{bmatrix} 0 & 0 & 1 & 0 \\ 0 & 0 & 0 & 1 \\ -\omega^2 & 0 & 0 & \omega \\ 0 & -\omega^2 & -\omega & 0 \end{bmatrix} \begin{bmatrix} v_d \\ v_q \\ \dot{v}_d \\ \dot{v}_q \end{bmatrix} \tag{4.8}$$

The complete rotating reference frame model of the SAPF system can be written as

$$\begin{bmatrix} \dot{i}_d \\ i_q \\ v_d \\ v_q \\ \dot{v}_d \\ \dot{v}_q \end{bmatrix} = \bar{A} \begin{bmatrix} i_d \\ i_q \\ v_d \\ v_q \\ \dot{v}_d \\ \dot{v}_q \end{bmatrix} + \bar{B} \begin{bmatrix} u_d \\ u_q \end{bmatrix} \tag{4.9}$$

$$y_{dq} = \bar{C} \begin{bmatrix} i_d \\ i_q \\ v_d \\ v_q \\ \dot{v}_d \\ \dot{v}_q \end{bmatrix} \tag{4.10}$$

where

$$\bar{A} = \begin{bmatrix} -\dfrac{R_f}{L_f} & \omega & \dfrac{1}{L_f} & 0 & 0 & 0 \\[2mm] -\omega & -\dfrac{R_f}{L_f} & 0 & \dfrac{1}{L_f} & 0 & 0 \\[2mm] 0 & 0 & 0 & 0 & 1 & 0 \\[2mm] 0 & 0 & 0 & 0 & 0 & 1 \\[2mm] 0 & 0 & -\omega^2 & 0 & 0 & \omega \\[2mm] 0 & 0 & 0 & -\omega^2 & -\omega & 0 \end{bmatrix},$$

$$\bar{B} = -\begin{bmatrix} \dfrac{v_{dc}}{L_f} & 0 \\[2mm] 0 & \dfrac{v_{dc}}{L_f} \\[2mm] 0 & 0 \\[2mm] 0 & 0 \\[2mm] 0 & 0 \\[2mm] 0 & 0 \end{bmatrix} \quad \text{and} \quad \bar{C} = -\begin{bmatrix} 1 & 0 & 0 & 0 & 0 & 0 \\ 0 & 1 & 0 & 0 & 0 & 0 \end{bmatrix}$$

4.3.3 LQR

LQR has been widely applied to several applications where optimal control is required for state regulation, output regulation and tracking. The LQR strategy implementation uses state feedback where the state weightings can be chosen and the control output is properly designed to satisfy a performance criterion [97][98][99][100]. In this control strategy, the states weighting gains are obtained through the solution of an associated algebraic Ricatti equation, which includes a performance index. LQR may be considered as a robust controller, minimizing satisfactorily the state variables. The Zero order Hold (ZOH) discrete time model of the system with sample period T_s is described as

$$x_{k+1} = A_d x_k + B_d u_k \tag{4.11}$$

$$y_k = C_d x_k \tag{4.12}$$

where

$$A_d = e^{\bar{A}T_s}, B_d = \bar{A}^{-1}(e^{\bar{A}T_s} - 1)\bar{B} \text{ and } C_d = \bar{C}$$

The switching function (control action) from LQR is given by $u_k = -K_{LQR}x_k$, which minimises the cost function

$$J_{LQR} = \frac{1}{2}\sum_{k=0}^{\infty}\left\{x_k^T Q_{LQR}x_k + u_k^T R_{LQR}u_k\right\} \tag{4.13}$$

where Q_{LQR} and R_{LQR} are the state and control weighting matrices which are square and symmetric. K_{LQR} Gains can be obtained solving the algebraic Riccati equation [88].

$$P_{LQR} = A_d^T P_{LQR}(A_d - B_d K_{LQR}) + Q_{LQR} \tag{4.14}$$

$$K_{LQR} = (B_d^T P_{LQR}B_d + R_{LQR})^{-1}B_d^T P_{LQR}A_d \tag{4.15}$$

The LQR calculates the gain vector K_{LQR} by using the model specified in Eq. (4.9).

The control structure of LQR is depicted in Fig. 4.2. It may be noted that this approach includes the entire system dynamics, with PCC voltage disturbance being compensated with the additional information that comes from the RECKF. The estimation of the state space variables related to the PCC voltages needed by the controller and the generation of current references are discussed in the next section.
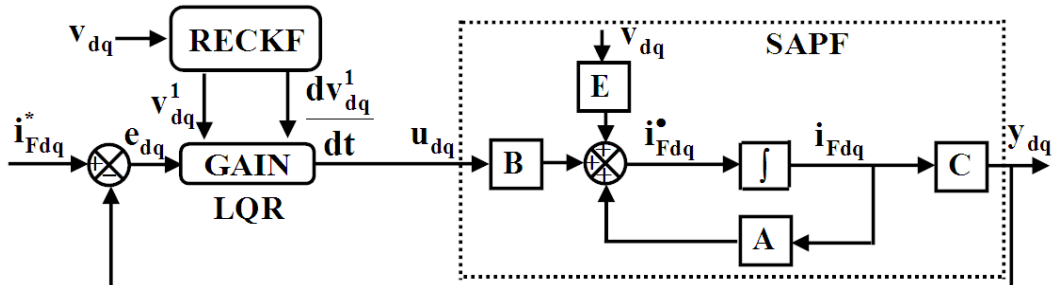
Figure 4.2: Structure of LQR for SAPF

4.3.4 Estimation of PCC State variables

The PCC modeling approach, presented in Section 4.2.2.1, requires the knowledge of the voltages at the PCC and their derivatives. It is impossible to differentiate a signal x by using the forward approximation $\dfrac{x_{k+1} - x_k}{T_s}$ when the system is affected by measurement noises, spikes and other unpredictable signal disturbances. Hence, this information has to be filtered. Considering that the voltage at the PCC is predominant at the fundamental frequency, the corresponding in phase and in quadrature components can be obtained by auxiliary algorithm based on proposed RECKF as displayed in Fig. 4.3. The in quadrature fundamental component can be obtained by 90 degree phase shifting of in phase fundamental being derived in Chapter 2.

$$v_{a_k} \Rightarrow \boxed{\textbf{RECKF}} \Rightarrow [v_{a_1}, v_{a_1}^{\perp}]_k$$

$$v_{b_k} \Rightarrow \boxed{\textbf{RECKF}} \Rightarrow [v_{b_1}, v_{b_1}^{\perp}]_k$$

$$v_{c_k} \Rightarrow \boxed{\textbf{RECKF}} \Rightarrow [v_{c_1}, v_{c_1}^{\perp}]_k$$
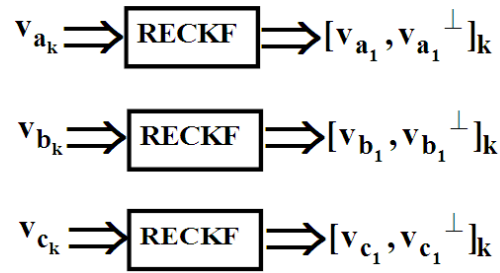
Figure 4.3: Identification of in phase and in quadrature fundamental voltages at PCC

It is possible to obtain the following relations for the fundamental component of voltage at the PCC v_{jl_k} and their respective derivatives $\dot{v}_{jl_k}$ that constitute state variables of the mathematical model.

$$v_{jl_k} = A_{v_{jl_k}} \sin(2\pi f_{1_k} T_s + \theta_{v_{jl_k}}) \tag{4.16}$$

$$\dot{v}_{jl_k} = \omega \hat{v}_{jl_k}^{\perp} = \omega A_{v_{jl_k}} \cos(2\pi f_{1_k} T_s + \theta_{v_{jl_k}}) \tag{4.17}$$

where $A_{v_{jl_k}}, \theta_{v_{jl_k}}$ are the amplitude and phase of the fundamental component of PCC voltage at the instant k, j represents the phase and v_{jl_k}, $v_{jl_k}^{\perp}$ are the in phase and in quadrature components respectively.

4.3.5 Generation of Reference current

The proposed reference current scheme (Fig. 4.1(b)) is the modification of reference scheme developed in Chapter 3 by including an error value originated from the difference between the estimated fundamental amplitudes of source current and load current. The estimation technique is based upon proposed RECKF algorithm and the formulations for fundamental amplitudes have already been described in Chapter 2. This error value is further added to the fundamental amplitude of load current to give a desired peak value of source current i_{sm}, which enhances the reference tracking capability of dc link voltage without involving any PI controller loop. The implementation of source reference currents i_{Sabc}^{*} are already prescribed in Chapter 2. Finally, for implementation of the LQR, the reference compensating currents i_{Fabc}^{*} can be found out by using the following equation.

$$i_{Fabc}^{*} = i_{Labc} - i_{Sabc}^{*} \tag{4.18}$$

4.3.6 Results and Discussions

4.3.6.1 Simulation Results

In order to evaluate the harmonic compensation performance of the proposed RECKF-LQR method, the SAPF system shown in Fig. 4.1 is implemented using MATLAB/Simulink. For the implementation of the LQR, the built-in 'lqrd' function of MATLAB is used. The selection of Q_{LQR} and R_{LQR} matrices in LQR design is based on the performance specifications and a certain amount of trial and error [108] is required with an interactive computer simulation before arriving at satisfactory design results. Since the matrices Q_{LQR} and R_{LQR} are symmetric, there are six distinct elements in Q_{LQR} and two distinct elements in R_{LQR} need to be selected. The matrices Q_{LQR} and R_{LQR} should be positive definite. The value of the elements in Q_{LQR} and R_{LQR} are related to their contribution to the cost function J_{LQR}.

$$Q_{LQR} = \begin{bmatrix} 3700 & 0 & 0 & 0 & 0 & 0 \\ 0 & 4970 & 0 & 0 & 0 & 0 \\ 0 & 0 & 0 & 0 & 0 & 0 \\ 0 & 0 & 0 & 0 & 0 & 0 \\ 0 & 0 & 0 & 0 & 0 & 0 \\ 0 & 0 & 0 & 0 & 0 & 0 \end{bmatrix}, R_{LQR} = \begin{bmatrix} 1 & 0 \\ 0 & 1 \end{bmatrix} \tag{4.19}$$

Fig. 4.4 shows the behavior of proposed RECKF-LQR approach considering phase 'a'. The response of a RECKF estimator, when extracting in phase and in quadrature fundamental components of PCC voltage, is depicted in Fig. 4.4(a). It is shown in Fig. 4.4(a) that estimation results are quite matched with the actual ones indicating a good performance of RECKF. The dc voltage stabilization capacity of proposed RECKF-LQR based SAPF system is presented in Fig. 4.4(b). It is realized from Fig. 4.4(b) that there is no overshoot present in the waveform and a settling time of 0.1sec is required to set at the reference voltage resulting a good voltage regulation performance of RECKF-LQR approach. The current output of SAPF is superimposed with its respective reference and is shown in Fig. 4.4(b). It is inferred that the filter injected current harmonics track their references with high level of accuracy.

Fig. 4.4(c) represents the current quality obtained with proposed RECKF-LQR after compensation with SAPF. As can be seen, the source current is sinusoidal and balanced. The spectrum analysis of source current depicted in Fig. 4.4(d) indicates that the THD of the source current is reduced to 3.4% after compensation. Hence, the effectiveness of proposed RECKF-LQR can be realized.

4.3.6.2 Real-time Simulation Results

Real-time simulated results of proposed SAPF system are shown in Fig. 4.5 (a), (b), (c) and (d) respectively. From Fig. 4.5(a), it is found that compensating current is able to track the reference perfectly by means of reducing the tracking error. Capacitor voltage is found to be set at 220V as depicted in Fig. 4.5(b). Both source voltage and source current waveforms are presented in Fig. 4.5(c) to analyze the performance of proposed RECKF-LQR. It is observed from Fig. 4.5(c) that the source current is in phase with source voltage with power factor close to unity. The compensating effect of proposed SAPF is analyzed in Fig. 4.5(d) and it is found that the THD of source current is reduced from 26.4% to 3.46%., very close to simulation result (i.e., 25.9% to 3.41%). Hence, all the

real time simulated results displayed in Fig. 4.5 are well agreed with the simulation results depicted in Fig. 4.4.
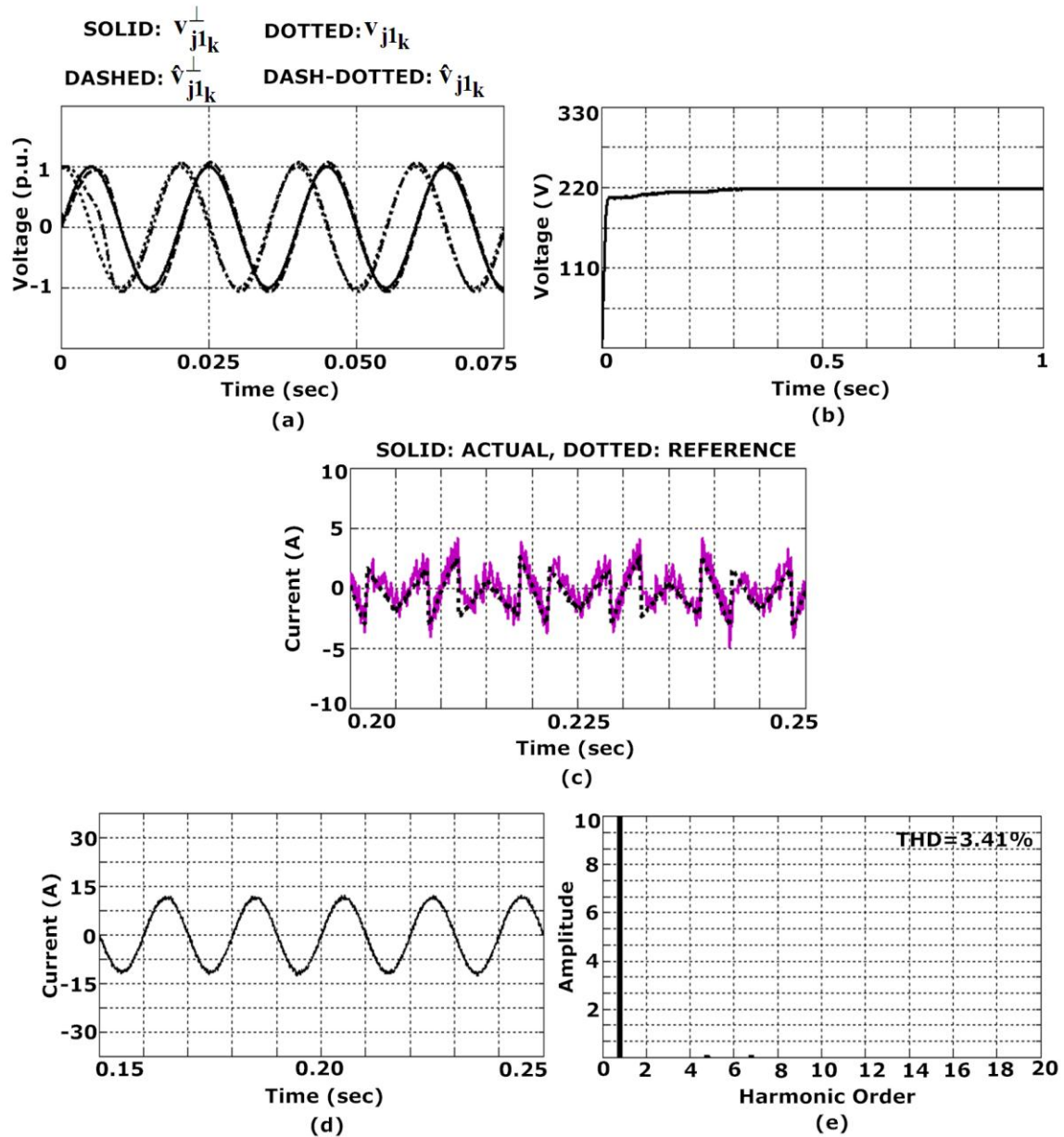
Figure 4.4: Response of RECKF-LQR based SAPF using MATLAB, (a) In phase and in quadrature fundamental components of PCC voltage, (b) Capacitor voltage, (c) Reference and actual compensating current, (d) Source current, (e) THD of source current

86
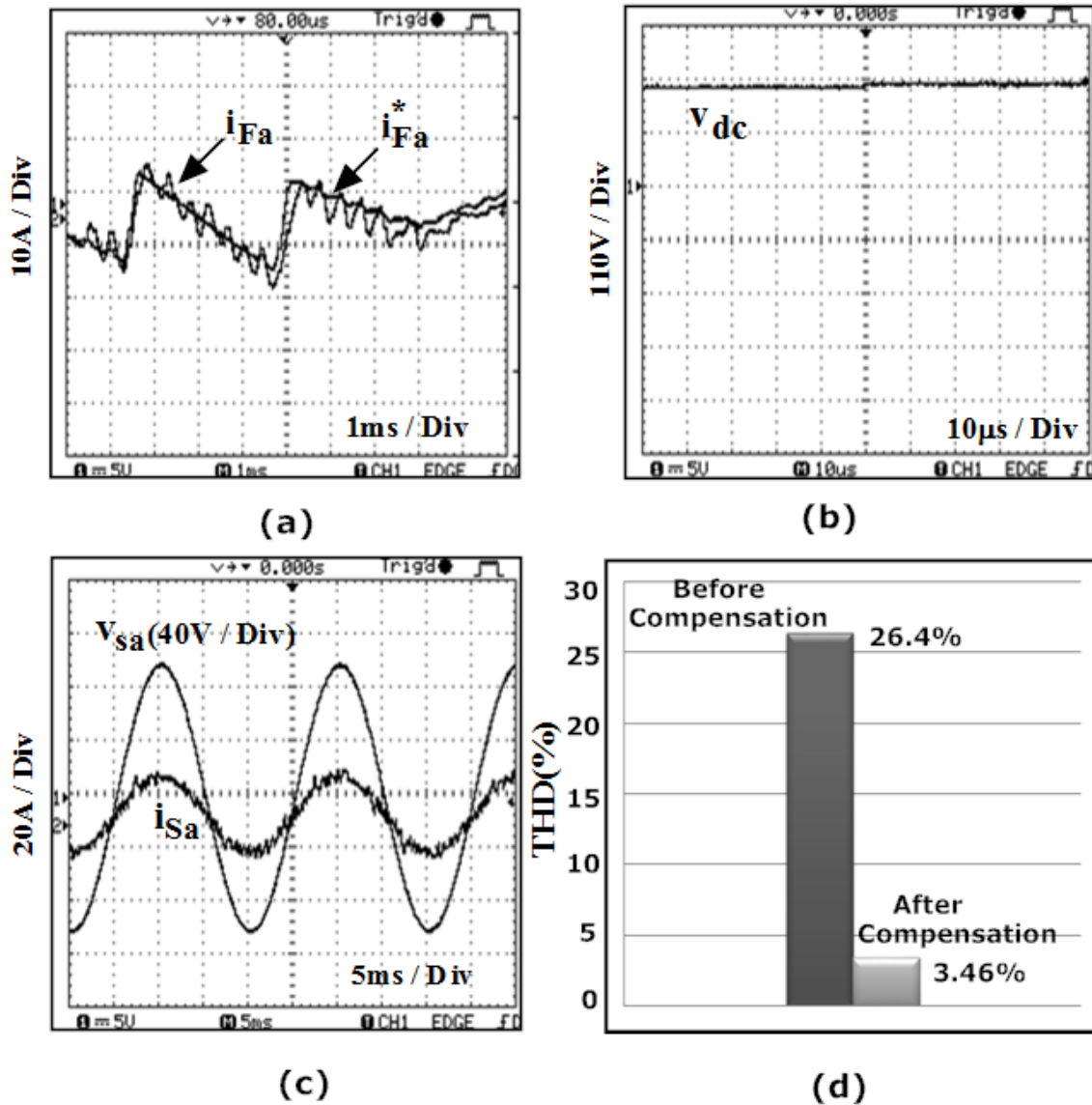
Figure 4.5: Response of RECKF-LQR based SAPF using Opal-RT, (a) Reference and actual compensating current, (b) Capacitor voltage, (c) Source voltage and source current after compensation, (d) THD before and after compensation

Table 4.1 shows a THD summarization of different control structures of SAPF such as RECKF-SMC, RECKF-DBC, RECKF-MPC and RECKF-LQR using simulation and real-time simulation results. It envisages a superiority of RECKF-LQR (3.46%) over other SAPF approaches.

Table 4.1 THD Factor of Control Structures of SAPF

(RECKF-SMC, RECKF-DBC, RECKF-MPC, RECKF-LQR)

Control Structure of SAPF	**THD% of Source Current After Compensation**	
	Simulation Results	Real-Time Simulation Results
RECKF-SMC	4.45	4.54
RECKF-DBC	4.26	4.31
RECKF-MPC	3.82	3.89
RECKF-LQR	3.41	3.46

4.4   Chapter Summary

This chapter proposed a RECKF-LQR control approach for improvement of current harmonics compensation capability of SAPF system. LQR is chosen here due to its well known features of tracking, disturbance rejection as well as robust performance. This technique carries the dynamic information of distorted voltage signal at the PCC and aims to have a more realistic representation of the SAPF system. For LQR implementation, the state space variables related to the PCC voltages, are very properly estimated using proposed RECKF based algorithm and have fast convergence. Moreover, the dc voltage stabilization is improved with a new reference generation scheme based on RECKF avoiding PI controller loop and as a consequence, harmonics cancellation effect is more in case of RECKF-LQR approach (THD=3.41%). From the obtained simulation and real-time results, the performances of the proposed RECKF-LQR are verified and it is found that the proposed SAPF exhibits good tracking behavior and PCC voltage disturbance rejection capability resulting towards a robust performance of SAPF system. Furthermore, RECKF-LQR is observed to be more effective in harmonics cancellation as compared to RECKF-SMC, RECKF-DBC, and RECKF-MPC.

CHAPTER 5

Robust Extended Complex Kalman Filter and Linear Quadratic Gaussian Servo Controller based SAPF

5.1 Introduction

This chapter proposes a Linear Quadratic Gaussian (LQG) servo controller for the current control of SAPF. It has been discussed in Chapter 2, 3, and 4 that RECKF is the most appropriate for estimation approach because of its fastest convergence. Further, reference current generation schemes employed in the above Chapters consider both voltage and current measurements and to achieve the dc-link capacitor voltage steady after a time delay of 0.15sec. Hence, in this chapter, voltage regulation of dc-link capacitor is further improved by employing a new and faster reference generation scheme based on RECKF, which can be achieved by only current measurements indicating a cost effective approach. Although, LQR approach developed in Chapter 4 provides robustness and disturbance rejection, but complete cancellation of load current harmonics was not obtained i.e. THD of the source current is 3.41%. Hence, in this Chapter, it is intended to develop effective robust technique such that higher disturbance rejection can be achieved.

Various control schemes have been applied in SAPF [109][110][111] under both balanced and unbalanced loading conditions. However, these control strategies have not considered some important aspects, such as variations in the SAPF parameters, including load impedance and grid perturbations. Due to parametric uncertainties present in the load, the problem of compensating the SAPF becomes more complicated which adversely effects towards its satisfactory operation.

A linear quadratic control combined with an integral control has been employed to control a three phase three wire SAPF to achieve unity power factor at PCC of a highly distorted and unbalanced load currents [107]. This control uses the full state vector available for feedback, but this is unrealistic as there is always a measurement noise. LQR with KF was proposed in [23] supported LQR and KF was proposed considering measurement noise, load currents and grid voltage transients. However, PCC voltage has not been considered as a disturbance in the SAPF model. LQR law is based on the

availability of the complete state vector, which may not be completely measurable in most of the real-world situations. To overcome this, a LQG servo controller was proposed in a voltage source converter, where KF was employed to estimate the state vector [112]. In this case, the control strategy is not far more sensitive to grid disturbances. Hence, tracking error is not reduced effectively and stability of the system is minimally improved. To resolve the above issues, in this Chapter, a suitable feedback compensator is proposed in a LQG servo controller in the proposed SAPF. However, using a LQG servo controller in SAPF framework is not very popular. The idea behind this feedback compensator is to achieve gain stability, less distortion and increased system bandwidth.

It is not possible to supply quality power to the special equipment e.g. programmable logic controller (PLC), distributed control system (DCS), converters in AC drives through conventional control schemes [23][107][111][113] employed in SAPF. This results in malfunctioning of the above type of equipment, which necessitates pure power even with fast changing disturbances occurring in the power system. Hence a fast and robust control action is necessary to supply pure and distortion less power to above equipment with all perturbations taken into account. In view of aforementioned issues, this Chapter focuses on the development of a robust LQG servo controller with a faster reference current estimation scheme in SAPF, which permits all perturbations such as PCC disturbances, parametric variations of load and tracking error variations so that compensation ability of the overall SAPF system can be enhanced with less consumption of time.

Fig. 5.1 shows the basic structure of LQG servo controller. The basic idea in a LQG servo control is to ensure that the output y tracks the reference command r while rejecting process disturbances w_i and measurement noise v_i. The plant in this figure subjects to disturbances w_i and is driven by controls u. The servo controller relies on the noisy measurements y to generate these controls. The plant state and measurement equations are described by the following equation.

$$\dot{x} = Ax + Bu + Gw_i$$
$$y = Cx + Du + Hw_i + v_i$$

$$(5.1)$$

where both w_i and v_i are modeled as white noise.
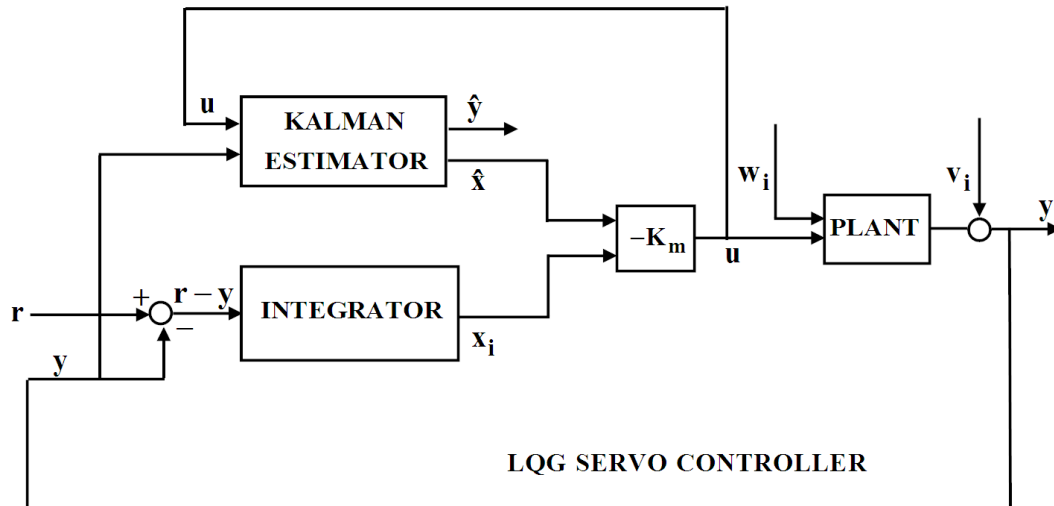
Figure 5.1: Basic Structure of LQG Servo Controller

5.2   Chapter Objectives

1. To self-regulate the dc-link voltage which avoids external PI controller loop.

2. To make SAPF robust against parameter variations of load.

3. To improve current harmonics compensation effect of SAPF.

4. To design a feedback compensator to increase the tracking error reduction, noise and external disturbances in SAPF system.

5. To make an inexpensive control strategy by reducing the number of voltage sensors.

6. To develop a prototype experimental set up in our Laboratory with dSPACE DS1104 controller board to investigate the robust performance of proposed control technique.

5.3   Proposed RECKF-LQG Servo based SAPF

5.3.1   Description of proposed RECKF-LQG Servo based SAPF system

The proposed SAPF system is developed by LQG servo current controller technique and RECKF based new reference current generation scheme as presented in Fig. 5.2. RECKF is employed for estimation of in phase fundamental component of load current in p.u. value U_{abc} and also the fundamental amplitude of source current i_{sm}, which give rise
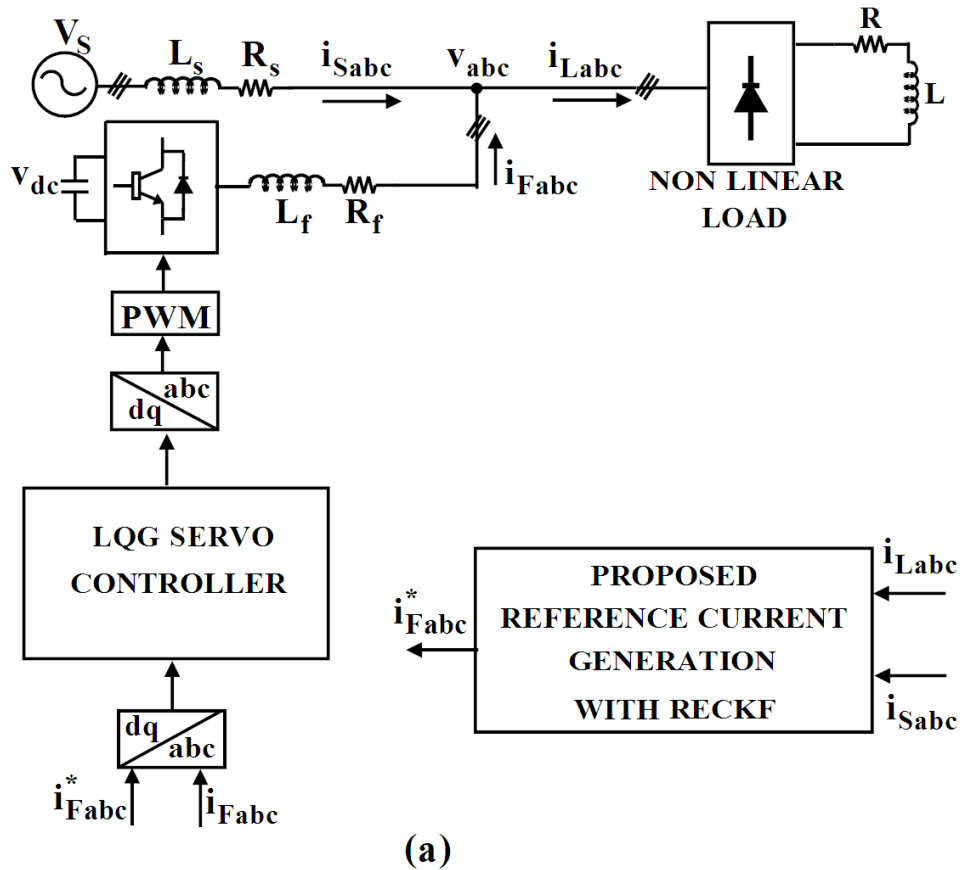
(a)
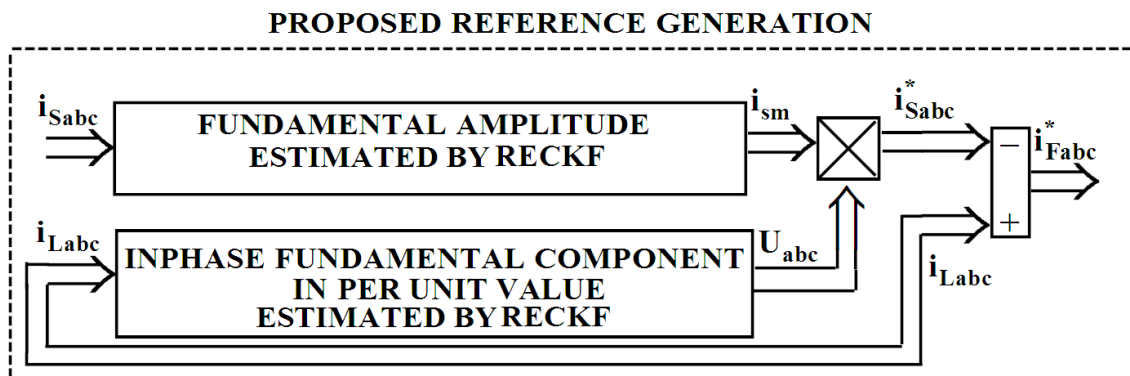
(b)

Figure 5.2: Proposed RECKF- LQG Servo based SAPF, (a) Block Diagram of Proposed RECKF- LQG Servo based SAPF, (b) Proposed Reference Current Generation

to source reference current i^*_{Sabc}. Further subtraction of this source reference i^*_{Sabc} from load current i_{Labc} provides reference compensating current i^*_{Fabc}, which supports the implementation of LQG servo current controller. The whole SAPF is implemented in dq-

reference frame. The LQG servo current controller is designed with a combination of KF and LQR receiving a tracking error between the actual and reference compensating current, which acts as an input to this controller. Then the switching action of IGBT inverter takes place by providing switching pulses through triangular carrier based PWM method realized in abc-reference frame.

The control algorithms in the development of proposed SAPF in two distinct steps namely reference generation and current controller implementation are described subsequently as below.

5.3.2 Proposed Reference Current Generation Scheme

The proposed scheme is based on source reference generation principle and the reference compensating currents i^*_{Fabc} are generated by subtracting the source references i^*_{Sabc} from the load currents i_{Labc} as shown in Fig. 5.2(b). Source reference current generation is implemented by the modulation of the estimated peak value of source current (i_{sm}) with the estimated in phase fundamental components (U_{abc}) of load currents in per unit value, equations of which are provided below.

$$i^*_{Sabc} = i_{sm} \times U_{abc} \tag{5.2}$$

$$i^*_{Fabc} = i_{Labc} - i^*_{Sabc} \tag{5.3}$$

For an accurate estimation of reference current, the unit template U_{abc} must be undistorted and this condition is fulfilled by the estimation algorithm developed by proposed RECKF. Further when load parameter varies, average voltage across the dc link capacitor deviates from its reference value and the real power supplied by the source is not enough to supply the load demand. The SAPF can not immediately respond to the load change since it takes a longer interval to calculate a new reference current. This drawback is overcome by the proposed reference scheme with a fast and adaptive estimation of peak value of source reference current, which has the capability of delivering real power equivalent to conduction and switching losses occurred during capacitor voltage deviation. A PI controller [114][115][116] is usually employed for determining this peak value of reference current and its performance is satisfactory up to steady state level. As a result, it is expected that the proposed reference generation scheme can overcome the demerits of PI control and makes the dc link capacitor voltage

stable at the reference point. This reference estimation approach does not require voltage sensors and synchronisation circuits for hardware, thus it becomes cost effective.

5.3.3 Proposed LQG Servo current controller

LQG servo controller with integral action allows us trade off of regulation/tracker performance and control effort and to take into account process disturbances and measurement noise. To design the proposed LQG servo controller as shown in Fig. 5.3, the following steps are to be performed.
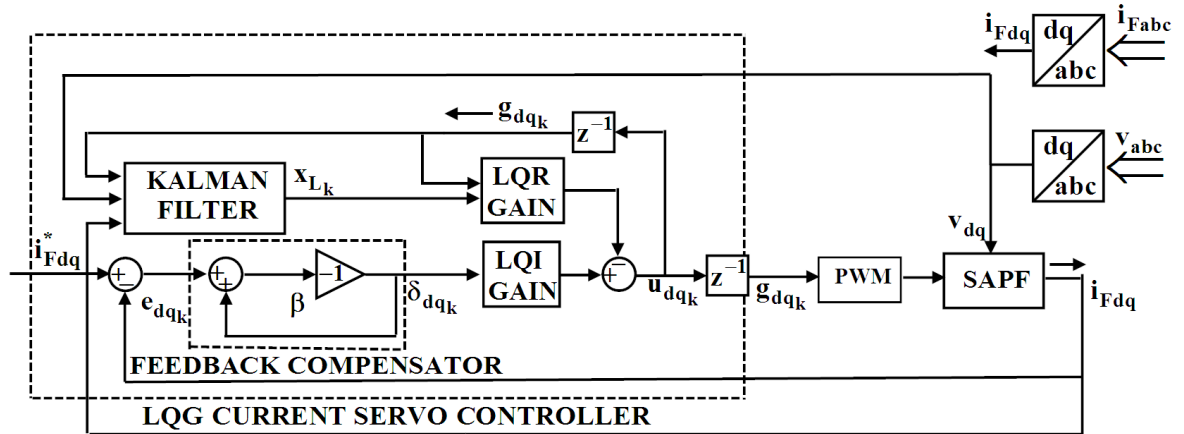
Figure 5.3: Proposed LQG Servo Current Controller Strategy

5.3.3.1 Development of State Space Model of SAPF

The SAPF model in the dq frame can be given in eq (5.4) considering PCC voltage as a disturbance.

$$\frac{di_{Fdq}(t)}{dt} = Ai_{Fdq}(t) + Bu_{dq}(t) + Ev_{dq}(t)$$

$$y_{dq}(t) = Ci_{Fdq}(t)$$

(5.4)

where the specifications for A, B, E and C are as given in Section 4.2.2 in Chapter 4. The discretized representation of the above state space model can be expressed as

$$i_{Fdq_{k+1}} = Gi_{Fdq_k} + Hu_{dq_k} + Zv_{dq_k}$$

$$y_{Fdq_k} = C_l i_{Fdq_k}$$

(5.5)

where

$$
\begin{aligned}
G &= e^{AT_s} = L^{-1}\{(sI - A)^{-1}\}|_{t=T_s} \\
H &= A^{-1}\left(e^{AT_s} - I\right)B \\
Z &= A^{-1}\left(e^{AT_s} - I\right)E \\
C_l &= C
\end{aligned}
\tag{5.6}
$$

5.3.3.2 Construction of Optimal State Feedback Gain

For a full state feedback control design, LQR design seeks to minimize the total transfer of energy from system input to output. The associated Riccati equation solution provides the optimal state feedback controller (K_{LQRm}) that can minimize the cost function of the closed loop system given below.

$$
J_{LQRm} = \frac{1}{2}\sum_{k=0}^{\infty}\{x_{dq_k}^T Q_{LQRm} x_{dq_k} + u_{dq_k}^T R_{LQRm} u_{dq_k}\}
\tag{5.7}
$$

where

$$
x_{dq_k} = \begin{bmatrix} i_{Fd} & i_{Fq} \end{bmatrix}, u_{dq_k} = \begin{bmatrix} u_d & u_q \end{bmatrix}
\tag{5.8}
$$

and Q_{LQRm} is a positive semi definite matrix (state weighting matrix) and R_{LQRm} is a positive definite matrix (control weighting matrix). The entries of matrices Q_{LQRm} and R_{LQRm} are chosen such that fastest dynamic response in SAPF system can be achieved. The gain K_{LQRm} can be obtained by solving the algebraic Riccati equation.

$$
P_{LQRm} = G^T P_{LQRm}(G - HK_{LQRm}) + Q_{LQRm}
\tag{5.9}
$$

which gives

$$
K_{LQRm} = (H^T P_{LQRm} H + R_{LQRm})^{-1} H^T P_{LQRm} G
\tag{5.10}
$$

5.3.3.3 Construction of Kalman State Estimator

For linear systems contaminated with additive noise, KF is found to be an optimum estimator [117][118][119]. In this paper, we need Kalman state estimator for LQG servo

control because we cannot implement LQ optimal state feedback without full state measurement.

The model given in eq (5.5) can be rewritten as

$$x_{dq_{k+1}} = Gx_{dq_k} + Su_{Fdq_k} + w_{i_k}$$
$$y_{dq_k} = Cx_{dq_k} + v_{i_k}$$

(5.11)

where the PCC voltage acts as an input to the estimator. w_{i_k} and v_{i_k} are modeled as white noise and the associated noise covariance matrices are given by

$$E(w_{i_k} w_{i_k}^T) = Q_n, \quad E(v_{i_k} v_{i_k}^T) = R_n$$

(5.12)

and

$$S = [H \quad Z], u_{Fdq_k} = \begin{bmatrix} g_{dq_k} & v_{dq_k} \end{bmatrix}^T$$

(5.13)

where

$$g_{dq_k} = u_{dq_{k-1}}$$

(5.14)

One inherent computational delay is considered within the switch input to the SAPF system due to finite computation time. Here PCC voltage acts as an input to the estimator and its inclusion allows KF to correctly estimate the state values even if it is not controlled.

5.3.3.4 Formulation of Proposed LQG Servo Controller

The proposed LQG servo controller (Fig. 5.3) ensures that the filter output current of SAPF (i_{Fdq}) tracks the reference command (i_{Fdq}^*) while rejecting process disturbances w_i and measurement noise v_i. The servo controller is the combination of optimal Kalman estimator and optimal state feedback controller and both designs are solved separately, based on the "separation principle". The estimator design has already been specified above.

The state space equations of the feedback controller LQR can be specified along with the consideration of computational delay (eq (5.14)) and PCC voltage as a disturbance. From eq (5.5), it can be written as

$$x_{L_{k+1}} = A_L x_{L_k} + B_L u_{dq_k}$$

$$y_k = C_L x_{L_k} \tag{5.15}$$

where

$$x_{L_k} = \begin{bmatrix} i_{Fdq_k} \\ \cdots \\ g_{dq_k} \end{bmatrix} = \begin{bmatrix} i_{Fd_k} & i_{Fq_k} & g_{d_k} & g_{q_k} \end{bmatrix}^T, A_L = \begin{bmatrix} G & \vdots & H \\ \cdots & \vdots & \cdots \\ 0 & \vdots & 0 \end{bmatrix},$$

$$\tag{5.16}$$

$$B_L = \begin{bmatrix} 0 \\ \cdots \\ I \end{bmatrix} = \begin{bmatrix} 0 & 0 & 1 & 1 \end{bmatrix}^T, C_L = \begin{bmatrix} C_l & \vdots & 0 \end{bmatrix} = \begin{bmatrix} 1 & 0 & 0 & 0 \\ 0 & 1 & 0 & 0 \end{bmatrix}$$

The following equations describe servo control laws.

$$u_{dq_k} = K_{LQI} \delta_{dq_k} - K_{LQRm} x_{dq_k} \tag{5.17}$$

$$\delta_{dq_k} = e_{dq_k} \times \beta \tag{5.18}$$

$$e_{dq_k} = i^*_{Fdq_k} - i_{Fdq_k} \tag{5.19}$$

where δ_{dq_k} is the output of the proposed feedback compensator and e_{dq_k} is the tracking error of the SAPF system. β is the gain of feedback compensator and the corresponding gain value is determined as $\left(-\dfrac{1}{2} \right)$. K_{LQI} and K_{LQRm} are the linear quadratic integrator and linear quadratic regulator gains of the proposed LQG servo controller respectively and the values of above gains can be achieved from the solutions of the state space model of LQG Servo controller. Finally the extended state space model of the proposed LQG servo controller equations is given below:

$$x_{servo_{k+1}} = A_{servo} x_{servo_k} + B_{servo} u_{dq_k} \tag{5.20}$$

$$y_k = C_{servo} x_{servo_k} \tag{5.21}$$

$$u_{dq_k} = -K_m x_{servo_k} \tag{5.22}$$

where

$$x_{servo_k} = \begin{bmatrix} i_{Fd_k} & i_{Fq_k} & g_{d_k} & g_{q_k} & \delta_{d_k} & \delta_{q_k} \end{bmatrix}^T \tag{5.23}$$

$$A_{servo} = \begin{bmatrix} A_L & \vdots & 0 \\ \cdots & \vdots & \cdots \\ -C_L A_L & \vdots & 1 \end{bmatrix}, \; B_{servo} = \begin{bmatrix} B_L \\ \cdots \\ -C_L B_L \end{bmatrix} \tag{5.24}$$

$$C_{servo} = \begin{bmatrix} C_L & \vdots & 0 \end{bmatrix}, \; K_m = \begin{bmatrix} K_{LQRm} & \vdots & -K_{LQI} \end{bmatrix} \tag{5.25}$$

5.4 Simulation Results and Discussions

A simulation model for the three phase SAPF (Fig. 5.2) with the same parameters shown in Table 2.1 in Chapter 2 has been developed using MATLAB/Simulink. A triangular carrier based PWM method is employed for driving three phase IGBT inverter. The objective is to verify the robustness of the proposed control scheme under parametric variations of load. The proposed LQG servo controller algorithm was implemented using MATLAB-Function "lqgtrack" in an Embedded MATLAB-Function block that allows simulation of a discrete model.

For the LQR design, weighting matrices Q_{LQRm} and R_{LQRm} are used considering the conventional model of eq (5.5) expanded to include different elements inside the state vector eq (5.23). These values are set to guarantee satisfactory response. These values are first generated through simulation analysis of responses obtained using sim power system in MATLAB/ Simulink. In order to optimize the behavior of chosen output variables, the methodology to set the values of eq (5.26), is based on output indexes i.e., the maximum value for control law, voltage at capacitors, current at inductors, among others. Correlation among state variables is disregarded.

$$Q_{LQRm} = \begin{bmatrix} 0.0031 & 0 & 0 & 0 & 0 & 0 \\ 0 & 0.0035 & 0 & 0 & 0 & 0 \\ 0 & 0 & 0 & 0 & 0 & 0 \\ 0 & 0 & 0 & 0 & 0 & 0 \\ 0 & 0 & 0 & 0 & 0.91 & 0 \\ 0 & 0 & 0 & 0 & 0 & 0.93 \end{bmatrix}, \; R_{LQRm} = \begin{bmatrix} 1 & 0 \\ 0 & 1 \end{bmatrix} \tag{5.26}$$

For Kalman filter design, zero mean white measurement noise is considered. The covariance of measurement noise is set to $R_n = 200A^2$ and arises from the covariance used in the generation of the measurement noise in the simulations. The covariance of the process noise is set to $Q_n = 0.05\,I_{22}A^2$. In fact in practice, both matrices Q_n and R_n can be identified by using whitening techniques as presented in [71].

The simulation results obtained with the proposed RECKF-LQG servo based SAPF are shown in Fig. 5.4 ,5.5 and 5.6 considering two cases of parameter uncertainties of the load (Case-1: Load impedances are at 100% (Base case); Case-2: Load impedances are increased by 100%). Fig. 5.4 presents the steady state performance of SAPF when the load impedances are kept at base value (100%). The supply voltage, load current, compensating current, source current and the capacitor voltage are shown for three phases in top to bottom order. The compensated source current is found to be in phase with the source voltage.

Similar results are found for Case-2 as seen in the respective graphs shown in Fig. 5.5. The robustness of LQG servo controller for the SAPF is analyzed here. The THD of the source current for phase 'a' in both cases when LQG servo controller is used are shown in Fig. 5.6. In Case-1, the source current THD is reduced from 25.6% to 2.23%. When load impedance is increased by 100%, the THD is reduced from 21.9% to 1.98% and also the harmonics compensation ratio (HCR) is differed by only 0.33% as summarized in Table 5.1. However, THDs of the source current are extremely far behind the permissible limit of 5%. As a result, this proposed SAPF model is unaffected by the parametric variations of the load. This shows the robustness of proposed RECKF-LQG servo controller based SAPF under parametric variations of the load. The HCR factor is calculated as follows:

$$HCR = \frac{THD\%\ After\ Compensation}{THD\%\ Before\ Compensation} \times 100\%$$
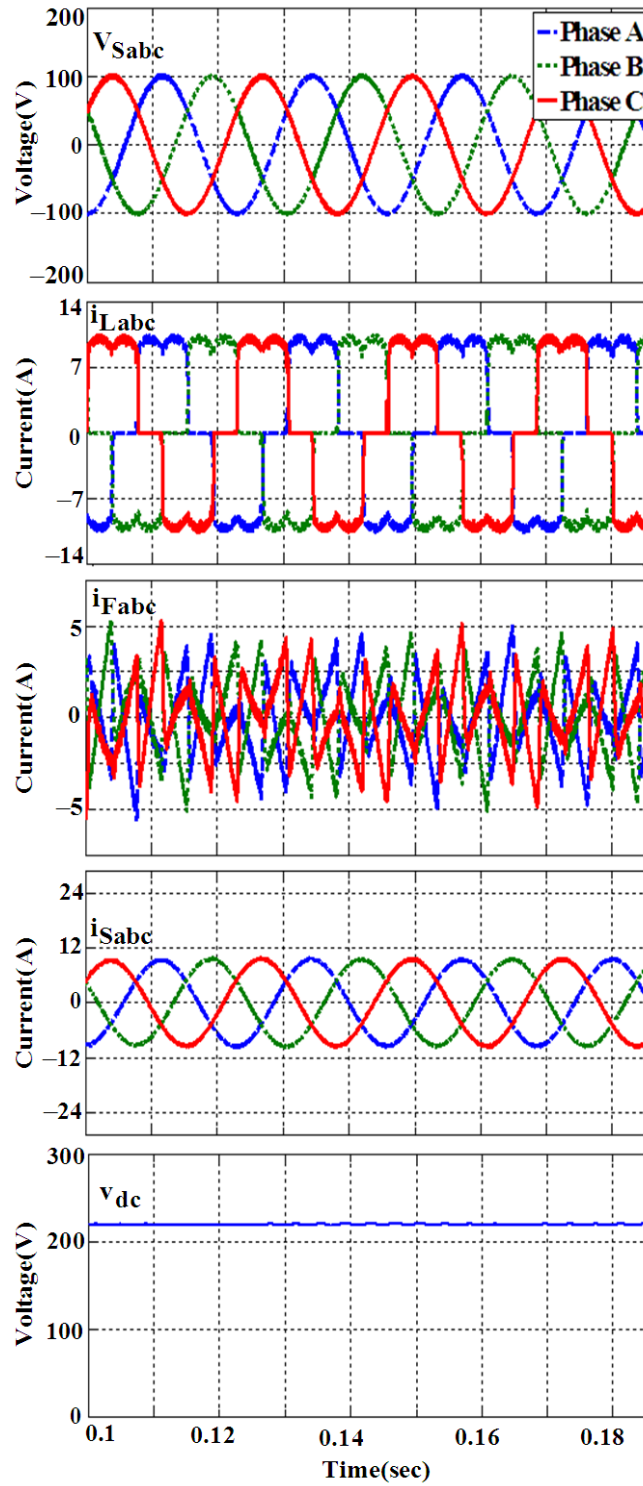
Figure 5.4: Response of RECKF-LQG Servo based SAPF in Case-1 using MATLAB
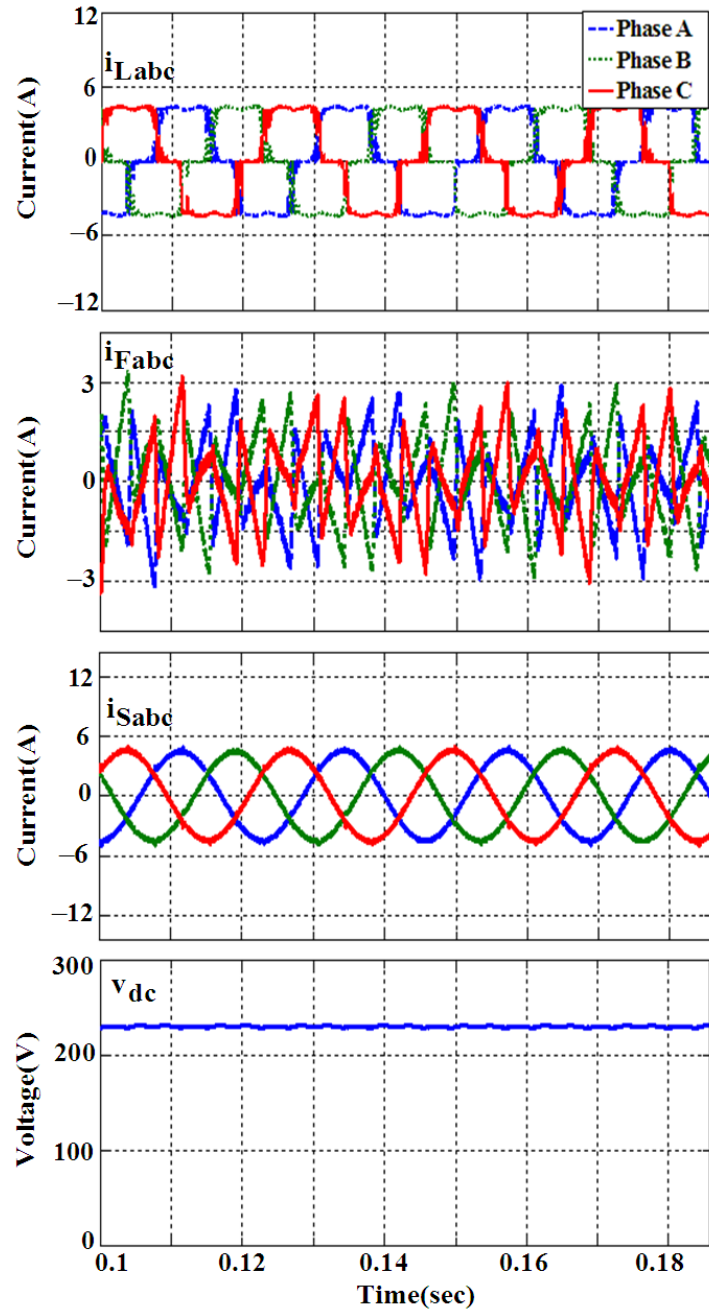
Figure 5.5: Response of RECKF-LQG Servo based SAPF in Case-2 using MATLAB

(i)

(ii)
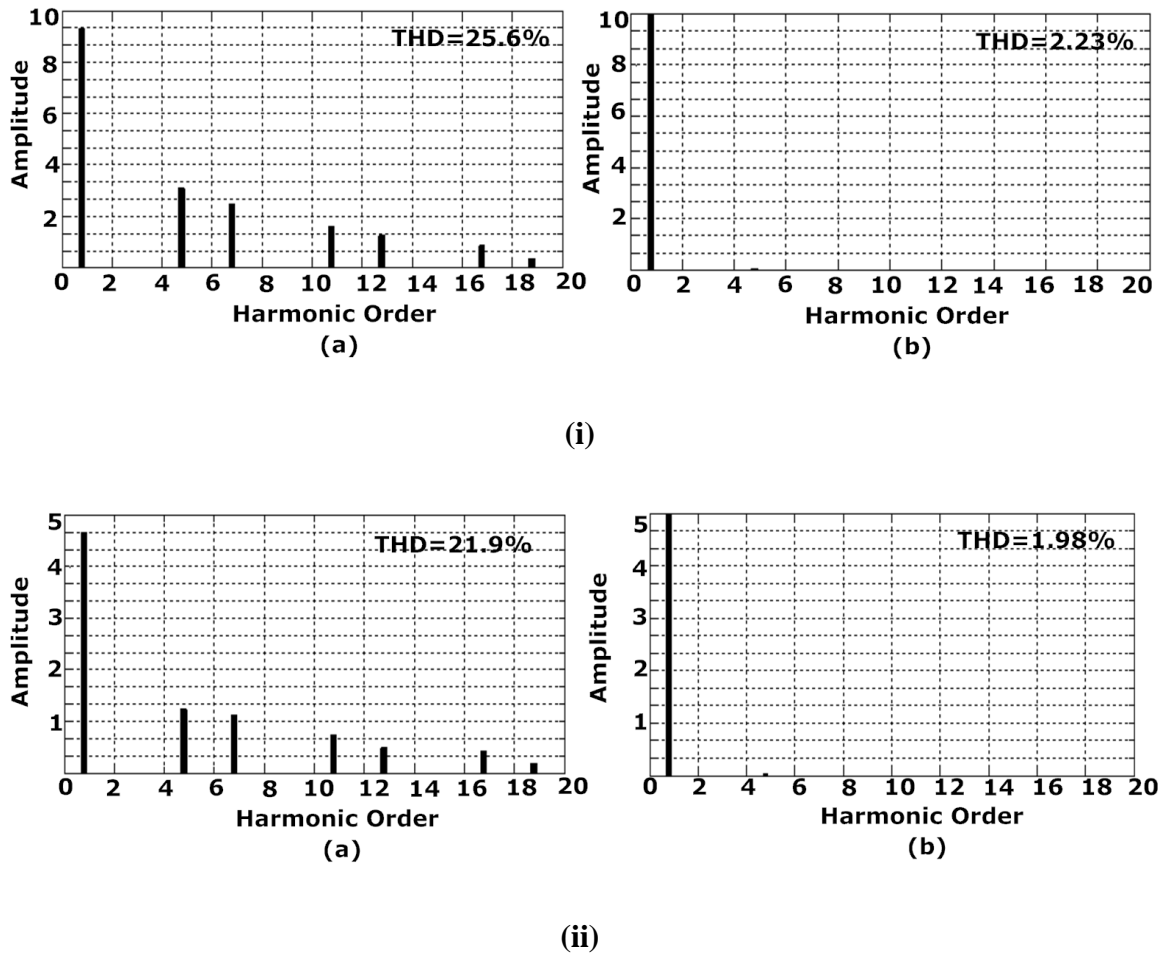
Figure 5.6: Compensation Effect of RECKF-LQG Servo based SAPF using MATLAB,

(i) Case-1, (ii) Case-2

(a) Load current spectrum, (b) Source current spectrum

Table 5.1 THD of the phase-a source current in RECKF-LQG Servo based SAPF

(Simulation)

Cases	THD% of Phase-a Source Current		
	Before Compensation THD (%)	After Compensation THD (%)	Harmonics Compensation Ratio (HCR) (%)
Case-1 (Steady State)	25.6	2.23	8.71
Case-2 (Load impedances are increased by 100%)	21.9	1.98	9.04

Fig. 5.7 shows the waveform of the tracking error signal at the three stages of controller in d-axis frame. From the input and output waveforms of the feedback compensator, it indicates that the compensator is able to reduce the amplitude distortion, noise and is more sensitive to external disturbances in the SAPF system. Hence gain stability and system bandwidth can be improved. Further, larger reduction of error signal at the controller output yields an efficient, robust and stable operation of current controller.
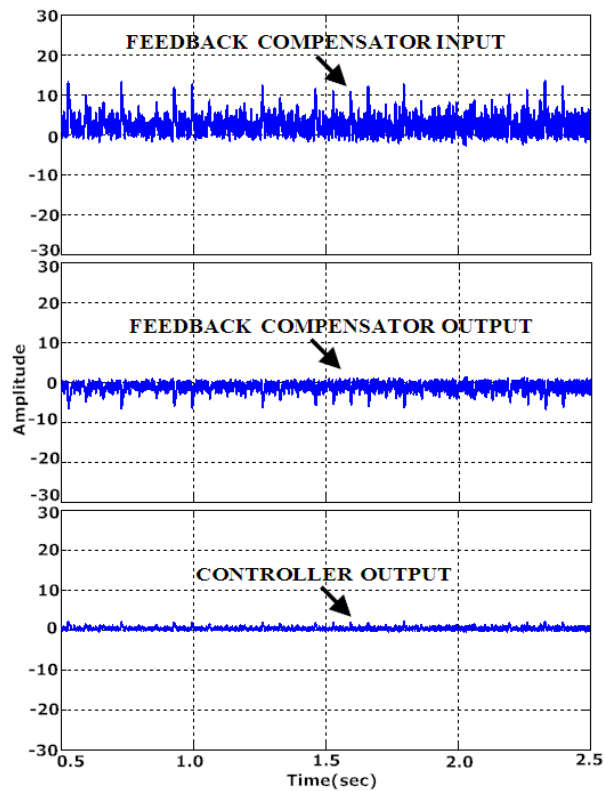
Figure 5.7: Response of Tracking Error Signal

From the above simulation results, it is observed that the proposed SAPF system is not only able to mitigate harmonics to a large extent, but also shows robustness against parameter variations of load. Moreover, this THD is completely satisfactory as compared to RECKF-SMC, RECKF-MPC and RECKF-LQR approach developed in Chapter 2, 3, and 4. This has motivated to develop a prototype experimental set up in our Laboratory using dSPACE DS1104 R & D controller board for validating the effectiveness of the LQG servo controller and the details of experimental implementation have been described in the next section.

5.5   Experimental Implementations

The basic topology of a prototype SAPF developed in the laboratory prototype is presented in Fig. 5.8. This topology is composed of a voltage source inverter (VSI) connected to PCC through filter impedances. A nonlinear load comprising of a three phase diode bridge rectifier with RL load is considered. The control of SAPF is achieved by LQG servo controller based algorithm implemented with dSPACE1104. The interface between MATLAB/Simulink and dSPACE1104 permits running the control algorithm. The dSPACE-CLP1104 combined connector panel acts as an interface between the input-output signals and the DS1104 R & D controller card. All computational tasks are processed by the DS1104 R & D controller card which is connected to the host PC where all the control is handled. The switching signals generated from the PWM port of
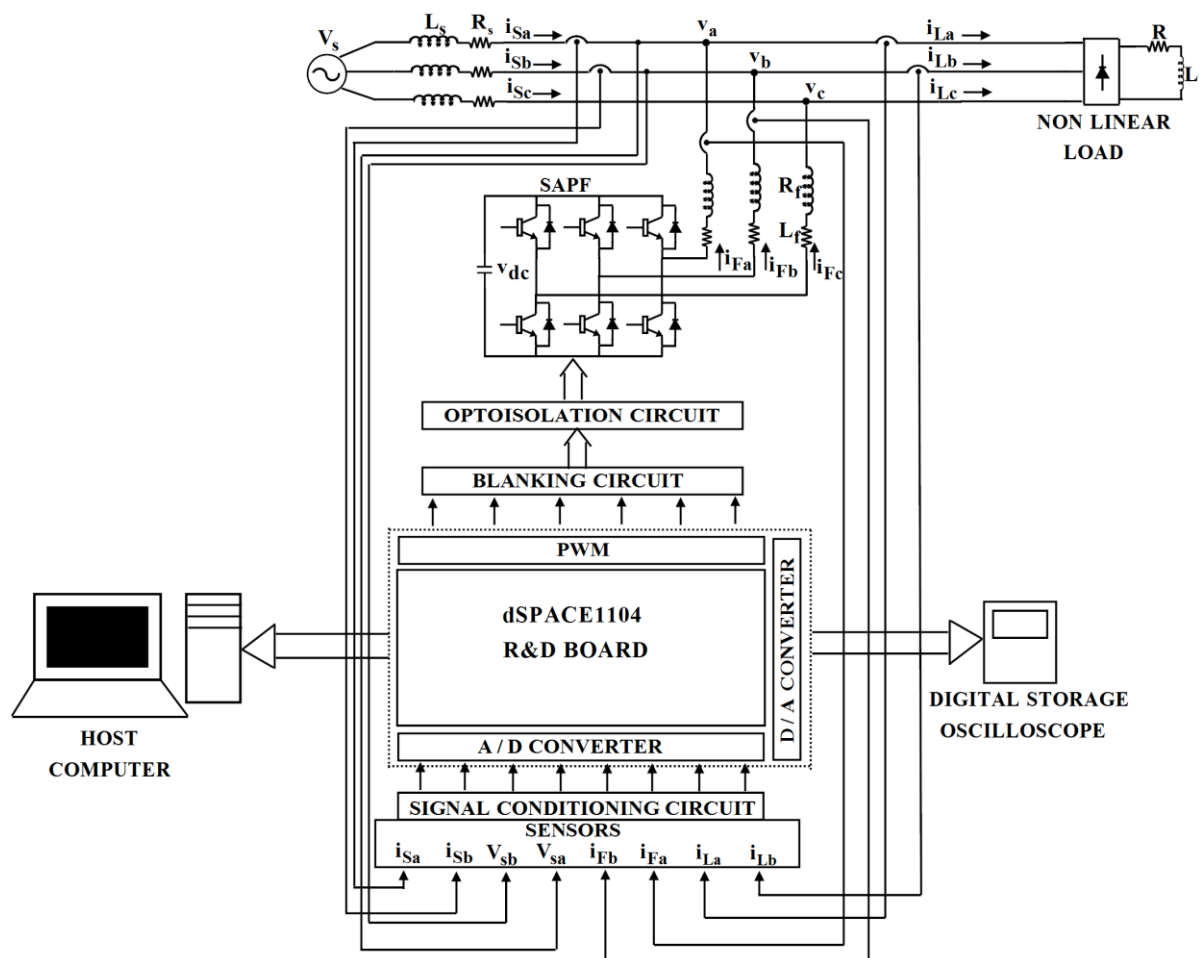
Figure 5.8: Control and Power Circuit of SAPF

CLP1104 connector panel are fed to blanking circuit and opto-isolation circuit, which finally provide gate pulses for the three phase insulated IGBT bridge, where the PWM frequency is set to 12.5 kHZ . The dead time for each leg of IGBT is set to 4 µs. The compensating currents (i_{Fa}, i_{Fb}) of phase 'a' and 'b' are sensed using Hall effect current sensors and then fed to the A/D converter (ADC) port of CLP1104 panel after passing through signal conditioning circuit. Since it is a three wire system, phase 'c' current can be calculated as $i_{Fc} = -(i_{Fa} + i_{Fb})$. Similarly the source currents and load currents for phase 'a' and 'b' are sensed. To sense the voltage signals of phase 'a' and 'b', two voltage sensors are used. The D/A converter (DAC) ports are provided for observing desired results through Digital Storage Oscilloscope (DSO). A photograph of the experimental setup is shown in Fig. 5.9.
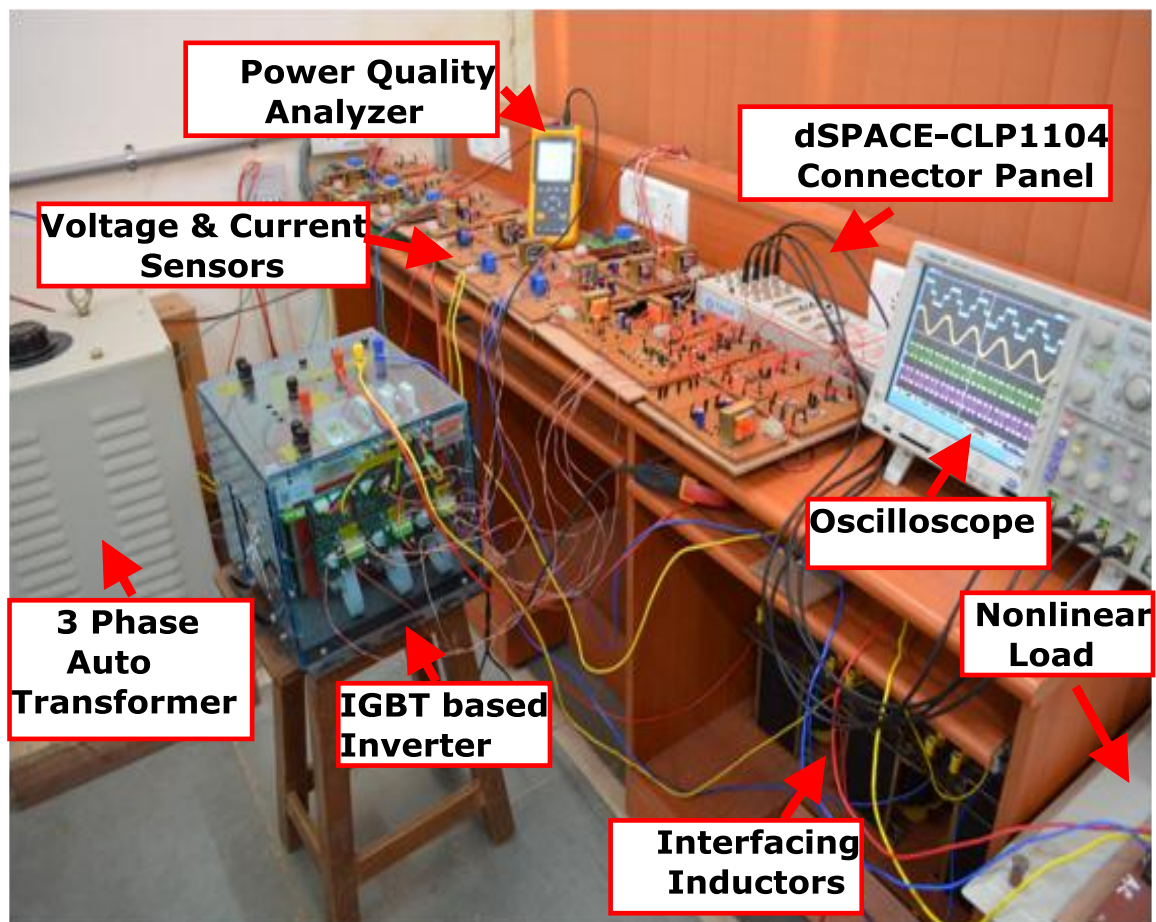
Figure 5.9: Experimental Setup

This experimental setup is composed of the following components.

- Control Platform:
    - dSPACE-1104 R & D Controller Board
    - Connector panel CLP1104

- Three-phase IGBT based inverter with following specifications:
    - IGBT module: SKM150GB12V (3 nos)
    - IGBT drivers: SKYPER 32R (3 nos)
    - DC-link: Semikron made 4700 µF/450 V (2 nos)
    - Input DC voltage: 600V
    - Output AC voltage: 415V 3- ϕ
    - Output Current: 35A max
    - Output Frequency: 50 Hz
    - Switching Frequency: 25 kHz max

- Three-phase Auto-transformer:
    - Max. Current capacity: 28A per phase
    - Voltage Range: 0-415V
    - Over-voltage Range: 0-470V

- The measuring system includes:
    - Voltage Transducer-LEM LV 25-P [120]
    - Current Transducer-LEM LA 55-P [121]

- Nonlinear Load:
    - Three-phase Diode Bridge Rectifier with a series RL load (R=0-100Ω, L=0-30mH)

- Interfacing Inductors

- Blanking Circuit

- Opto-isolation Circuit

- DC Power supply:
    - $\pm$ 15V DC supply
    - 5-0-5V DC supply

- Power Quality Analyzer (Single Phase-Fluke 43b)

The detail overviews of above components are presented in the next section.

5.5.1 dSPACE Control Platform

DSPACE^R provides complete solutions for electronic control unit (ECU) software development. It is a powerful development tool for dedicated services in the field of function prototyping, target implementation, and ECU testing. Real time control systems can be built using dSPACE and the control logic can be implemented. The dSPACE works on Matlab/Simulink platform which is a common engineering software and easy to understand. Another feature of the dSPACE is the Control desk which allows the graphical user interface. Through the control desk the user can observe the response of the system. Real-time Interface (RTI) is the link between dSPACE's real-time systems and the development software MATLAB/Simulink from the Math Works. It extends Real-Time Workshop (C-code generation) for the seamless and automatic implementation of our Simulink Models on the dSPACE Real-time Hardware. This allows us to concentrate fully on the actual design process and to carry out fast design iterations.

To implement a real-time control loop using dSPACE and MATLAB we need following items.

1. dSPACE DS1104 R&D Controller Board
2. Connector Panel CLP1104

5.5.1.1 dSPACE DS1104 R&D Controller Board

The DS1104 R&D Controller Board is a standard board that can be plugged into a PCI slot of a PC shown in Fig. 5.10. The DS1104 is specifically designed for the development of high-speed multivariable digital controllers and real-time simulations in various fields. It is a complete real-time control system based on a 603 Power PC floating-point processor running at 250 MHz. For advanced I/O purposes, the board includes a slave-DSP subsystem based on the TMS320F240 DSP microcontroller. For purposes of rapid control prototyping (RCP), specific interface connectors and connector panels described below provide easy access to all input and output signals of the board. Thus, the DS1104 R&D Controller Board is the ideal hardware for the dSPACE Prototype development system for cost-sensitive RCP applications. It executes all computational and control tasks for the shunt connected converter.

Figure 5.10: DS1104 R&D Controller Board

A schematic description of the features input and output ports of the DS1104 Board are given in Fig. 5.11. Some of the main features of the board include the main processor, a PowerPC 603e with a 250MHz CPU clock frequency and a slave DSP from Texas instruments (DSP TMS 320F240). The dSPACE1104 board also consists of Digital I/O ports, Slave I/O PWM ports, ADC and DAC channels, an incremental encoder interface and a UART interface. In this Chapter, the Slave I/O ports as well as the ADC channels are used. The technical details of the board are described below.
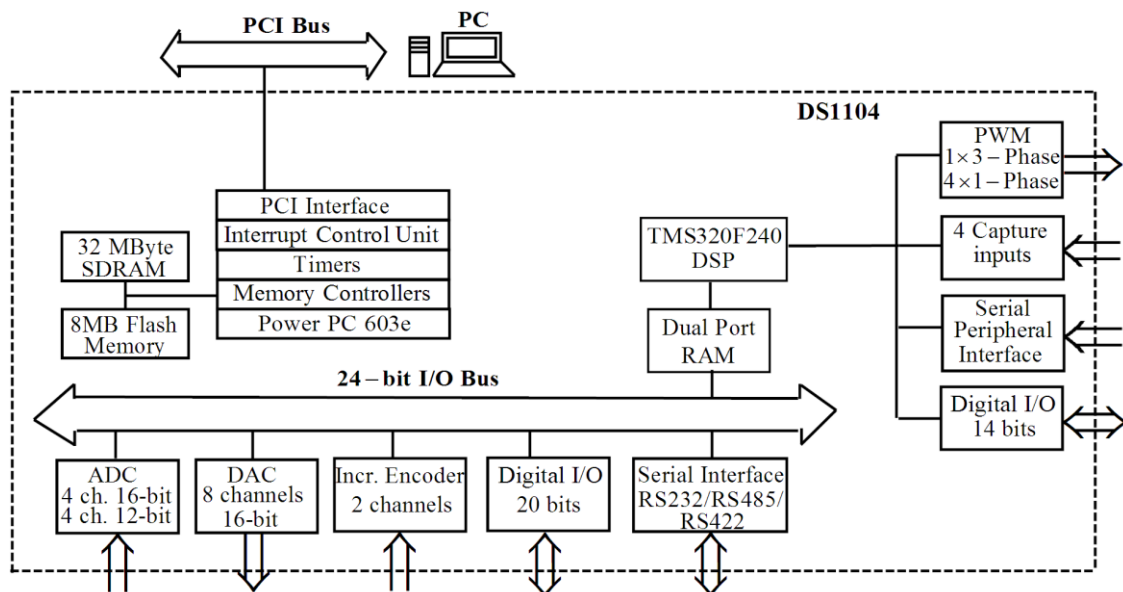
Figure 5.11: Features of the DS1104 R&D Controller Board

Technical Details:

- **Main Processor**
    - MPC8240, PowerPC 603e core, 250 MHz
    - 32 kByte internal cache

- **Timers**
    - 1 sample rate timer, 32-bit downcounter
    - 4 general purpose timers, 32 bit
    - 64-bit time base for time measurement

- **Memory**
    - 32 MByte synchronous DRAM (SDRAM)
    - 8 MByte boot flash for applications

- **Interrupt Control Unit**
    - Interrupts by timers, serial interface, slave
      DSP, incremental encoders, ADC, host PC
      and 4 external inputs
    - PWM synchronous interrupts

- **Analog Input**
    - 4 ADC inputs, 16 bit, multiplexed
    - ± 10 V input voltage range
    - 2 µs sampling time
    - 80 dB signal-to-noise ratio
    - 4 ADC channels, 12 bit
    - ± 10 V input voltage range
    - 800 ns sampling time
    - > 65 dB signal-to-noise ratio

- **Analog Output**
    - 8 channels, 16 bit, 10 µs max. settling time
    - ± 10 V output voltage range

- **Incremental Encoder Interface**
    - Two digital inputs, TTL or RS422
    - 24-bit digital incremental encoders
    - Max. 1.65 MHz input frequency, i.e. fourfold pulse counts up to 6.6 MHz
    - 5V / 0.5 A sensor supply voltage

- **Digital I/O**
    - 20-bit digital I/O (bit-selectable direction)
    - ± 5 mA output current

- **Serial Interface**
    - Serial UART (RS232, RS485 and RS422)

- **Slave DSP Subsystem**
    - Texas Instruments' DSP TMS320F240
    - 4 kWord of dual-port RAM
    - Three-phase PWM outputs plus
    - 4 single PWM outputs
    - 14 bits of digital I/O (TTL)

- **Physical Characteristics**
    - Power supply 5 V, 2.5 A / -12 V, 0.2 A / 12 V, 0.3 A
    - Requires one 32-bit PCI slot

5.5.1.2 The CLP1104 Combined Connector/ LED Panel

Specific interface connector panels provide easy access to all the input and output signals of the DS1104 R&D Controller Board.The CLP1104 Connector Panel provides easy-to-use connections between the DS1104 R&D Controller Board and devices to be connected to it. Devices can be individually connected, disconnected or interchanged without soldering via BNC connectors and Sub-D connectors. This simplifies system construction, testing and troubleshooting. Fig. 5.12 shows the dSPACE CLPI104 Panel
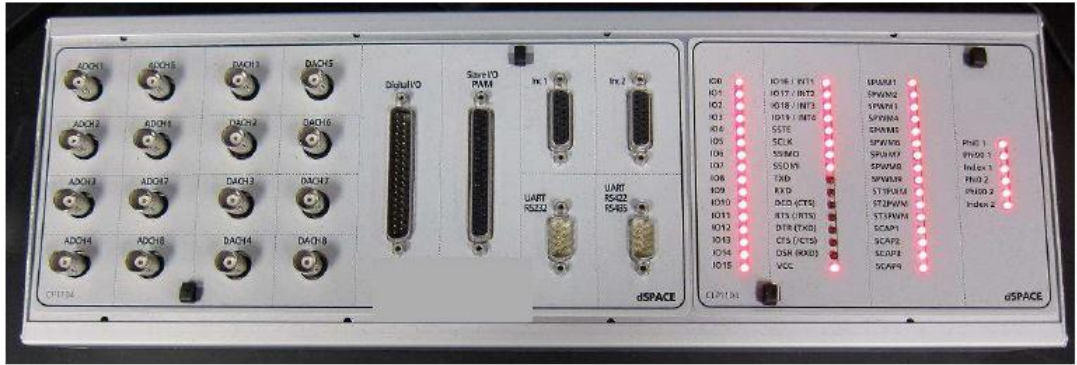
Figure 5.12: CLP1104 Connector/LED Panel

and the LED panel on the right of the board indicates the state of the ports and is very useful for debugging. The currents and voltage signals are taken into the DS1104 using BNC connectors CP1-CP8 on the CLP1104 connector panel.The analog signal inputs are shown in Table 5.2. The PWM signals can be connected using a CP18 Sub- D connector. Table 5.3 represents the output of digital signal used for PWM.

Table 5.2 Analog Signal Input

Channel	1	2	3	4	5	6	7	8
Signal	V_{sa}	V_{sb}	i_{Sa}	i_{Sb}	i_{La}	i_{Lb}	i_{Fa}	i_{Fb}

Table 5.3 Slave I/O PWM Connector (CP18)

Pin	Signal	Pin	Signal
7	SPWM1	26	SPWM2
8	SPWM3	27	SPWM4
9	SPWM5	28	SPWM6

5.5.2 Three-phase IGBT based inverter

The inverter consists of three Semikron IGBT modules (SKM150GB12V). These lGBTs are driven by SKYPER 32R drivers, which get their switching signals from the CLPI104 panel via blanking and optoisolation circuit [122]. The gate driver controls the dynamic behavior of IGBT and its short circuit protection. The interlocking time between the input signals is 4µs. Two capacitors are connected in the series in DC side to have equivalent capacitance of 2350 µF/900V. All the above components are encapsulated in acrylic case for protection from electrical shock as shown in Fig. 5.13.
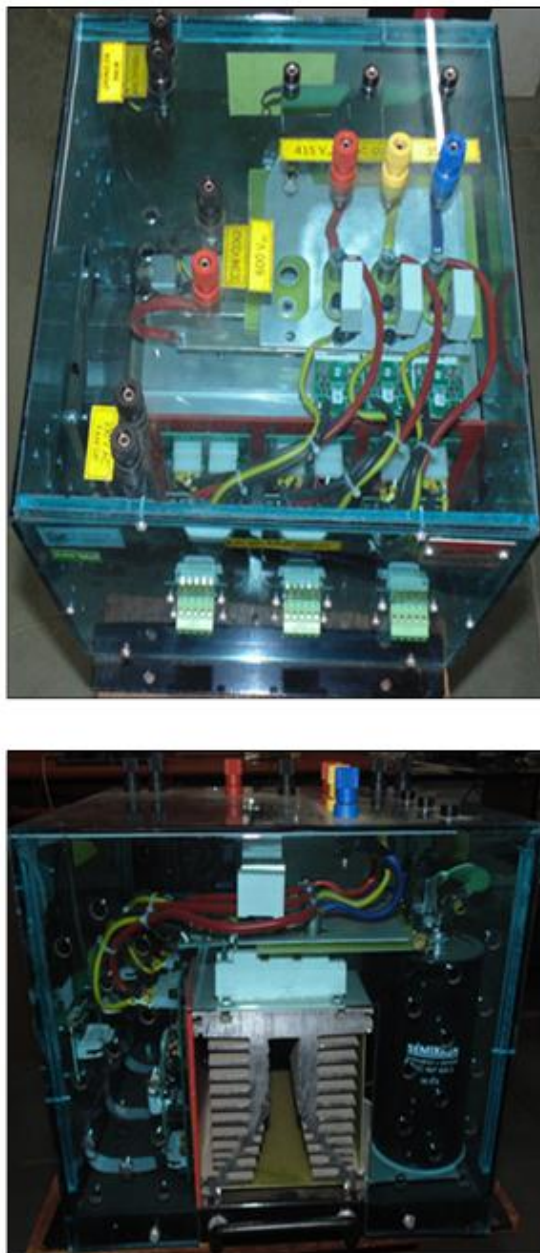
Figure 5.13: Three-phase IGBT based inverter

5.5.3 Three-phase Auto-Transformer

A layout of three-phase auto transformer is shown in Fig. 5.14, which provides a variable AC supply. Hence we can test the SAPF model with different supply voltages. Supply voltage can be varied from 0 to 415V with a maximum current capacity of 28A.

Figure 5.14: Three-phase Auto-Transformer

5.5.4 Transducer Circuits

Hall effect current and voltage transducer circuits measure high currents and voltages and transform them to a low voltage signal. These transducers offer many advantages. Some of these are:

- Very good linearity
- Low temperature drift
- Excellent accuracy

With knowledge of the magnitude of the currents and voltages to be measured, tranducer circuits are selected. Thus, the LEM LV 25-P and the LEM LA 55-P are used as voltage and current transducers respectively and the schematic diagrams of which are represented in Fig. 5.15 and Fig. 5.16 respectively. Both transducers require a $\pm 15V$ supply voltage as well as external resistors to determine the ratio between the input signal and the output signal. This ratio is determined by the magnitude of the maximum current or voltage that must be measured on the primary side of the tansducer circuits as well as
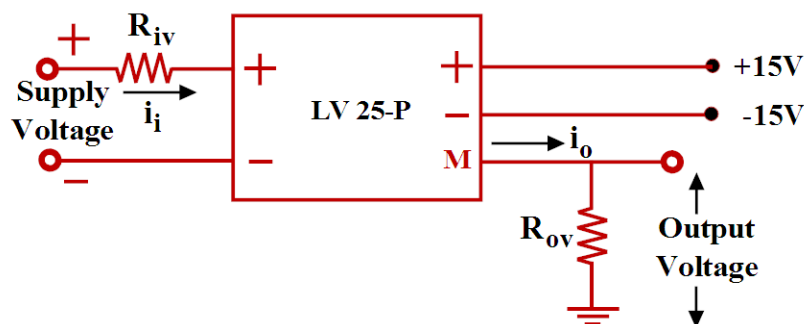
Figure 5.15: Schematic Diagram of Voltage Sensor
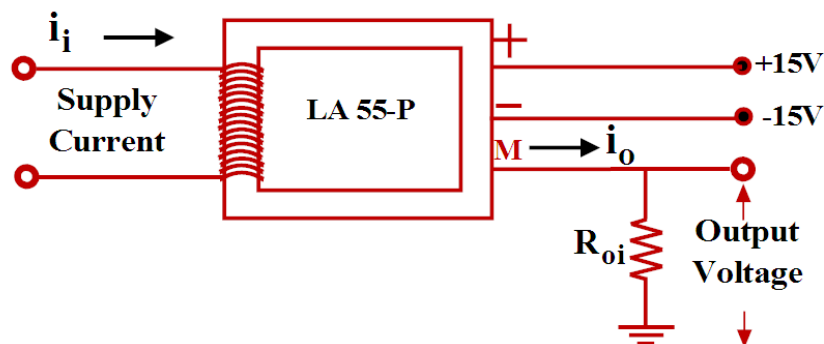
Figure 5.16: Schematic Diagram of Current Sensor

by the magnitude of the desired output voltages on the secondary side. The transducer circuits provide isolation between the power network and the signal level circuits. The output signals must be restricted to $\pm 10\text{V}$, which is the maximum allowable voltage of the ADC of the DS 1104 Controller board.

5.5.4.1 Design of Voltage Transducer Circuit

In the experimental set up, the supply voltage is scaled down from $\pm 100\text{V}$ to the $\pm 10\text{V}$ range. Referring the data sheet of the transducer [120], the input resistance R_{iv} is chosen so as to fall the output resistance R_{ov} in the range of 100-350Ω.

The input current i_i can be obtained from $v_i = 100\text{V}$ and $R_{iv} = 15\text{k}\Omega$.

$$i_i = \frac{v_i}{R_{iv}} = \frac{100}{15 \times 10^3} = 6.67\text{mA} \tag{5.27}$$

With conversion ratio of 2500:1000 for transducer, the output current is calculated as

$$i_o = i_i \times \frac{2500}{1000} = 6.67 \times 2.5 = 16.67\text{mA} \tag{5.28}$$

The output resistance is chosen to be 300 Ω so that transducer output voltage lies in the range of $\pm 10\text{V}$ and hence the transducer output voltage becomes,

Output voltage= $R_{ov} \times i_o = 300 \times 16.67 \times 10^{-3} = 5\text{V}$ \hfill (5.29)

5.5.4.2 Design of Current Transducer Circuit

A current of $\pm 10\text{A}$ in the power network is converted to $\pm 10\text{V}$. The number of primary turns (N_p) is chosen such that the output resistance falls in the range of 50-160 Ω as specified in the datasheet of transducer [121].

With conversion ratio of 1:1000, $N_p = 5$ and $i_i = 10\text{A}$, the output current can be computed as

$$i_o = N_p \times i_i \times \frac{1}{1000} = \frac{5 \times 10}{1000} = 0.05\text{A} \tag{5.30}$$

The output resistance is chosen to be 100 Ω so that transducer output voltage lies in the range of $\pm 10\text{V}$ and hence the transducer output voltage becomes,

Output voltage$= R_{oi} \times i_o = 100 \times 0.05 = 5V$ (5.31)

5.5.4.3 Signal Conditioning Circuit

The low level voltage signals ($\pm 5V$) obtained from the voltage and current transducers are passed through the signal conditioning circuit (Fig. 5.17) to make them compatible with the ADC channel of dSPACE-1104 connector panel ($\pm 10V$). OPAMP TL064 has been used in this signal conditioning circuit and a DC supply of $\pm 15V$ is applied.
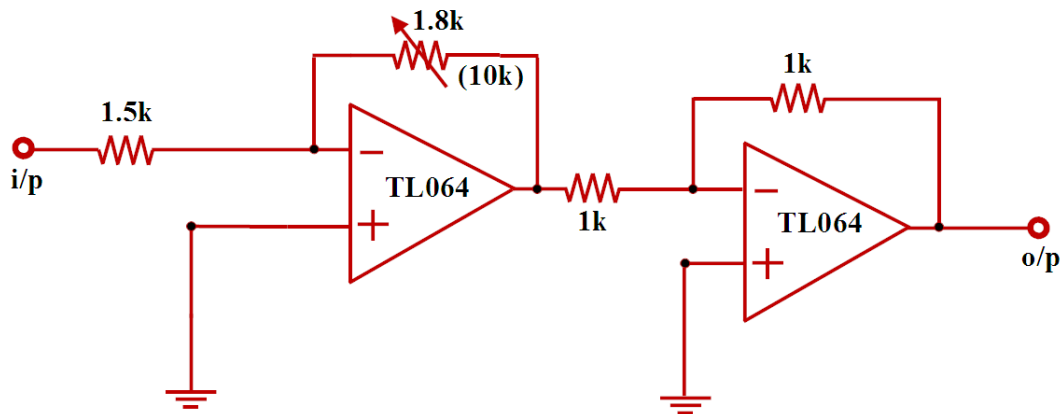
Figure 5.17: Schematic Diagram of Signal conditioning Circuit

5.5.5 Non-Linear Load

An assembly of nonlinear load is provided in Fig. 5.18, which is consisting of a three phase diode bridge rectifier (Fig. 5.18(a)), a resistive load (Fig. 5.18(b)) and an inductive load (Fig. 5.18(c)). The resistive and inductive loads are connected in series with the rectifier bridge. The load current can be changed with a variation of resistance (0-100Ω) of resistive load since there are ten different tapping available in this load. The same numbers of tapping are also available in the inductor to vary the load inductance from 0 to 30 mH.

5.5.6 Interfacing Inductors

A picture of three filter inductors is shown in Fig. 5.19. The inductors have maximum current capacity of 25A and we can change the value of inductance from 0 to 30mH with the usage of ten numbers of tapping. The inductance value is chosen according to the power circuit design of SAPF already prescribed in Section 2.2.4.1 in Chapter 2.

(a)

(b)
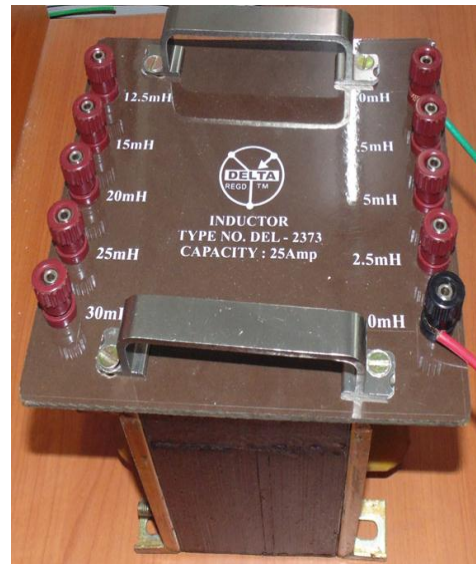
(c)

Figure 5.18: Nonlinear Load, (a) Three-phase diode bridge rectifier, (b) Resistive Load, (c) Inductor

Figure 5.19: Filter Inductor

5.5.7 Blanking Circuit

The switching pulses generated from the PWM port of dSPACE CLP-1104 panel are not directly fed to the IGBT switches of inverter. They are passed through the blanking circuit to avoid short circuit of the dc-link capacitor during the turning ON and OFF of both switches in the same leg of inverter. Hence, a dead band time is provided between turning ON and turning OFF of the switches in the same leg. Fig. 5.20(a) shows the blanking circuit used for phase 'a'. Its inputs are the switching pulses S_a and $\overline{S}_a$ generated from the dSPACE1104. The detailed circuit diagram for two channels of the blanking circuit using mono-stable multi-vibrator (SN74LS123) is shown in Fig. 5.20(b). This unit generates two shot pulses S_{as} and $\overline{S}_{as}$ with a duration of t_d. The gate signal G_a is generated by ANDing S_a and S_{as} using IC 7408 and passing this signal through a buffer (CD4050). Similarly, the complementary gate signal $\overline{G}_a$ can be achieved. The timing diagram of the blanking circuit including signals $S_a, \overline{S}_a, S_{as}, \overline{S}_{as}$, G_a and $\overline{G}_a$ is depicted in Fig. 5.20(c).

The expression for obtaining dead beat time 't_d' of mono-stable multi-vibrator [123] is given as follows.

$$t_d = 6 + 0.05C_{E1} + 0.45R_{E1}C_{E1} + 11.6R_{E1} \tag{5.32}$$

where, R_{E1} and C_{E1} are the external resistance and capacitance in kΩ and pF respectively. In this experiment, a dead beat time of 4μs is chosen by considering the values of R_{E1} and C_{E1} as 18 kΩ and 470 pF respectively in the above eq (5.32).

5.5.8 Opto-isolation Circuit

The gate signals obtainable from the blanking circuit can't be directly applied to the gates of the IGBT switches which consist of the high power network. Hence, high speed optocouplers (ICHCPL2601) with isolated dc power supplies are used for providing isolation between the logic control units and the power network. The schematic diagram of optocoupler circuit [124] is presented in Fig. 5.21.
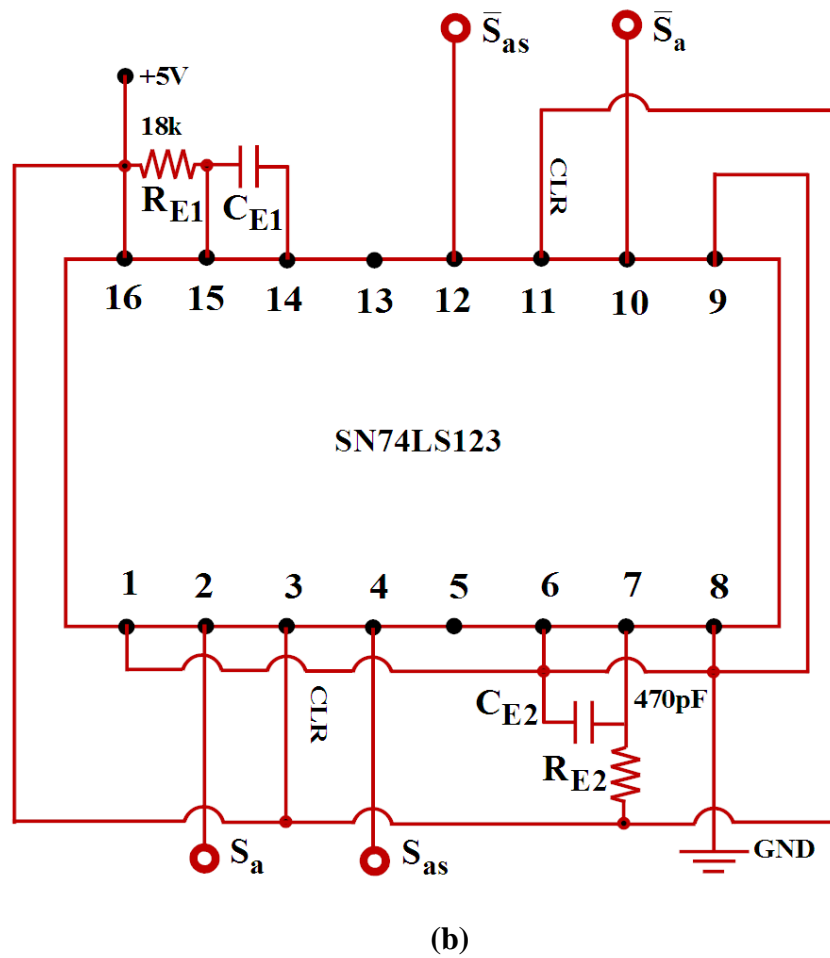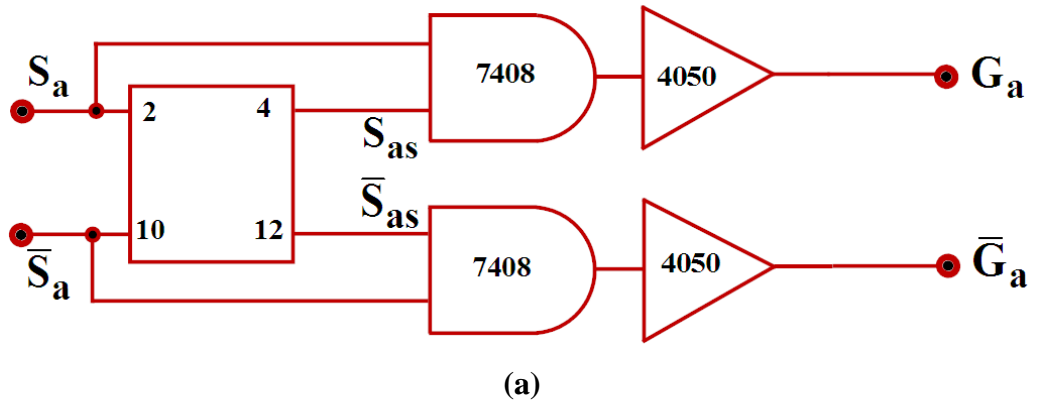
Figure 5.20: Blanking Circuit, (a) Schematic circuit diagram, (b) Monostable multivibrator circuit connection diagram, (c) Timing diagram
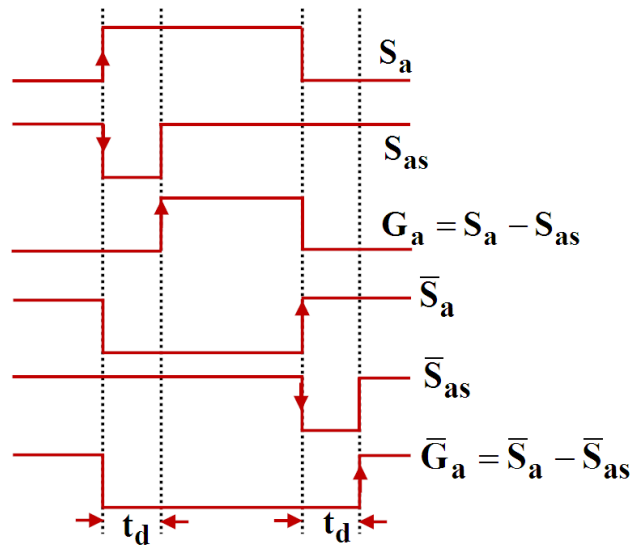
(c)

Figure 5.20: Continued
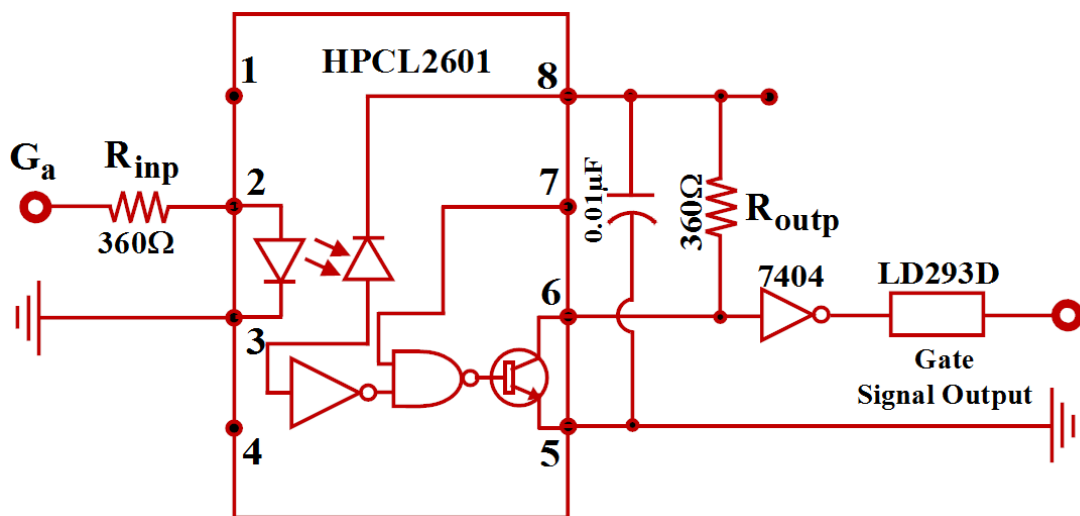
Figure 5.21: Opto-Coupler Circuit

5.5.9 DC Power Supply

The DC regulated power supplies of different voltage levels are required for implementing the experimental set up. A 230/18-0-18 V centre-tapped step-down transformer of 750 mA rating is used for generating a ± 15V bipolar dc regulated supply as shown in Fig. 5.22. A full-bridge diode rectifier (IN4007) consisting of four diodes D1-D4, is utilized for converting ac voltage into dc. Two equal electrolytic capacitors (

C_{dc}) of value 2200µF are used to smoothen the output voltage. The centre tap of the transformer and the mid-point of the capacitors are connected to the ground. The unregulated dc voltages +15V and -15V are given as input to the positive voltage regulator IC7815 and negative voltage regulator IC7915 respectively to generate dc output voltages of $\pm$ 15V. Further to generate a +5 V dc supply, a 230/9-0-9 V centre-tapped step-down of 750 mA and positive voltage regulator of IC7805 are used.
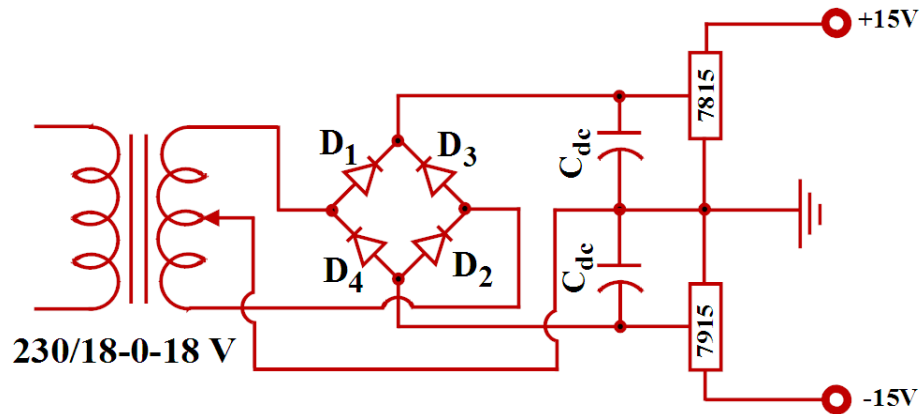
Figure 5.22: DC regulated power supply

5.6   Experimental Results and Discussions

The proposed RECKF-LQG servo control algorithm has been implemented in real-time on the experimental set up developed in our Lab. The efficacy of the proposed scheme is verified with the obtained experimental results. Two cases of parametric variations of nonlinear load are considered and the performance of the control algorithm is presented in the following sections. The design specifications and circuit parameters in laboratory prototype are same as employed for simulation study mentioned in Table 2.1 of Chapter 2.

Case 1: Load Impedances are 100% (Base Case):

The performance of RECKF-LQG servo controller is analyzed with the base case load impedance (R=20 Ω, L=10mH). A diode bridge rectifier with a resistive-inductive load is chosen as the test load to study the operation of SAPF for load compensation. Fig. 5.23 and Fig. 5.24 show the load currents (i_{La}, i_{Lb}, i_{Lc}) and compensating currents (i_{Fa}, i_{Fb}, i_{Fc}) in phase a, b and c respectively. The overall performance of the LQG servo

controller is shown in Fig. 5.25. The waveforms shown in this figure are phase-a source voltage, compensating current, source current and dc bus voltage. The three phase source currents (i_{Sa}, i_{Sb}, i_{Sc}) are found to be almost sinusoidal as depicted in Fig. 5.26. The harmonic spectra are analyzed using power quality analyzer and the recorded harmonic spectra for uncompensated as well as compensated phase 'a' current are shown in Fig. 5.27. The THD in the load current is as high as 27.9%, but the THD in the source current has been lowered to 2.5%. A wide reduction of %THD is due to good tracking characteristics of the current references of SAPF.

Case 2: Load Impedances are increased by 100%:

In this case, the load impedances have been increased by 100% from the base case without alternating any other parameters of the system. Fig. 5.28 shows the three phase load currents, where the amplitude is reduced by 4A as compared to Case-1. The source voltage is kept at 100V and the dc link voltage is maintained at 220V. Fig. 5.29 shows the compensation characteristics of SAPF. Fig. 5.30 shows the three phase source currents which are all balanced and sinusoidal in the proposed SAPF. The harmonic spectra are evaluated for phase-a source current before and after compensation in Case-2, which are shown in Fig. 5.31.The THD of the load current is reduced up to an extent of 2.2%.
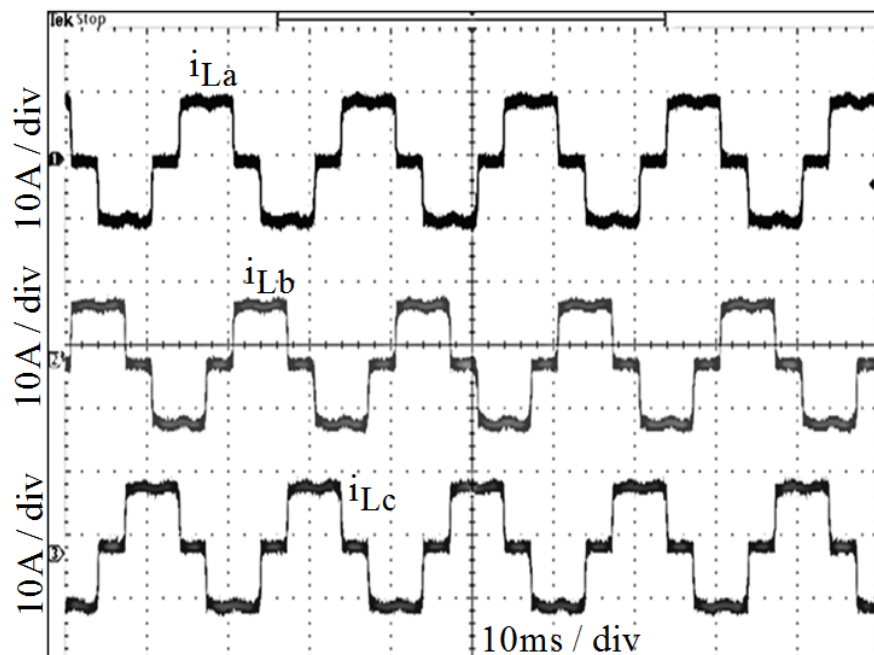
Figure 5.23: Waveforms of three phase load currents in Case-1
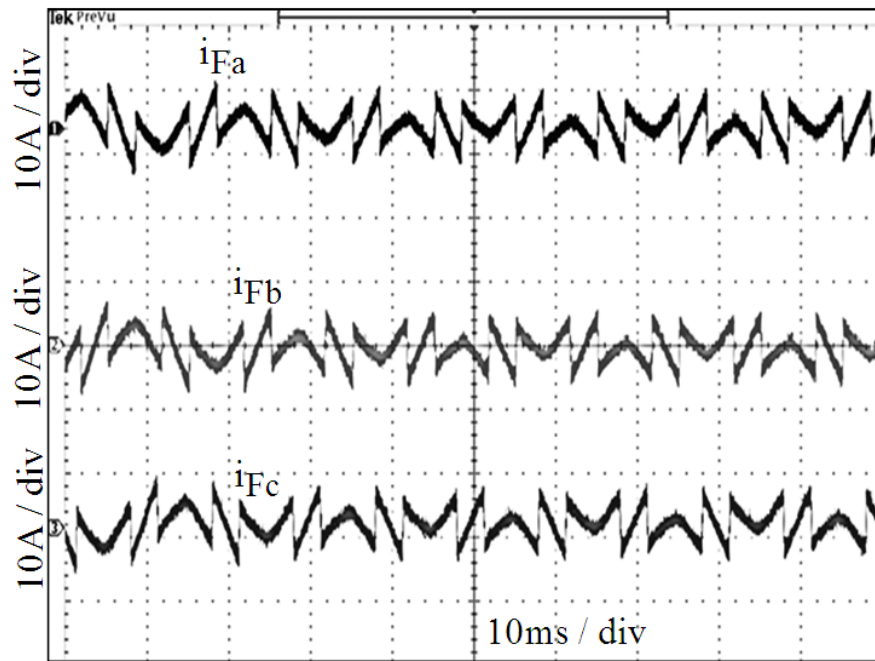
Figure 5.24: Waveforms of three phase compensating currents in Case-1
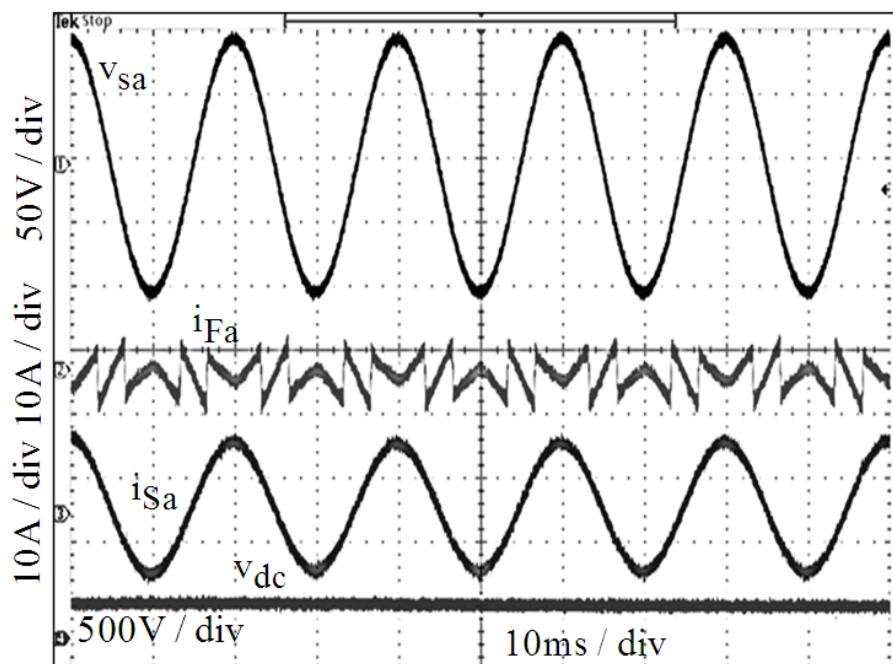
Figure 5.25: Waveforms showing phase-a quantities in Case-1
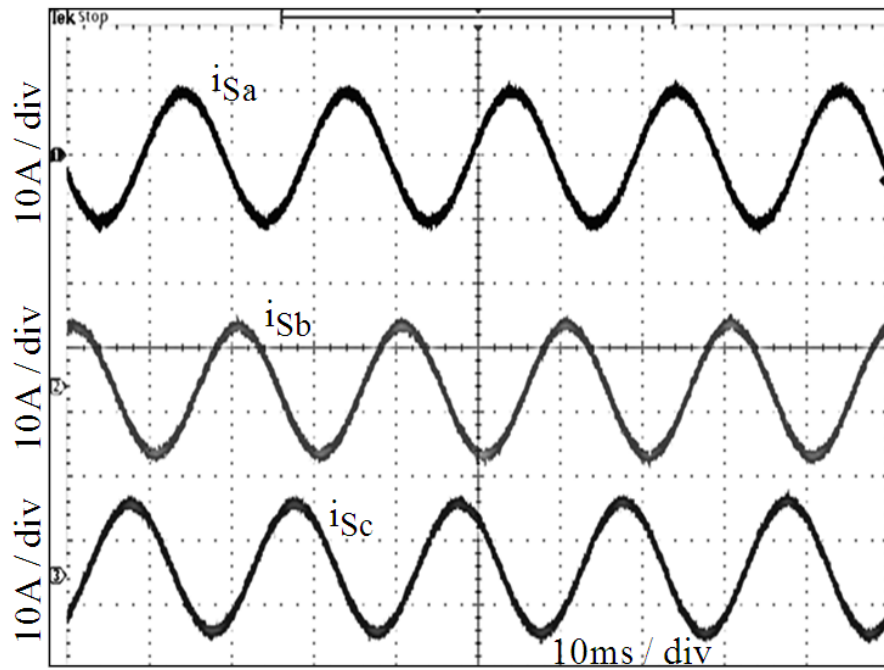
Figure 5.26: Waveforms of three phase source currents in Case-1
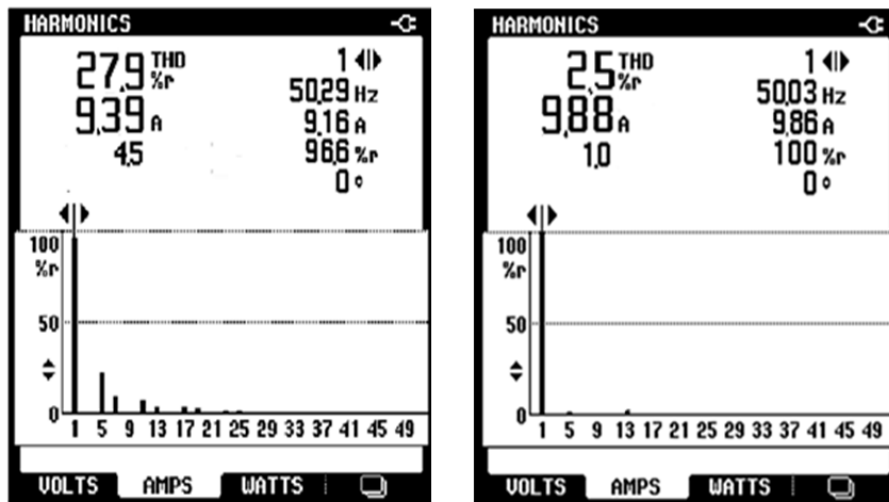
(a)

(b)

Figure 5.27: Harmonic spectra of (a) phase-a load current, (b) phase-a source current of proposed RECKF-LQG Servo based SAPF in Case-1

124
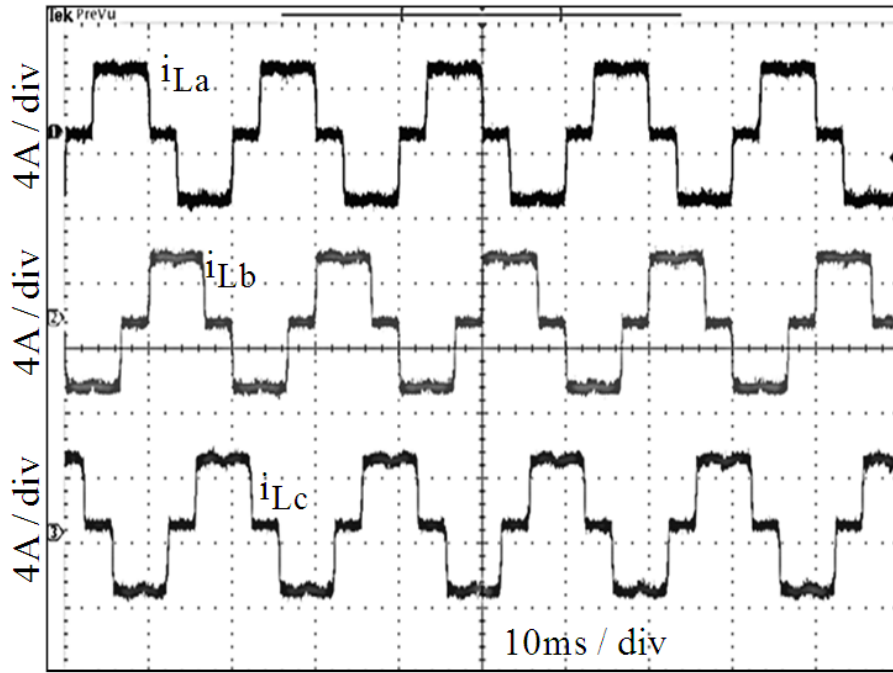
Figure 5.28: Waveforms of three phase load currents in Case-2
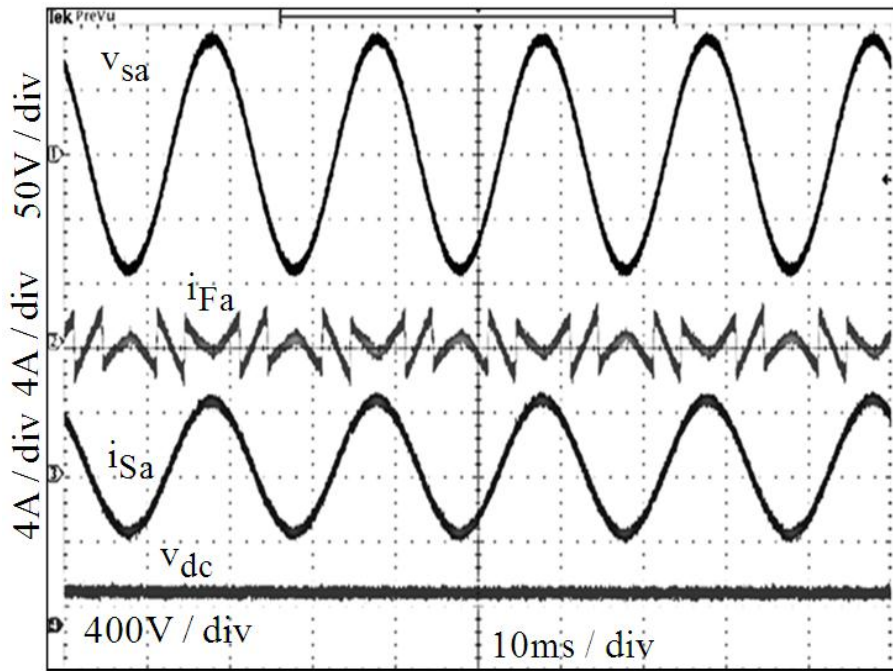
Figure 5.29: Waveforms showing phase-a quantities in Case-2
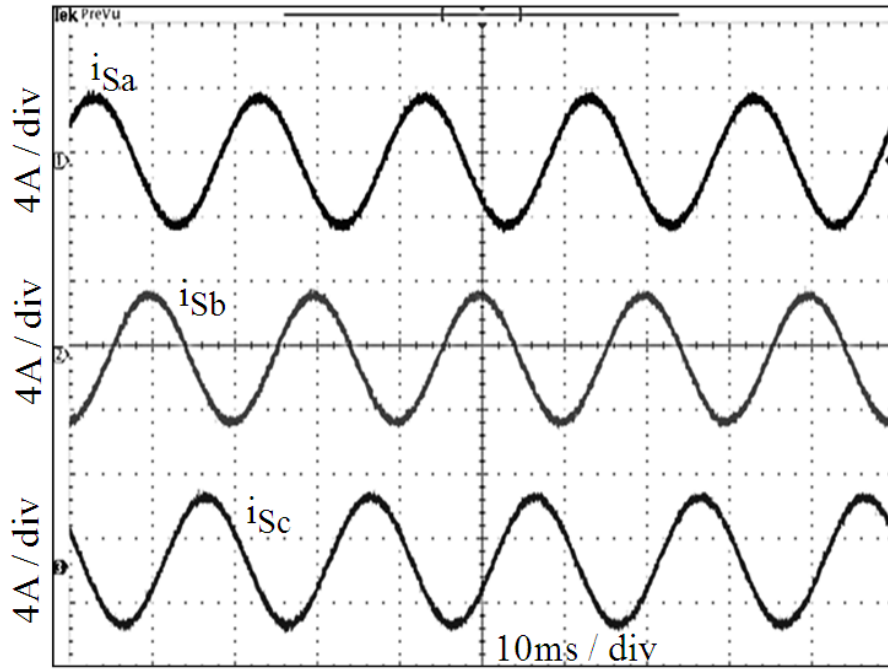
Figure 5.30: Waveforms of three phase source currents in Case-2

(a)   (b)
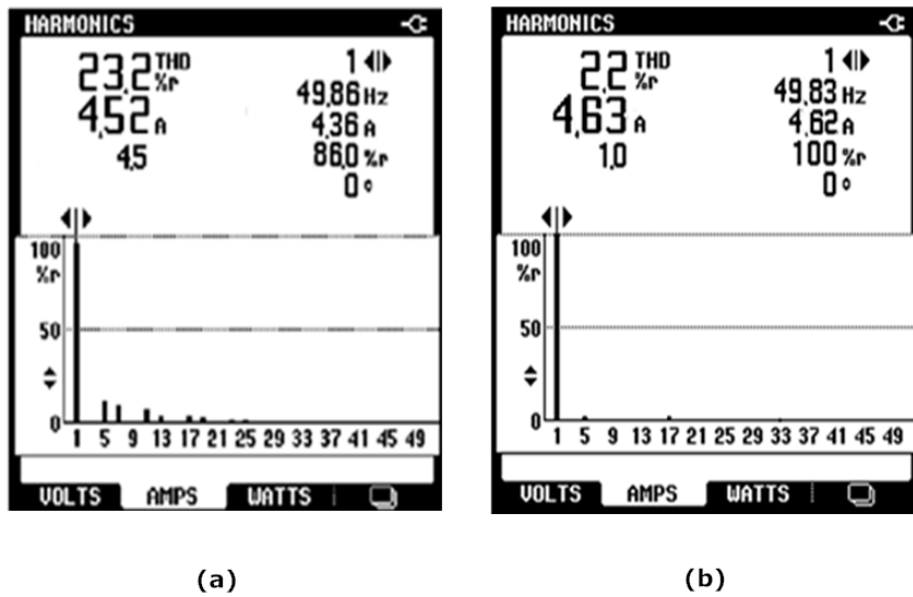
Figure 5.31: Harmonics spectra of (a) phase-a load current, (b) phase-a source current of proposed RECKF-LQG Servo based SAPF in case-2

To evaluate the robustness performance of the proposed RECKF-LQG servo controller considering above two Cases, HCR factors are calculated and summarized in Table 5.4. The results in Table 5.4 demonstrate that in both cases, HCR factors are maintained nearly same (i.e. a deviation of 0.5% only) and these factors are unaffected by

any parametric variations of load, which makes SAPF system more robust.

Table 5.4 THD of the phase-a source current in RECKF-LQG Servo based SAPF (Experimental)

Cases	THD% of Phase-a Source Current		
	Before Compensation THD (%)	After Compensation THD (%)	Harmonics Compensation Ratio (HCR) (%)
Case-1 (Steady State)	27.9	2.5	8.9
Case-2 (Load impedances are increased by 100%)	23.2	2.2	9.4

5.7   Chapter Summary

This Chapter presented design of a robust LQG servo controller for a SAPF. The robustness of the proposed LQG servo controller strategy has been verified by analyzing the performance at various operating conditions in SAPF. From the obtained simulation as well as experimental results, the proposed SAPF has been observed to provide current harmonics mitigation, reference current tracking and reactive power compensation with load parameter variations as well as grid disturbances.

In the presence of an additive white Gaussian noise, switching noise, and distortion at PCC voltage, Kalman filter is found to be the best option involving in current controller realization of SAPF. Further, the proposed reference scheme based on RECKF acts as a self-regulator of dc-link voltage escaping from external linear and nonlinear controller and hence an inexpensive control strategy can be implemented. The main feature of the LQG servo controller is the feedback compensator, which plays a significant role in achieving gain stability, perfect reference tracking, less current harmonics distortion as well as improved bandwidth. Hence the proposed RECKF-LQG servo control scheme is an effective solution for SAPF that requires integrated functionalities.

CHAPTER 6

Robust Extended Complex Kalman Filter and H∞ Control based SAPF

6.1 Introduction

This Chapter proposes a robust H∞ control scheme in the current control loop for a three phase SAPF system. With the purpose of achieving high stability and high disturbance rejection, a mixed sensitivity approach has been employed in the synthesis of this H∞ controller. Further, the reference generation scheme employed in the Chapter 5 considers current measurements (both load and source current) to achieve a cost effective SAPF system. Hence, a new current reference scheme is proposed in this Chapter, which concerns with the measurement of source current only in order to achieve a more reliable and cost efficient SAPF.

The proposed reference scheme is based upon a fast and adaptive estimation of peak and fundamental of source reference current, which has the capability of delivering real power equivalent to conduction and switching losses occurred during capacitor voltage deviation. Robust extended complex Kalman filter is employed here for fast estimation of positive sequence from the fundamental component of supply current, which leads to generate source reference because negative and zero sequence components can degrade the harmonics compensation efficiency of SAPF. It is demanded that proposed reference generation scheme not only overcomes the problems of PI controller, but also self-regulates the dc-link voltage with sensing supply current only.

In recent years, power line uncertainties such as random variation of load, unexpected failure of power system components, high disturbance environment and involved sensor nonlinearities are the most challenging issues that might affect the dynamic performance of SAPF. Moreover parameters of SAPF may vary due to component aging, thermal drift and saturation effects caused by the operating environment. Hence it is essential to design robust controllers that provide good disturbance rejection and robustness against uncertainties in the system dynamics. Furthermore, application of robust control scheme is not very popular in distribution of power system and is limited to medium voltage level DVR [125][126], where H∞

controller is employed for the purpose of voltage control only. However, H∞ control of SAPF has not been actively investigated for the purpose of harmonics and reactive power compensation so far. In view of addressing all the aforementioned issues, an H∞ robust controller is proposed, designed and investigated in this Chapter for mitigating current harmonics as well as reactive power to achieve unity power factor in SAPF. H∞ controller is synthesized using mixed sensitivity approach for achieving stability and high disturbance rejection in SAPF.

6.2   Chapter Objectives

1. To make reference generation scheme simple, reliable and self dc-link voltage regulating.

2. To achieve stability and disturbance rejection in SAPF.

3. To show a high degree of robustness against parametric variations of the load.

4. To improve the PQ more effectively in terms of tracking error minimization and efficient current harmonics compensation.

5. To make a cost-effective SAPF system.

6. To validate the robustness of proposed control system with experimental set up under different parameters of load.

6.3   Proposed RECKF-H∞ based SAPF

The proposed control scheme for the SAPF is summarized in Fig. 6.1. The control system consists of a current loop including H∞ controller so that the current injected $\left(I_{Fabc}\right)$ into the grid could track the reference current $\left(I_{Fabc}^{*}\right)$. The transformation from abc to dq frame has been performed for current controller implementation. The output of the current controller is then transformed to the abc frame and subsequently passed to the pulse width modulation (PWM) generator to give switching pulses to IGBT based inverter.

The whole system is designed to inject current into the line such as to compensate the harmonic content of the load current. The compensation must be accomplished considering model uncertainty, parameter variations of load, and several disturbances on the grid which may affect the dynamic behavior of SAPF. Under this scenario, this

Chapter focuses on designing of a robust H$_\infty$ controller to cope with all perturbations mentioned before.
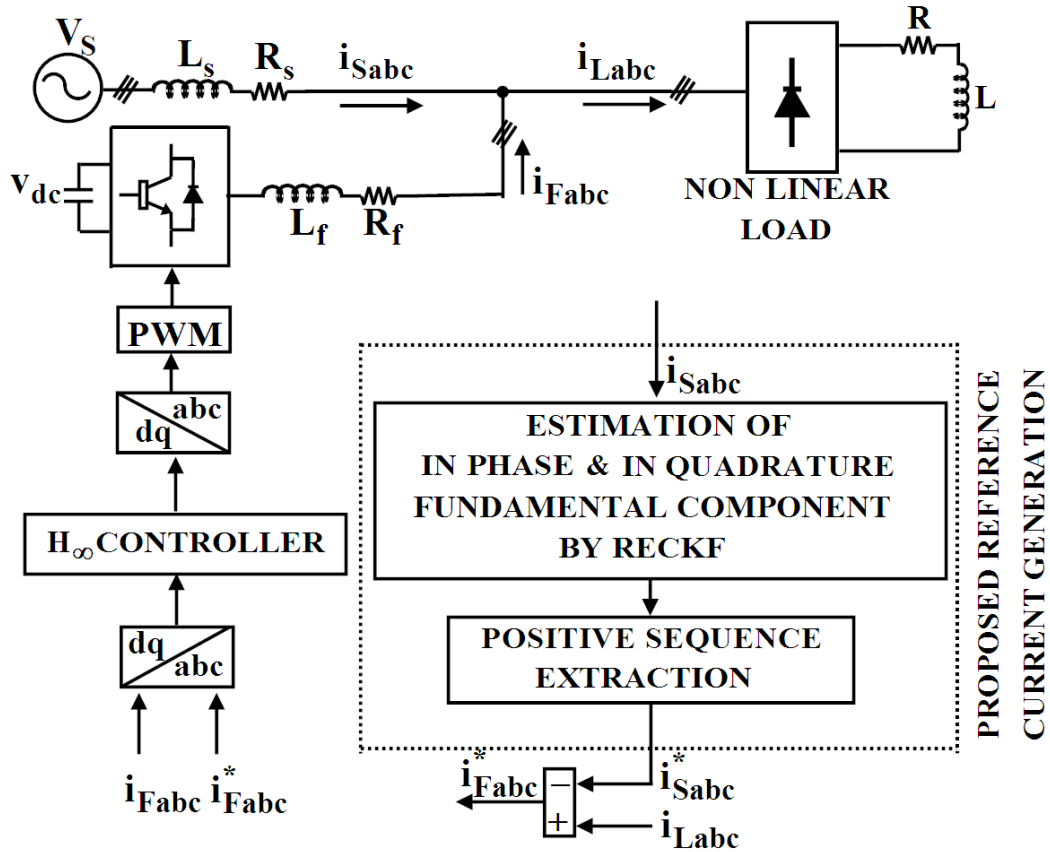
Figure 6.1: Proposed RECKF-H$_\infty$ based SAPF system

6.4   Design of H$_\infty$ Controller

Robustness is of crucial importance in control systems design, because real world systems are vulnerable to external disturbance and measurement noise, and there are always discrepancies between mathematical models developed for design and the actual system. To achieve certain performance levels in the presence of disturbance signals, noise interference, unmodeled plant dynamics and plant parameter variations, the H$_\infty$ control method has been implemented in VSI [127][128][129], dc-dc converter [130] and single phase UPS inverter [131]. H$_\infty$ controller can be synthesized using different techniques, but H$_\infty$ loop shaping is gaining very high acceptance since the performance requirements can be incorporated in the design stage as performance weights. In the H$_\infty$ loop shaping

technique a plant model is augmented with certain weight functions like sensitivity weight function (W_1), complementary weight function (W_3) and control sensitivity weight function (W_2) so that closed loop transfer function of the plant will have desired performances.

The standard H_∞ configuration for current control of a SAPF is shown in Fig. 6.2, where $G_H(s)$ is the nominal plant transfer function; $K_H(s)$ is the desired H_∞ controller;
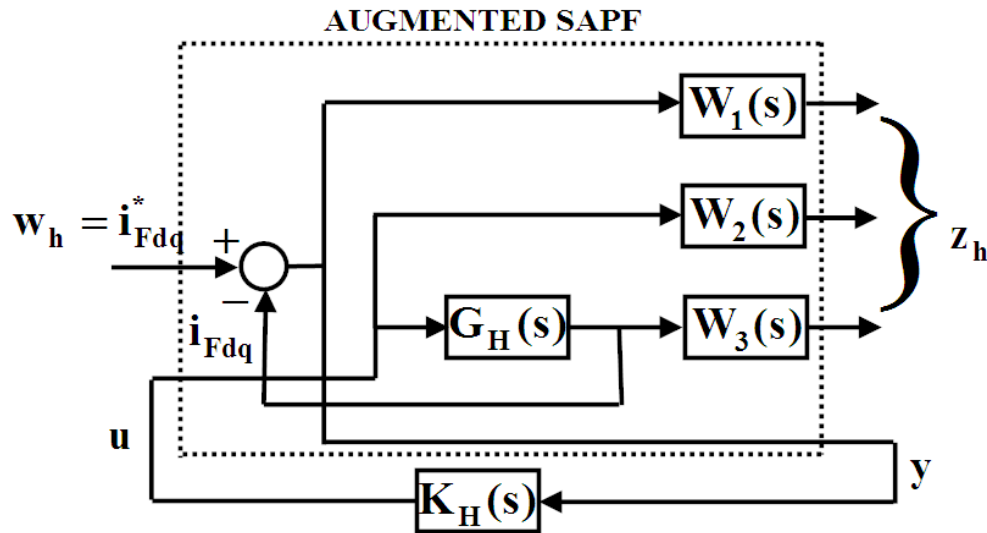
Figure 6.2: H_∞ control configuration with weighting functions

w_h, u, y and z_h are the exogenous input, control input, measured output and controlled output respectively.

The transfer function of the nominal plant or SAPF can be expressed as

$$G_H(s) = \frac{1}{1.5T_sL_fs^2 + (1.5T_sR_f + L_f)s + R_f} \tag{6.1}$$

There are many delays in the control loop (e.g. processing time of the control algorithm, analog to digital conversion time, delay time of the converter) which have to be taken into account for the control design. Here, a processing delay of $1.5T_s$ is taken into account for the control design due to the inclusion of 1) Digital processor dSPACE1104 , where analog to digital conversion process involves with a delay of T_s, and 2) PWM converter, where the PWM pattern are implemented with a delay of $0.5T_s$.

Mixed sensitivity problem is to find $K_H(s)$ and make H$_\infty$ norm of the transfer function from w_h to z_h be less than unity. This can be expressed as

$$\left\| \begin{matrix} W_1 S_H \\ W_2 K_H S_H \\ W_3 T_H \end{matrix} \right\|_\infty < 1 \quad \text{or equivalent} \quad \left\| T_{w_h z_h} \right\|_\infty < 1$$

(6.2)

where $S_H(s) = \left(1 + G_H(s)K_H(s)\right)^{-1}$ is the sensitivity transfer function, $K_H(s)S_H(s)$ is the input sensitivity transfer function and $T_H(s) = G_H(s)K_H(s)(1 + G_H(s)K_H(s))^{-1}$ is the complementary sensitivity transfer function. By proper selection of weighting functions W_1, W_2, W_3, their corresponding transfer functions can be shaped.

6.4.1 Weighting function selection for Tracking error performance

It is well-known that the quality of the step response can be quantified by rise time t_r, settling time t_s and percent overshoot $100M_p\%$. These performance indices can be approximately calculated as follows.

$$t_r = \frac{0.6 + 2.16\xi}{\omega_n}, \ 0.3 \le \xi \le 0.8; \ t_s = \frac{4}{\xi\omega_n}; \ M_p = e^{-\frac{\pi\xi}{\sqrt{\left(1-\xi^2\right)}}}, \ 0 < \xi < 1$$

Since, the performance objectives are related to the sensitivity function, a relationship is considered between these time domain indices (ω_n, ξ) with the frequency response of the sensitivity function.

$$S_H(s) = \left(1 + G_H(s)K_H(s)\right)^{-1} = \frac{s(s + 2\xi\omega_n)}{s^2 + 2\xi\omega_n s + \omega_n^2} \tag{6.3}$$

The closed loop bandwidth can be regarded as $\omega_b \approx \omega_n / \sqrt{2}$, since beyond this frequency the closed-loop system will not be able to track the reference and the disturbance will be amplified. Further, a gain for high frequency disturbance M_s can be represented by the following equation.

$$M_s = \|S_H(s)\|_\infty = |S(j\omega_{max})| = \frac{\gamma\sqrt{\gamma^2 + 4\xi^2}}{\sqrt{\left(1-\gamma^2\right)^2 + 4\xi^2\gamma^2}} \tag{6.4}$$

where $\gamma = \sqrt{0.5 + 0.5\sqrt{1+8\xi^2}}$ and $\omega_{max} = \gamma\omega_n$. The overshoot can be excessive if M_s is large. Hence, a good control design should not have a very large M_s. The above requirements can be approximately represented as

$$|S_H(s)| \leq \left|\frac{s}{s/M_s + \omega_b}\right|, \quad s{=}j\omega \tag{6.5}$$

Or, equivalently, $|W_1 S_H| \leq 1$ with

$$W_1 = \frac{\dfrac{s}{M_s} + \omega_b}{s} \tag{6.6}$$

For the steady state error with respect to a step input not being greater than e_s (i.e., $|S_H(0)| \leq e_s$), it is sufficient to choose a weighting function W_1 satisfying $|W_1(0)| \geq 1/e_s$ so that $\|W_1 S_H\|_\infty < 1$ can be achieved as shown in Fig. 6.3(a). Hence, a possible choice of W_1 can be obtained by modifying the weighting function in eq (6.6).

$$W_1 = \frac{\dfrac{s}{M_s} + \omega_b}{s + \omega_b e_s} \tag{6.7}$$

6.4.2 Weighting function selection for Control effort

Here the control inputs are kept to be small by the allowable cost of control effort and saturation limit of the actuators; hence the maximum gain of input sensitivity can be fairly large, while the high frequency gain is essentially limited by the controller bandwidth and the noise frequencies. We would like to roll off as fast as possible beyond the desired control bandwidth so that the high frequency noises are attenuated as much as possible. Hence the control weighting function for the input sensitivity shaping (Fig. 6.3(b)) can be determined as follows,

(a)

(b)

(c)
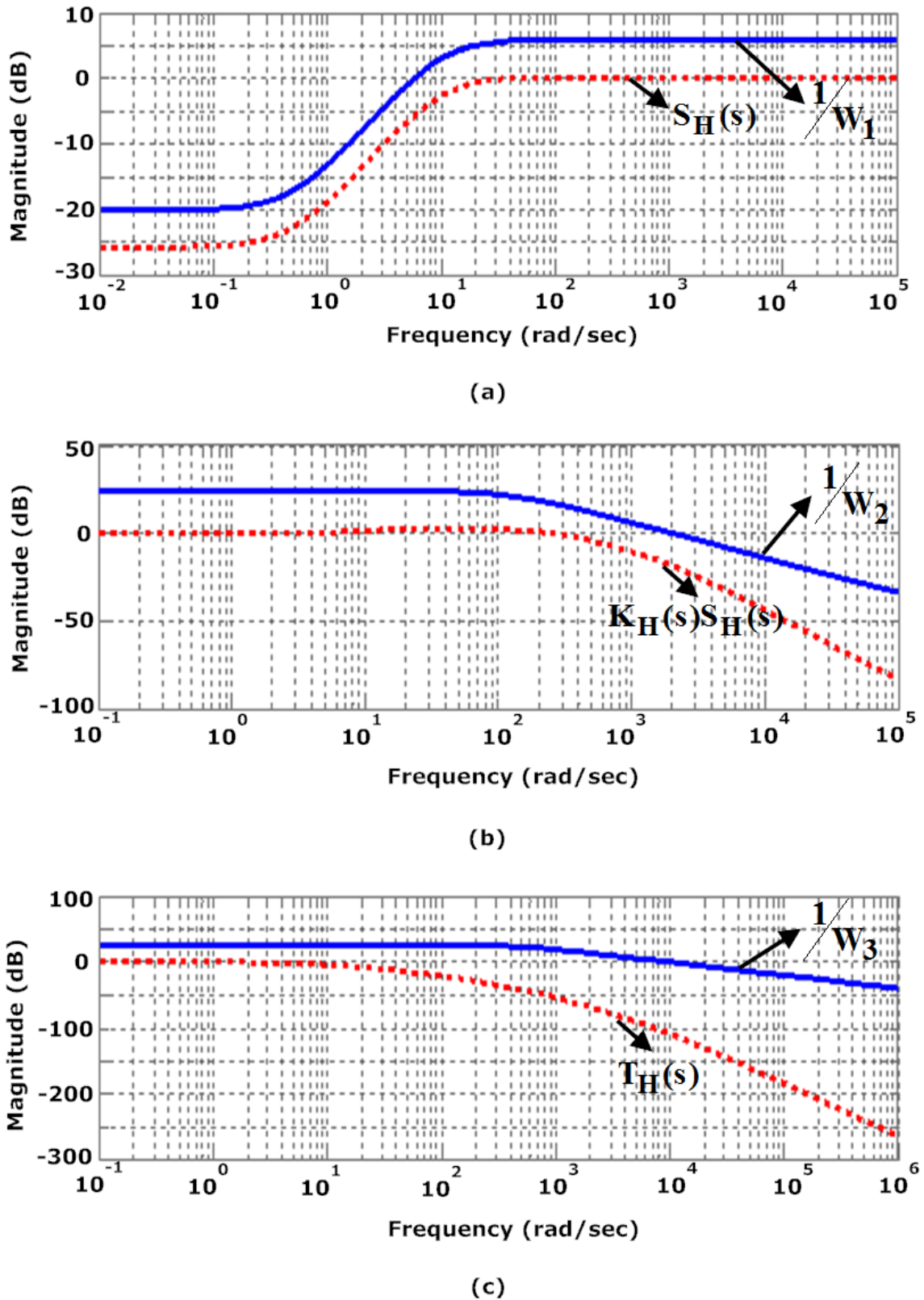
Figure 6.3: Waveforms for (a) Performance weight $1/W_1$ and desired S_H, (b) Control weight $1/W_2$ and desired $K_H S_H$, and (c) Complementary weight $1/W_3$ and desired T_H

135

$$W_2 = \frac{s + \dfrac{\omega_{bc}}{M_u}}{e_u s + \omega_{bc}} \tag{6.8}$$

where e_u stands for gain for low frequency control signal.

6.4.3 Weighting function selection for Robust performance

The complementary sensitivity function is weighted to achieve stability robustness characteristics (e.g., insensitivity to noise and unmodeled dynamics). Because noise has most of its energy concentrated at high frequencies, a high pass weight is used on the complementary sensitivity function. This has the same form as the input sensitivity weighting function and when S_H is decreased, T_H has to be increased since $S_H + T_H = 1$. The standard form of a complementary sensitivity weight function is,

$$W_3 = \frac{s + \dfrac{\omega_{bt}}{M_t}}{e_t s + \omega_{bt}} \tag{6.9}$$

The nomenclature for ω_{bt}, M_t, e_t are the same as previous weighting functions. An iteration procedure with assumed initial values is conducted to find out the above weighting functions. The initial choices for weighting functions are given in eq (6.10).

$$e_s = 0.1, \ M_s = 1, \ e_u = 0.01, \ M_u = 1, \ e_t = 0.01, \ M_t = 1 \tag{6.10}$$

The performance criteria for H$_\infty$ controller mentioned in (eq (6.2)) are checked along with the shaping of closed loop responses of the weighting functions. The selection of weighting function needs a careful iteration procedure, for example, if the first iteration of the derived specification given in eq (6.10) were not satisfied then subsequent iterations had to be pursued. The objective of the H$_\infty$ controller is to modify the weights until the various performance criterions such as tracking error performance, control effort performance as well as robust performance can be achieved simultaneously.

6.5   Proposed Reference Current Generation

Presence of negative and zero sequence components in the fundamental current may be ineffective in generation of source reference as they degrade the performance of SAPF system. Hence it is necessary to disregard these components and the proposed reference

current scheme only deals with the positive sequence component extraction from the fundamental component of supply current, which acts as source reference signal as shown in Fig. 6.1. This scheme quickly adapts to load changes and accordingly self maintains the dc capacitor voltage by properly estimating the peak and fundamental of the source reference current.

RECKF is employed for estimation of in phase fundamentals $\left(i_{Sa_{1_k}}, i_{Sb_{1_k}}, i_{Sc_{1_k}}\right)$ and in quadrature fundamentals $\left(i^{\perp}_{Sa_{1_k}}, i^{\perp}_{Sb_{1_k}}, i^{\perp}_{Sc_{1_k}}\right)$ from the source currents $\left(i_{Sa_k}, i_{Sb_k}, i_{Sc_k}\right)$. The formulations for obtaining in phase and in quadrature fundamental components of a signal are described in Chapter 2. Then the determination of positive sequence currents $\left(i^{+}_{Sa_k}, i^{+}_{Sb_k}, i^{+}_{Sc_k}\right)$ are obtained by,

$$
\begin{bmatrix} i^{+}_{Sa_k} \\ i^{+}_{Sb_k} \\ i^{+}_{Sc_k} \end{bmatrix} = \frac{1}{3} \begin{bmatrix} 1 & \alpha & \alpha^2 \\ \alpha^2 & 1 & \alpha \\ \alpha & \alpha^2 & 1 \end{bmatrix} \begin{bmatrix} i_{Sa_{1_k}} \\ i_{Sb_{1_k}} \\ i_{Sc_{1_k}} \end{bmatrix} \tag{6.11}
$$

where $\alpha = e^{j120^{\circ}}$. Defining 90° phase shift operator as $e^{j90^{\circ}}$ and considering $\alpha = -(1/2) \pm \left(\sqrt{3}/2\right) e^{j90^{\circ}}$ then eq (6.11) becomes,

$$
i^{+}_{Sa_k} = \frac{1}{3} i_{Sa_{1_k}} - \frac{1}{6}\left(i_{Sb_{1_k}} + i_{Sc_{1_k}}\right) + \frac{\sqrt{3}}{6}\left(i^{\perp}_{Sb_{1_k}} - i^{\perp}_{Sc_{1_k}}\right)
$$
$$
i^{+}_{Sb_k} = -i^{+}_{Sa_k} - i^{+}_{Sc_k} \tag{6.12}
$$
$$
i^{+}_{Sc_k} = \frac{1}{3} i_{Sc_{1_k}} - \frac{1}{6}\left(i_{Sa_{1_k}} + i_{Sb_{1_k}}\right) + \frac{\sqrt{3}}{6}\left(i^{\perp}_{Sa_{1_k}} - i^{\perp}_{Sb_{1_k}}\right)
$$

Therefore the reference compensating currents for phase 'a', 'b' and 'c' are generated with the following equations,

$$
i^{*}_{Sabc_k} = i^{+}_{Sabc_k} \tag{6.13}
$$

$$
i^{*}_{Fabc_k} = i_{Labc_k} - i^{*}_{Sabc_k} \tag{6.14}
$$

6.6 Simulation Results and Discussions

A simulation model for the three phase SAPF (Fig. 6.1) has been developed using MATLAB/Simulink. After several iterations, the necessary weighting functions are defined with all parameters specified in Table 6.1. The typical plots for S_H, $K_H S_H$ and T_H with their corresponding inverse weighting functions are shown in Fig. 6.3 and from the figure, it is clear that a proper shaping of the sensitivity functions is achieved as described in Section 6.3. Using the MATLAB 'hinfsyn' algorithm, the H_∞ controller that nearly minimizes the H_∞ norm of the transfer function from w_h to z_h is obtained as

$$K_H\left(s\right) = \frac{\begin{array}{l}(0.0003296s^4 + 9.889 \times 10^5 s^3 + 6.593 \times 10^{14} s^2 + ... \\ ... + 9.422 \times 10^{18} s + 6.279 \times 10^{19})\end{array}}{\begin{array}{l}(s^5 + 1 \times 10^9 s^4 + 1.642 \times 10^{13} s^3 + 3.101 \times 10^{16} s^2 + ... \\ ... + 6.964 \times 10^{18} s + 3.479 \times 10^{18})\end{array}} \tag{6.15}$$

Using the balanced truncation method (modred function in MATLAB), the resulting reduced controller is given by the following eq (6.16).

$$K_H\left(s\right) = \frac{1.306s + 9.043}{s + 0.501} \tag{6.16}$$

Table 6.1 H∞ Performance Function Specification

Weighting Functions	Specifications		
W_1	$\omega_b = 5 \text{ rad}/s$	$M_s = 1.9946$	$e_s = 1 \times 10^{-1}$
W_2	$\omega_{bc} = 2 \times 10^3 \text{ rad}/s$	$M_u = 16$	$e_u = 1 \times 10^{-2}$
W_3	$\omega_{bt} = 3 \times 10^3 \text{ rad}/s$	$M_t = 18$	$e_t = 1 \times 10^{-2}$

The Bode plots of the original and reduced order controllers in the continuous time domain are shown in Fig. 6.4 for comparison. They are almost the same at low frequencies. The Bode plots in the discrete time domain are almost identical. Using MATLAB c2d (ZOH) algorithm, the discretized controller can be obtained as

$$K_H(z) = \frac{1.306z - 1.305}{z - 1} \qquad (6.17)$$
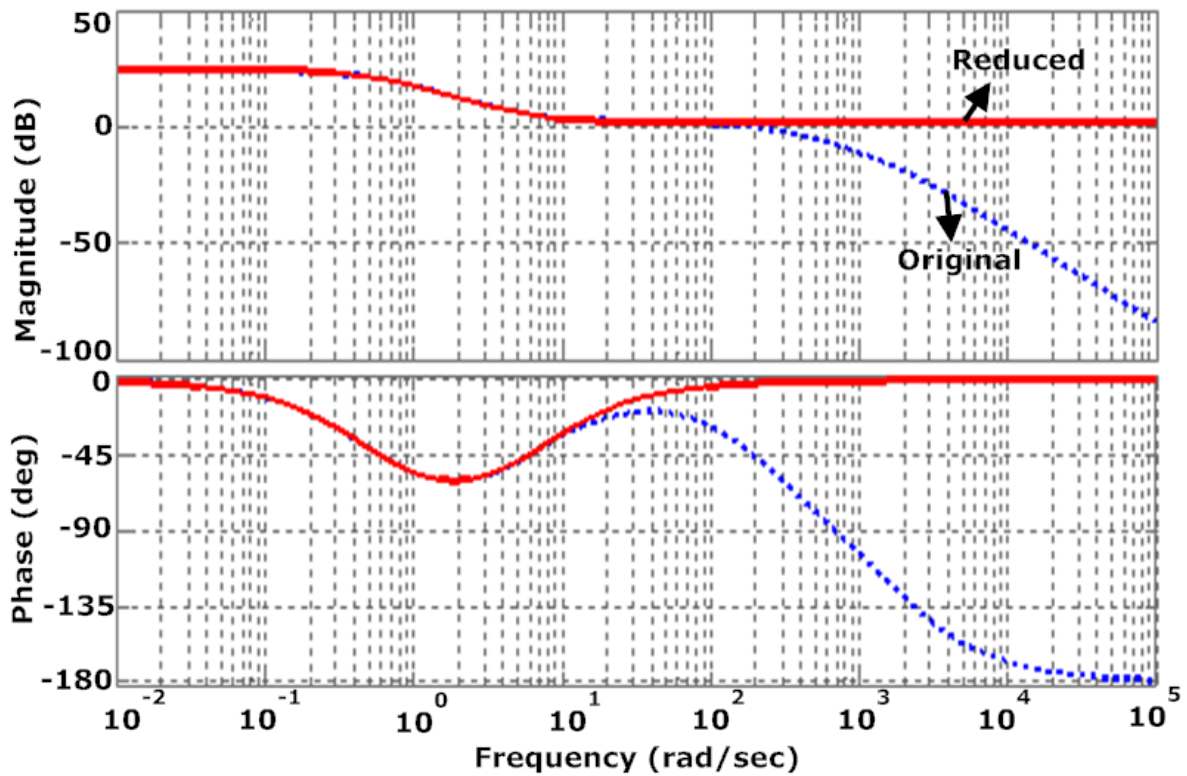
Figure 6.4: Bode plots of the original and reduced controllers

The resulting H∞ norm $\left\| T_{w_h z_h} \right\|_\infty$ is obtained as 0.5307 and hence the closed loop control system is stable [132]. The robustness of the system is very good.

To verify the robustness of the proposed scheme, simulation studies are performed considering two different load conditions as described in Section 5 and the simulation results are presented in Fig. 6.5, Fig. 6.6, and Fig. 6.7.

Fig. 6.5 presents the steady state performance of SAPF when the load impedances are kept at base value (Case-1). The load current, compensating current, source current and

the capacitor voltage are shown for three phases in top to bottom order. The compensated source current is found to be purely sinusoidal and distortion less. Also, a good response of capacitor voltage is observed maintaining towards a better voltage regulation in the SAPF system.
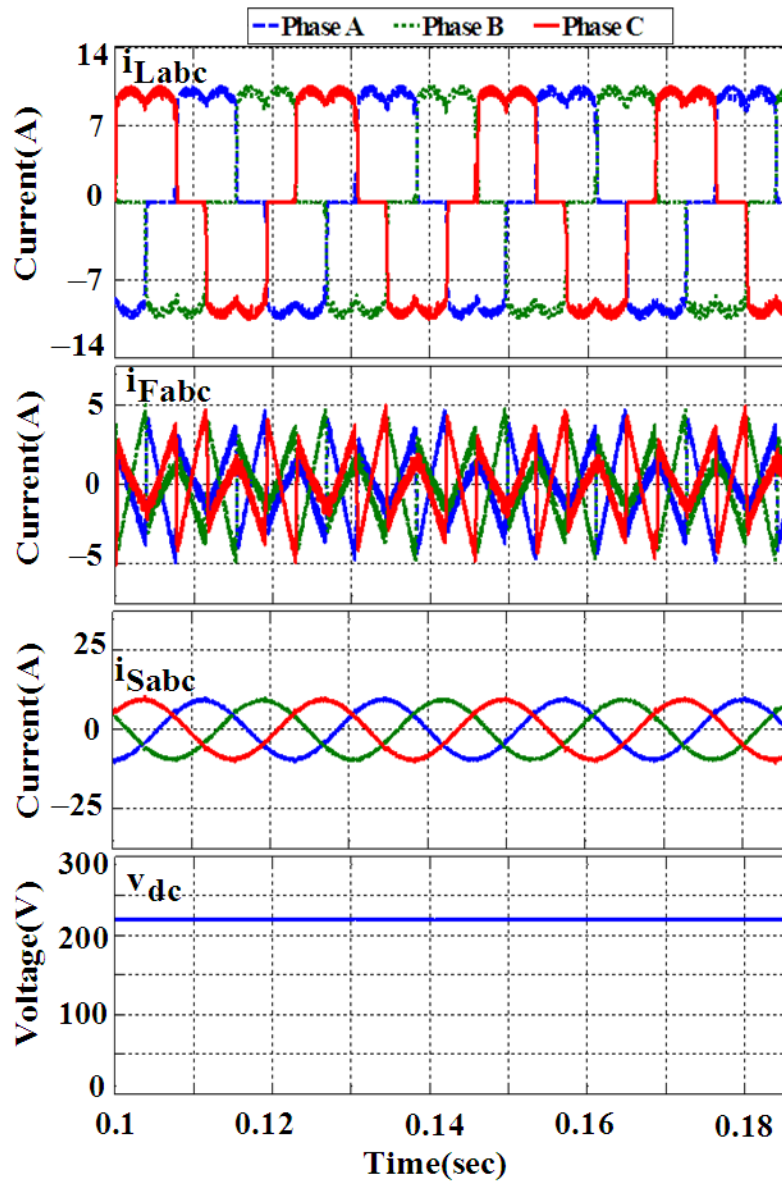
Figure 6.5: Response of RECKF-H∞ based SAPF in Case-1 using MATLAB

Similar results are obtained for Case-2 as viewed in the respective graphs shown in Fig. 6.6. Fig. 6.7 shows the THD of the source current for phase 'a' in two cases when H∞ controller is used. In Case-1, the source current THD is reduced from 25.6% to 1.9%,

whereas it is decreased to 1.67% when load impedance is increased by 100%. Hence, THDs of the source current are sufficiently small and far away from the permissible limit of 5%, indicating a complete and perfect harmonics cancellation in SAPF system. Here, the robustness of H_∞ controller for the SAPF is examined on the basis of harmonics compensation ratio.
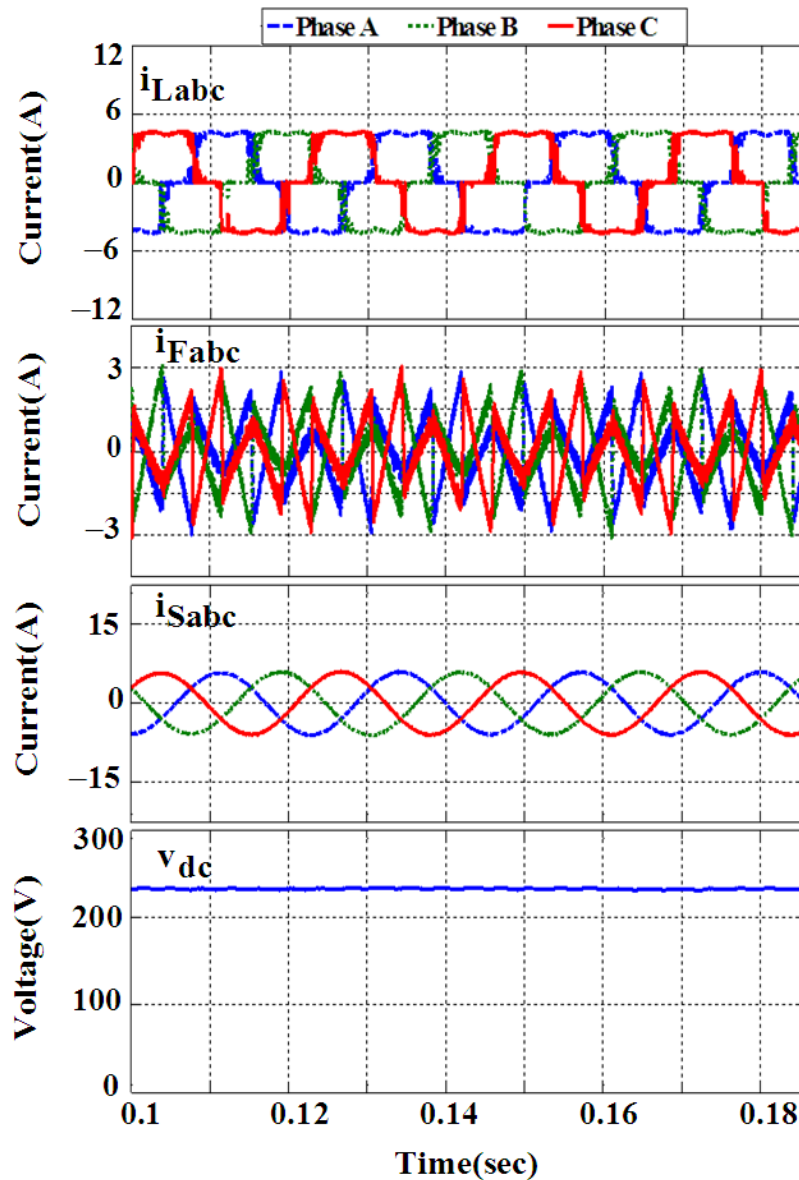
Figure 6.6: Response of RECKF-H_∞ based SAPF in Case-2 using MATLAB

Table 6.2 demonstrates that when load impedance is increased by 100%, the harmonics compensation ratio (HCR) is differed by only 0.20% (i.e., Case-1: 7.42% and

Case-2: 7.62%). This envisages a superior robustness of this proposed SAPF model against parametric variations of the load.

(i)

(ii)
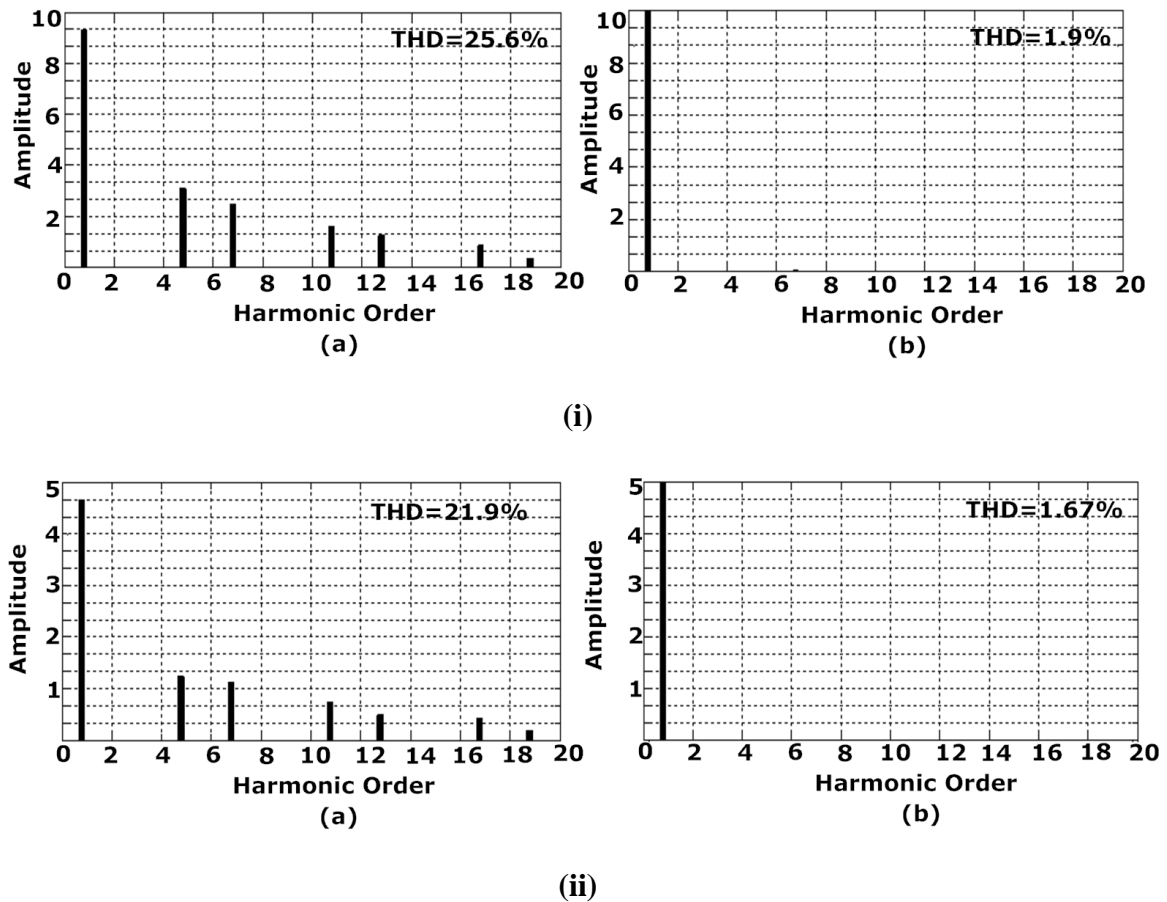
Figure 6.7: Compensation Effect of RECKF- H_∞ based SAPF using MATLAB,

(i) Case-1, (ii) Case-2

(a) Load current spectrum, (b) Source current spectrum

Table 6.2 THD of the phase-a source current in RECKF-H_∞ based SAPF

(Simulation)

Cases	THD% of Phase-a Source Current		
	Before Compensation THD (%)	After Compensation THD (%)	Harmonics Compensation Ratio (HCR) (%)
Case-1 (Steady State)	25.6	1.9	7.42
Case-2 (Load impedances are increased by 100%)	21.9	1.67	7.62

6.7 Experimental Results and Discussions

The power circuits of the proposed SAPF are shown in Fig. 6.8. The details regarding experimental set up have already been described in Section 5.4 of Chapter 5. The control of SAPF is realized by RECKF-H$_\infty$ controller based algorithm implemented with dSPACE1104. Firstly, the controller is implemented using MATLAB/Simulink and the real time workshop is used to generate C code for real time applications. The interface between MATLAB/Simulink and dSPACE-1104 facilitates running the control algorithm. The source currents (i_{Sa}, i_{Sb}), compensating currents (i_{Fa}, i_{Fb}) and load currents (i_{La}, i_{Lb}) are sensed using current sensors and are fed to the ADC port of dSPACE1104 connector panel via signal conditioning circuits as depicted in Fig. 6.8 and the desired signals are observed through DSO. No voltage sensors are required for implementation of SAPF experimentally, which is the greatest advantage of this control strategy.
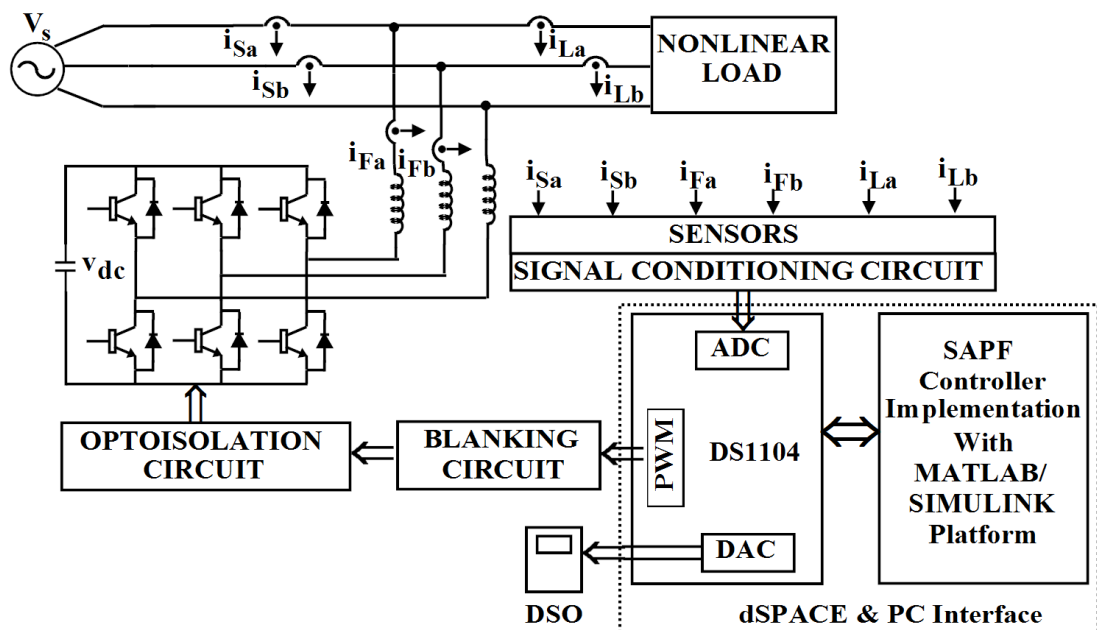
Figure 6.8: Control and Power circuit of SAPF Model

    The proposed control algorithm has been implemented in real-time on the experimental set up developed in the laboratory. The results are presented below.

Case 1: Load Impedances are 100% (Base Case):

The performance of RECKF-H$_\infty$ controller is investigated with the base case load impedance (R=20 Ω, L=10mH). The three phase source reference currents $(i^*_{Sa}, i^*_{Sb}, i^*_{Sc})$ generated with the help of RECKF are presented in Fig. 6.9. It is seen that source reference currents are undistorted and perfectly sinusoidal. The overall performance of the H$_\infty$ controller is shown in Fig. 6.10 and Fig. 6.11. The waveforms shown in Fig. 6.10 from top to bottom are, load current, compensating current, source current and dc bus voltage respectively. The source current is found to be perfect sinusoidal and the dc link voltage is nearly constant at its set-point value around 220V providing a good voltage regulation across the dc bus. A phase relation between source voltage and source current for phase-a is shown in Fig. 6.11. From Fig. 6.11, it is clear that the source current is exactly in phase with the source voltage. In Fig. 6.12, the source currents of three phases are nearly sinusoidal. The harmonic spectra are analyzed using a power quality analyzer and the recorded harmonic spectra for uncompensated as well as compensated phase 'a' current are shown in Fig. 6.13. The THD in the load current is as high as 27.9%, but the THD in the source current has been lowered to 2.1%. This is due to better harmonics rejection, control effort and tracking performance behavior of the controller.

Case 2: Load Impedances are increased by 100%:

In this case, the load impedances have been increased by 100% from the base case. Fig. 6.14 shows the three phase source reference currents, where the amplitude is reduced by 4A as compared to test case-1. Fig. 6.15 and Fig. 6.16 show the compensation characteristics of SAPF, where the source voltage is kept at 100V and the dc link voltage is maintained at 220V. Further, the amplitude of load current is reduced to 4.5A and source current is found to be sinusoidal and in phase with source voltage. Fig. 6.17 shows the three phase source currents which are all balanced and sinusoidal in the proposed H$_\infty$ controller based SAPF. The harmonic spectra of phase a load current and source current for the proposed SAPF are presented in Fig. 6.18. The THD of the load current is reduced up to an extent of 1.8% in case of proposed method.
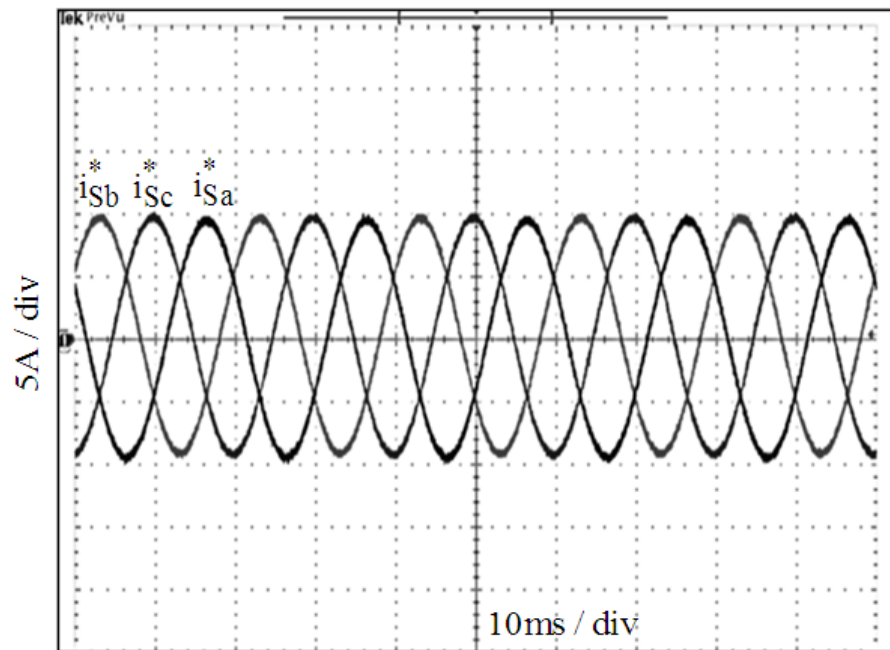
Figure 6.9: Experimental test case 1: Source reference current waveforms
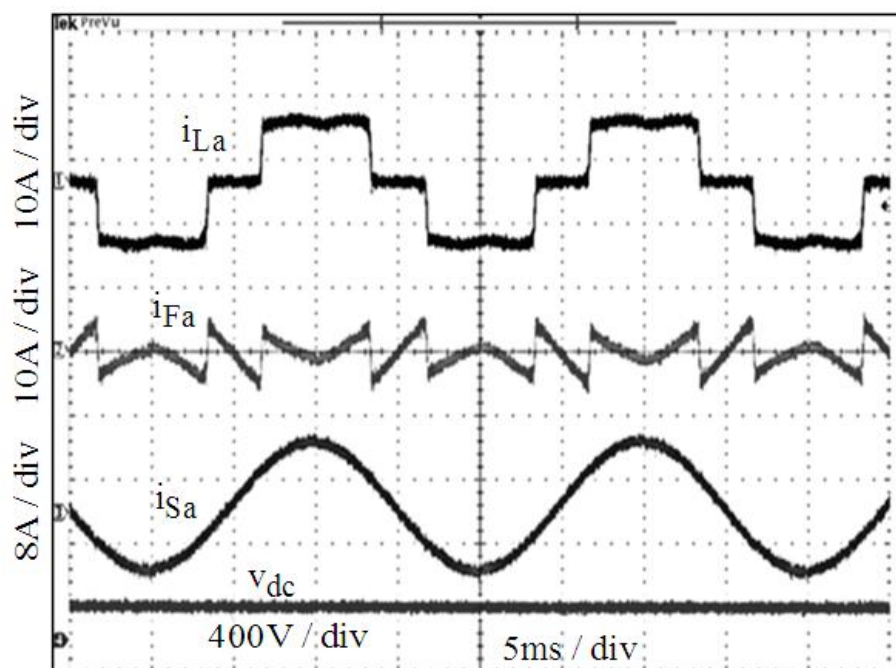
Figure 6.10: Experimental test case 1: Waveforms of compensation by SAPF

145
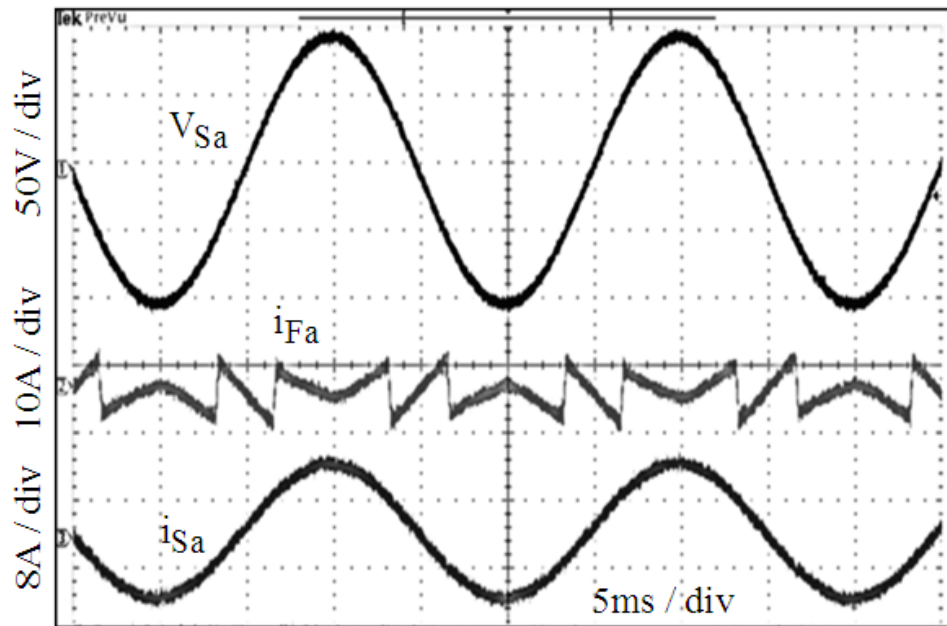
Figure 6.11: Experimental test case 1: Waveforms showing phase-a quantities
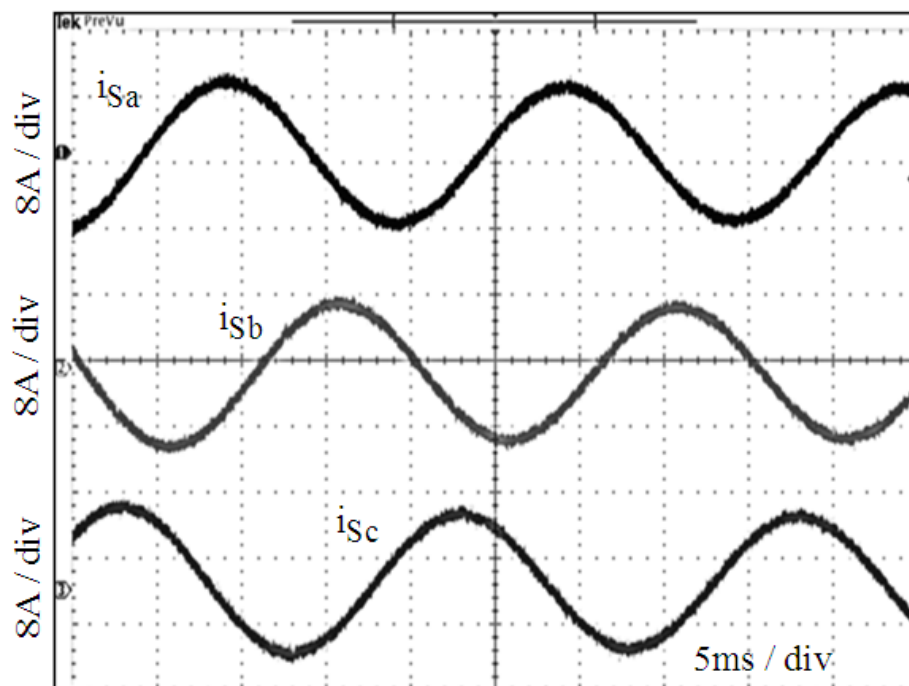
Figure 6.12: Experimental test case 1: three phase source current waveforms

146
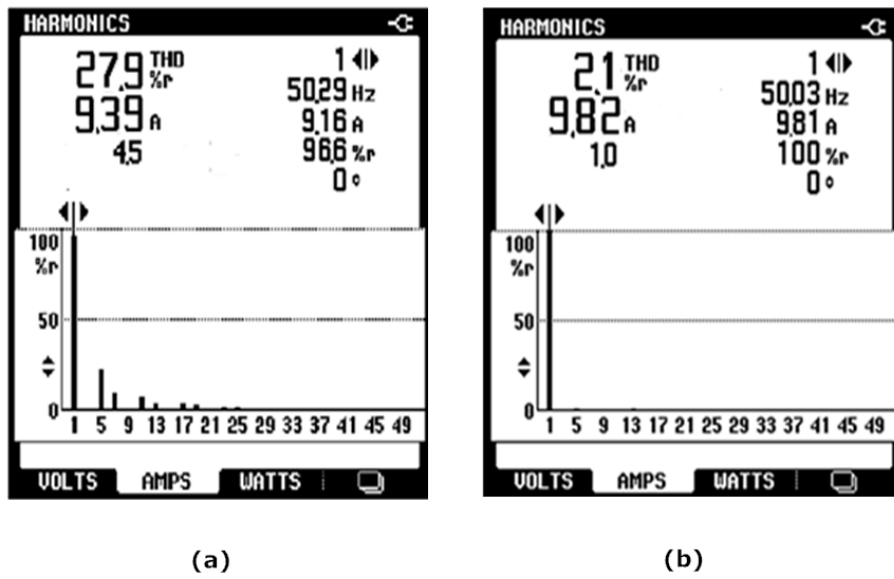
Figure 6.13: Experimental test case 1: Harmonic spectra of (a) phase-a load current, (b) phase-a source current
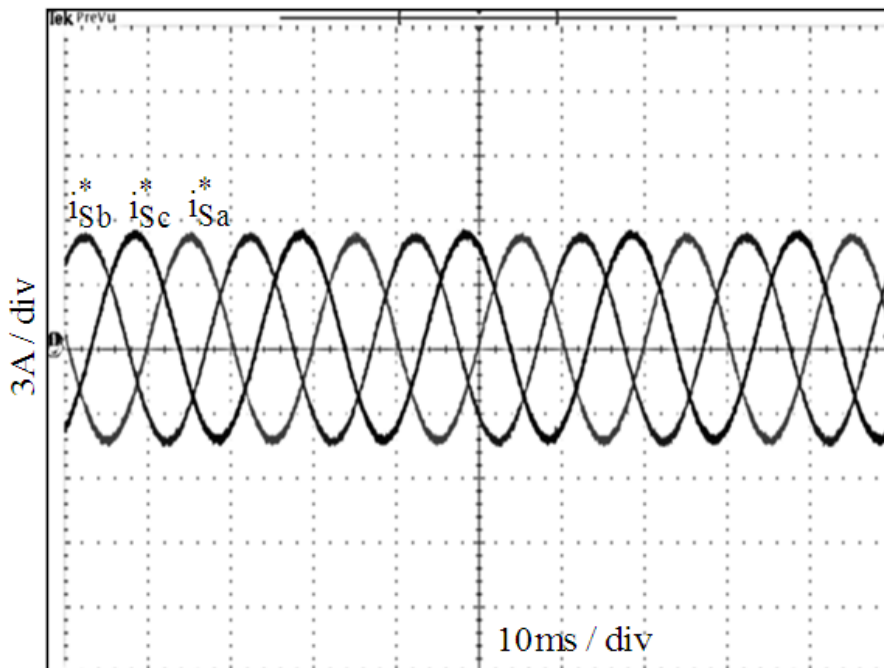
Figure 6.14: Experimental test case 2: Source reference current waveforms
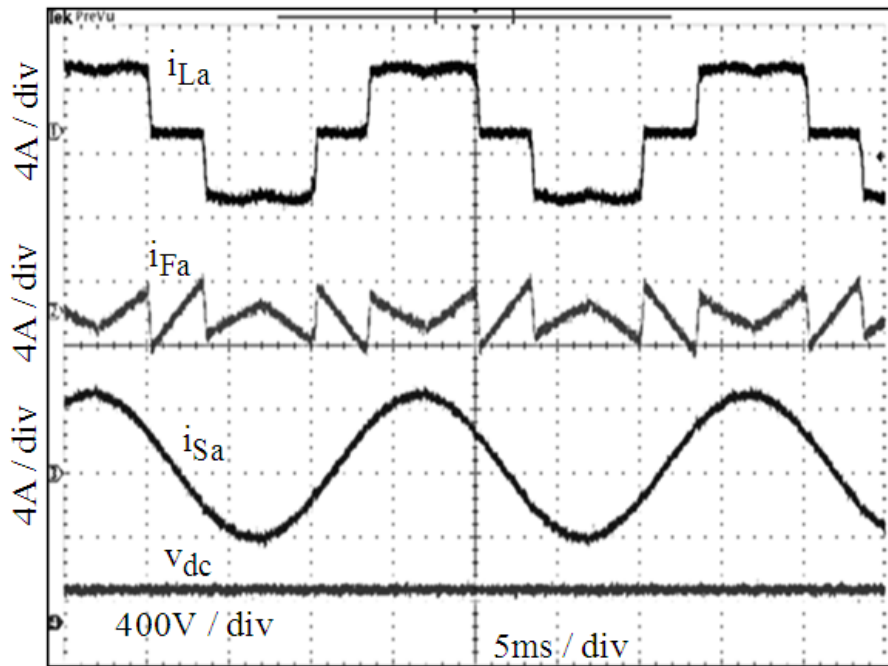
Figure 6.15: Experimental test case 2: Waveforms of compensation by SAPF
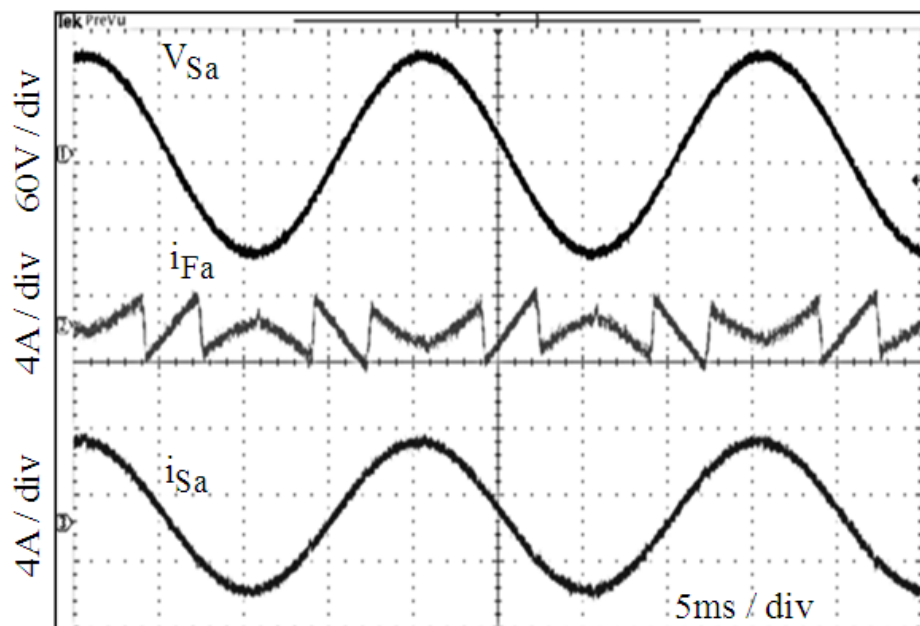
Figure 6.16: Experimental test case 2: Waveforms showing phase-a quantities
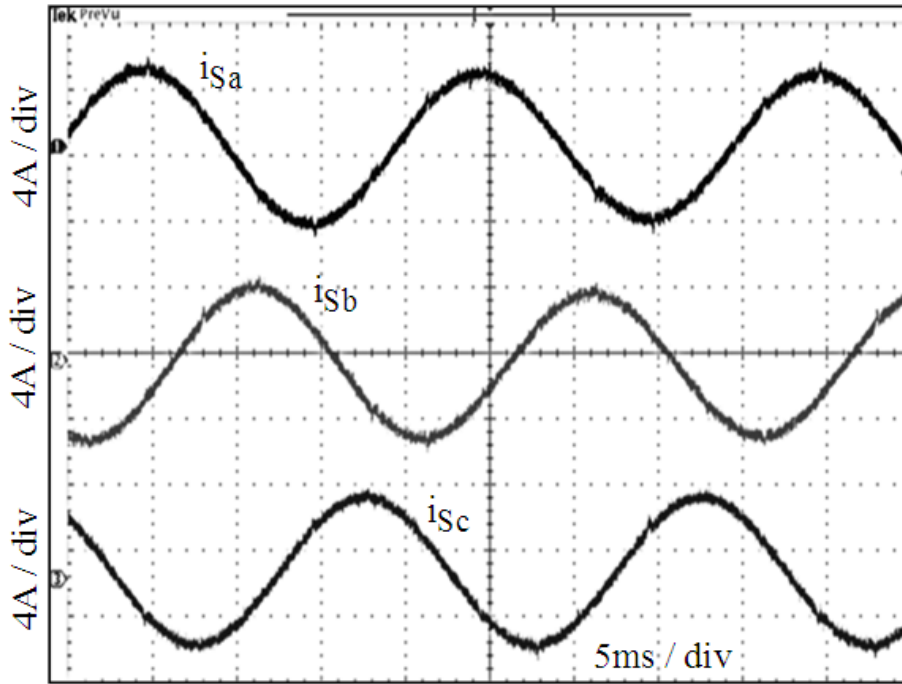
Figure 6.17: Experimental test case 2: three phase source current waveforms
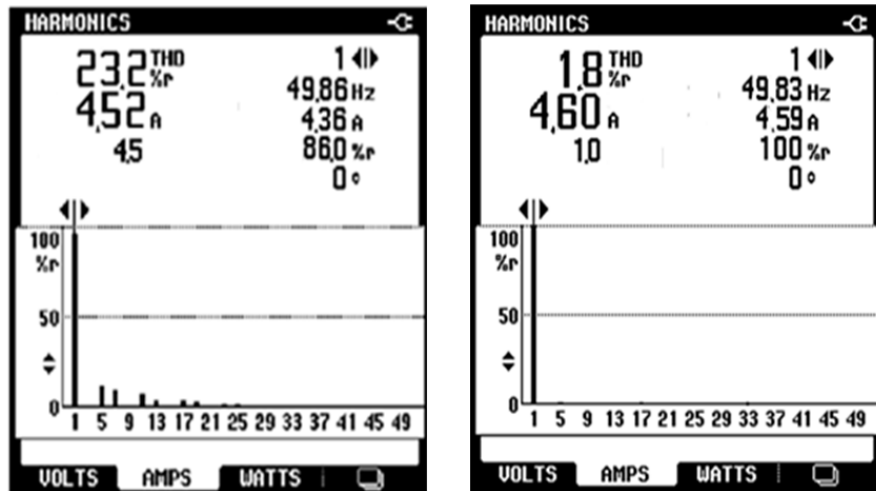
Figure 6.18: Experimental test case 2: Harmonic spectra of (a) phase-a load current, (b) phase-a source current

149

Experimental results for the proposed RECKF-H$_\infty$ controller are demonstrated in Table 6.3 using THD and HCR factors considering above two Cases. It is shown that HCR factors are maintained nearly same (i.e. a deviation of 0.23% only) and these factors are unaffected by any parametric variations of load.

Table 6.3 THD of the phase-a source current in RECKF-H$_\infty$ based SAPF
(Experimental)

Cases	THD% of Phase-a Source Current		
	Before Compensation THD (%)	After Compensation THD (%)	Harmonics Compensation Ratio (HCR) (%)
Case-1 (Steady State)	27.9	2.1	7.75
Case-2 (Load impedances are increased by 100%)	23.2	1.8	7.52

Moreover, to evaluate the robust performance of RECKF-LQG servo and RECKF-H$_\infty$ based SAPF considering above two cases, HCR factors are analyzed in Table 6.4 employing experimental results. The results in Table 6.4 show that a minimum difference of HCR factor (i.e. 0.23%) is achieved in case of proposed RECKF-H$_\infty$, when load is varied. From these it is confirmed that H$_\infty$ control based SAPF system provides excellent robust characteristics.

Table 6.4 Analysis of HCR factors in SAPF system
(Experimental)

Control Structure of SAPF		HCR (%)	HCR%(Case-2)-HCR%(Case-1)
RECKF-LQG Servo	Case-1	8.9	0.5
	Case-2	9.4	
RECKF-H$_\infty$	Case-1	7.52	0.23
	Case-2	7.75	

6.8   Chapter Summary

In this Chapter, a H$_\infty$ controller with a new reference current estimation scheme based on RECKF has been developed for a SAPF. This reference generation scheme is simple, reliable and self-regulator of dc-link voltage, which does not necessitate PI controller loop. A mixed sensitivity approach is adopted in the synthesis of H$_\infty$ controller for achieving stability and high disturbance rejection in SAPF. A proper selection of weighting functions has been performed to specify the robustness, control effort performance and error tracking performance of SAPF. Finally, the designed control scheme is tested on an experimental prototype SAPF model, where the controller performs extreme well at a particular load condition (base case), but a high degree of robustness of the proposed controller is also verified through its performance for the SAPF even under different load condition with changing load impedances.

Generally power line uncertainties such as fluctuation of load, variation of system parameter, sudden failure of power system components and sensor nonlinearities degrade the reliability and efficiency of the SAPF system. Moreover, grid perturbations such as harmonics, measurement noise, and distorted voltage are responsible for power quality deterioration. Hence, the objective of designing a robust control strategy in SAPF is achieved by accommodating all the possible perturbations occurring in the power system. From the experimental results, it is also observed that the proposed control approach to design a SAPF is found to be robust in face parametric uncertainties due to load perturbations yielding improvement in power quality more effectively in terms of tracking error reduction, efficient current harmonics mitigation as well as reactive power compensation. Moreover, the proposed SAPF system is less expensive since it uses only current sensors and has very good filtering performance with the reduced hardware. Finally, the superiority of proposed RECKF- H$_\infty$ based SAPF is verified through a comparative assessment with RECKF- LQG Servo based SAPF employing simulation and experimental results.

CHAPTER 7

Conclusion and Suggestions for future work

In this chapter, the conclusions of overall thesis are presented and some suggestions for future work are also proposed.

7.1 Overall Conclusion

The thesis has described development of new current controller techniques together with new reference current estimation schemes for performance enhancement of Shunt Active Power Filter (SAPF). Firstly, a Robust Extended Complex Kalman Filter (RECKF) estimation algorithm is employed which provides fast convergence under highly abnormal conditions such as PCC voltage distortion, harmonics and measurement noise. A number of controllers such as Hysteresis Current Controller (HCC), Sliding Mode Controller (SMC), Dead Beat Controller (DBC), Model Predictive Controller (MPC), Linear Quadratic Regulator (LQR), Linear Quadratic Gaussian (LQG) Servo Controller and H-infinity (H_∞) Controller are employed in SAPF for achieving tracking error minimization, which in turn provides cancellation of current harmonics in power system.

This thesis presents an extensive review on different control strategies in SAPF with emphasis on their merits and demerits, and evaluate with respect to their benefits, drawbacks and appliances.

HCC realized with a new reference current generation scheme are proposed for SAPF system in Chapter 2. This reference generation scheme involves a PI controller in the external loop. Further, the in phase fundamental components of distorted PCC voltages necessitated for this reference generation are estimated using the KF based algorithm. KF-HCC based SAPF performs under consideration of grid perturbations, but harmonics cancellation is not so fast owing to slower convergence rate of KF.

Hence, a robust controller SMC is employed with a faster reference scheme based on proposed RECKF. A new weighted exponential function is embedded into RECKF for fast estimation of a reference signal considering grid perturbations such as voltage distortion and measurement noise. The effectiveness of this RECKF-SMC is evaluated

with other variants of KF such as KF, EKF and ECKF with the results obtained from MATLAB/Simulink simulations as well as real-time simulation results obtained from Opal-RT. KF-SMC performs better than KF-HCC, but RECKF-SMC is analyzed to be more efficient in harmonics cancellation as compared to KF-SMC, EKF-SMC and ECKF-SMC based control strategies in SAPF.

With the growth of powerful and fast computing facilities with expensive computing platforms such as microprocessors, FPGA, recently increasing attention has been given to predictive control. Hence, predictive current control techniques called Dead beat control (DBC) and Model predictive control (MPC) with improved reference generation scheme are focused in Chapter 3. The reference generation is comprised of two components, namely estimation of in phase fundamental component of PCC voltage in p.u. value and estimation of fundamental amplitude of load current. The advantage of this reference scheme is that the need of a PI controller loop can be avoided to eliminate relatively large overshoots and undershoots associated with it, which may interrupt the stable operation of the inverter in protecting the switching devices. Further proposed RECKF is found to be excellent among KF, EKF and ECKF as investigated in Chapter 2. As a result, RECKF has been employed in reference generation scheme in Chapter 3.

Proposed RECKF-DBC scheme is very simple and it needs a modulator to provide gate drive signals to IGBT inverter. In DBC, the optimal actuation is the one that makes the error equal to zero in the next sampling instant, whereas a more flexible criterion is employed in MPC, expressed as a cost function to be minimized. There is no need of any modulators and the gate drive signals are generated directly by this MPC scheme. In the first proposed RECKF-DBC method, harmonics cancellation is not perfect (THD is above 4%) in spite of having kept the switching frequency of 12.5 kHz fixed in the SAPF. But, the second proposed RECKF-MPC method performs better as compared to RECKF-DBC. Furthermore, to examine the efficiency of this proposed RECKF-MPC over PI-MPC, a comparative study has been done applying both steady state and transient state conditions. It is observed from the simulation and real-time simulation results that the proposed RECKF-MPC based SAPF outperforms over PI-MPC in steady as well as transient condition.

Subsequently, this thesis presented development of an optimal Linear Quadratic Regulator (LQR) with a new reference current generation method in SAPF in Chapter 4 for further improvement of harmonics mitigation since MPC is very sensitive to model

mismatch and noise. LQR is chosen because it provides good tracking and disturbance rejection capability. For LQR designing, the state space variables related to the PCC voltages, are accurately estimated using proposed RECKF based algorithm. Furthermore, stabilization of capacitor voltage is improved with a new reference generation scheme based on RECKF, adding an error between fundamental amplitudes of source and load current. Consequently, harmonics cancellation effect is more in case of RECKF-LQR approach. Thus, RECKF-LQR is found to be more effective as compared to RECKF-SMC, RECKF-DBC and RECKF-MPC which are evidenced from both the obtained simulation as well as real-time simulation results.

Reference generation schemes employed in the Chapter 2, 3, and 4 consider both voltage and current measurements and make the dc-link capacitor voltage steady after some time delay. Hence, in Chapter-5, voltage regulation of dc-link capacitor is further improved by employing a new and faster reference generation scheme based on RECKF, which involves with only current measurements representing a cost effective approach. In spite of robustness and disturbance rejection capability of LQR approach, it is not successful in complete cancellation of current harmonics since the THD of the source current is found to be far more than 3%. Hence, a more robust technique called Linear Quadratic Gaussian (LQG) Servo controller with higher disturbance rejection capability has been developed in Chapter 5, which permits all perturbations such as PCC disturbances, parametric variations of load and tracking error variations so that compensation capability of the overall SAPF system can be enhanced (i.e., THD much less than 3%) with less consumption of time. From simulation results, LQG servo controller is not only analyzed to be robust against different load parameters, but also a satisfactory THD result has been achieved in SAPF. This has motivated to develop a prototype experimental set up in our Laboratory using dSPACE DS1104 R & D controller board for verifying the robustness of LQG servo controller. Finally, the experimental results agree with the simulation results.

Although RECKF-LQG servo based SAPF exhibits good robustness against parameter variations of load and also harmonics mitigation is superior than that of RECKF-LQR, RECKF-MPC and RECKF-SMC, but the stability of RECKF-LQG servo control cannot be guaranteed under high disturbance environment. In view of achieving stability, high disturbance rejection and high level of harmonics cancellation performance, H_∞ controller with a mixed sensitivity approach has been developed for

SAPF in the Chapter 6. This mix sensitivity approach involves with the robustness performance, control effort performance as well as error tracking performance of SAPF system by selecting appropriate weighting functions. Further, a new current reference scheme is proposed in this Chapter, which deals with the measurement of source current only ensuring whole SAPF a more reliable and a cost efficient system. This method does not require voltage sensor in realization of RECKF-H$_\infty$ based SAPF. The effectiveness of the proposed RECKF-H$_\infty$ based SAPF model is validated through both simulation and experimental studies. From the both simulation and experimental results, it is observed that the proposed RECKF-H$_\infty$ control approach to design a SAPF is found to be more robust as compared to RECKF-LQG servo control approach in face parametric uncertainties due to load perturbations yielding improvement in power quality more effectively in terms of tracking error reduction and efficient current harmonics mitigation (i.e., just touches the line of THD 2%). Moreover, the proposed RECKF-H$_\infty$ control based SAPF system yields the least THD i.e., 1.9% as compared to RECKF-SMC, RECKF-DBC, RECKF-MPC, RECKF-LQR and RECKF-LQG servo approaches employing both the simulation and real-time results.

7.2 Contributions of the Thesis

The contributions of the Thesis are as follows.

- A RECKF approach with an exponential robust term embedded for reference current estimation of SAPF system is proposed in Chapter 2, which handles all grid perturbations to estimate the reference signal quickly. Further, the current controller in the proposed SAPF has been designed using sliding mode approach because it is controlled by a variable structure approach with time varying nature of SAPF. [*A Robust Extended Complex Kalman filter and Sliding mode control based shunt active power filter," Electric Power Components and Systems (Taylor & Francis), vol. 42, no. 5, pp. 520-532, 2014.]*

- Predictive current control techniques called DBC and MPC are proposed in Chapter 3. DBC eliminates the classic linear controller by using a predictive model of the system. Another advanced predictive control called MPC takes advantage of the limited number of switching states of voltage source inverter for solving optimization problem and the main advantage of MPC lies in the direct

application of the control action to the inverter, without necessitating a modulation stage. Also a new and faster reference current estimation based on RECKF is proposed in this Chapter because predictive control techniques require an immediate and accurate response of reference current. This proposed reference scheme is based on estimation of fundamental amplitude of load current and also in phase fundamental component of PCC voltage; hence it is completely devoid of exterior PI controller loop and self-regulator of dc capacitor voltage. *[Model Predictive Based Shunt Active Power Filter with a New Reference Current Estimation Strategy," IET Power Electronics, vol. 8, no. 2, pp. 221–233, 2015.]*

- An optimal control technique called LQR is proposed in Chapter 4. LQR deals with state regulation, output regulation, and tracking. This approach includes the whole SAPF system dynamics, with PCC voltage disturbance being compensated with the aid of information that comes from RECKF algorithm. Further, a new reference current scheme based on RECKF is proposed here by adding an error between the fundamental amplitudes of load and source current in the reference scheme proposed in Chapter 3 and this facilitates better regulation of dc-link voltage.

- A Robust LQG Servo controller is proposed in Chapter 5. A feedback compensator is proposed in this LQG servo controller to achieve gain stability, less distortion and increased bandwidth. Voltage regulation of dc-link capacitor is improved by proposing a new and faster reference generation scheme based on RECKF, which comprises only current measurements i.e., fundamental amplitude estimation of source current and in phase fundamental component estimation of load current.

- A Robust H_∞ controller design is proposed for SAPF in Chapter 6. This H_∞ controller is synthesized using mixed sensitivity approach for realizing stability and high disturbance rejection in SAPF system. Moreover, in this Chapter, the proposed reference current scheme based on RECKF that uses sensing of the supply current only is making a more reliable and cost-effective SAPF system.

7.3   Suggestions for Future Work

- **Control Strategies for Unified Power Quality Conditioner (UPQC)**

  This thesis work is based upon shunt APF system, which attempts to solve PQ problems such as current harmonics through different control strategies. Since the modern distribution system demands a better quality of voltage being supplied and current drawn, integration of both shunt APF and series APF, i.e. UPQC [133] has great scope in actual practical implementation. Hence, an immediate extension of the thesis work is to apply above control strategies for UPQC.

- **Estimation Techniques**

  Estimation of amplitude and frequency problems can also be extended to different versions such as Unscented Kalman filter (UKF) [134], Particle filter [135], and H_∞ filter [136]. These can be applied with further comparative analysis of the methods presented in the thesis.

- **Robust Adaptive Control Design**

  The performance of robust control strategies such as LQG servo controller, H_∞ controller may not be satisfactory when severe model uncertainties are present in the SAPF system. Hence, robust performance of SAPF can be enhanced by employing adaptive LQG or adaptive H_∞ controller with suitable adaptive control laws [137] such that it can counteract the effects of the severe disturbances and thereby achieves PQ improvement.

THESIS DISSEMINATION

Journal Papers

1. R. Panigrahi, B. Subudhi, and P. C. Panda, "A Robust LQG Servo Control Strategy of Shunt Active Power Filter for Power Quality Enhancement," IEEE Transactions on Power Electronics, vol. 31, no. 4, pp. 2860-2869, 2016.

2. R. Panigrahi, B. Subudhi, and P. C. Panda, "Model Predictive Based Shunt Active Power Filter with a New Reference Current Estimation Strategy," IET Power Electronics, vol. 8, no. 2, pp. 221–233, 2015.

3. R. Panigrahi, P. C. Panda, and B. Subudhi, "A Robust Extended Complex Kalman filter and Sliding mode control based shunt active power filter," Electric Power Components and Systems (Taylor & Francis), vol. 42, no. 5, pp. 520-532, 2014.

4. R. Panigrahi, B. Subudhi, and P. C. Panda, "A Comparative Assessment of Hysteresis and Dead Beat Controllers for Performances of Three Phase Shunt Active Power Filtering," Journal of Power Technologies, vol. 94, no. 4, pp. 286-295, 2014.

5. R. Panigrahi, B. Subudhi, and P. C. Panda, "Performance Enhancement of Shunt Active Power Filter using a Robust H_∞ Control Strategy," IEEE Transactions on Power Electronics (Revision in Progress).

6. R. Panigrahi, B. Subudhi, and P. C. Panda, "New Control Strategy of Shunt Active Power Filter Based on Robust Extended Complex Kalman Filter," International Journal of Electrical Power and Energy Systems (Elsevier) (Revision in Progress).

Conference Papers

1. R. Panigrahi, P. C. Panda, and B. Subudhi, "Comparison of performances of hysteresis and dead beat controllers in active power filtering", IEEE 3rd International Conference on Sustainable Energy Technologies (ICSET), Kathmandu, Nepal, 24-27 September, 2012.

2. R. Panigrahi, P. C. Panda, and B. Subudhi, "Discrete Kalman filter applied in reference current estimation for control of single phase shunt active power filter", National Power System Conference (NPSC), Varanasi, 12-14 December, 2012.

3. R. Panigrahi, P. C. Panda, and B. Subudhi, "New strategy for generation of reference current in active power filters with distortion in line voltage", IEEE 7th International Conference on Industrial and Information Systems (ICIIS), Chennai, 6-9 August, 2012.

4. R. Panigrahi, P. C. Panda, B. Subudhi, and S. Swain, "Model Predictive Control of Shunt Active Power Filter with Kalman Filter based reference signal generation", 5th International Conference on Computer Applications in Electrical Engineering-Recent Advances (CERA), Roorkee, 3-5 October, 2013.

5. R. Panigrahi, P. C. Panda, and B. Subudhi, " Investigation on active power filter using Kalman filter based LQR modeling approach", International conference on Electronics Engineering and Image Processing (ICEEIT), Bangkok, Thailand, 1-2 April, 2014.

References

[1] J. D. Gomez, P. N. Enjeti and B. Woo, "Effect of voltage sags on adjustable-speed drives: a critical evaluation and an approach to improve performance," *IEEE Transactions on Industry Application*, vol. 35, no. 6, pp. 1440–1449, 1999.

[2] P. S. Harmonics, IEEE Working Group on Power System Harmonics, "Power System Harmonics: An Overview," *IEEE Transactions on Power Apparatus and Systems*, vol. PAS-102, no. 8, pp. 2455-2460, 1983.

[3] Mohd Izhar Bin A Bakar, "Active power filter with automatic control circuit for neutral current harmonic minimization technique," Ph.D thesis, University of Science, Malaysia, June 2007.

[4] G. T. Heydt, "Electric power quality: a tutorial introduction," *IEEE Transactions on computer applications in power*, vol. 11, no. 1, pp. 15-19, 1998.

[5] I. Hunter, "Power quality issues-a distribution company perspective," *Power Engineering Journal*, vol. 15, no. 2, pp. 75-80, 2001.

[6] J. Stones and A. Collinson, "Power Quality," *Power Engineering Journal*, vol. 15, no. 2, pp. 58-64, 2001.

[7] E. Muljadi and H. E. McKenna, "Power quality issues in a hybrid power system," *IEEE Transactions on industry applications*, vol. 38, no. 3, pp. 803-809, 2002.

[8] M. S. M. Cichowlas, "PWM Rectifier with Active filtering," Ph.D Thesis, Warsaw University of Technology, Poland, 2004.

[9] J. Arrillaga and N. R. Watson, *Power system harmonics*, second edition, New Zealand: John Wiley & Sons, 2003.

[10] J. S. Thorp, A. G. Phadke and K. J. Karimi, "Real-Time Voltage Phasor Measurements for Static-State Estimation," *IEEE Transactions on Power Apparatus and Systems*, vol. PAS-104, no. 11, pp. 3099-3106, 1985.

[11] P. Verdelho and G. D. Marques, "An active power filter and unbalanced current compensator," *IEEE Transactions on Industrial Electronics*, vol. 44, no. 3, pp. 321-328, 1997.

[12] A. M. Al-Zamil and D. A. Torrey, "A passive series, active shunt filter for high power applications," *IEEE Transactions on Power Electronics*, vol. 16, no. 1, pp. 101-109, 2001.

[13] J. L. Hurng and W. C. Jinn, "A novel active power filter for harmonic suppression," *IEEE Transactions on Power Delivery*, vol. 20, no. 2, pp. 1507-1513, 2005.

[14] S. Rahmani and A. Hamadi, "A Combination of Shunt Hybrid Power Filter and Thyristor-Controlled Reactor for Power Quality," *IEEE Transactions on Power Delivery*, vol. 61, no. 5, pp. 2152-2164, 2014.

[15] A. F. Zobaa, "Optimal multiobjective design of hybrid active power filters considering a distorted environment," *IEEE Transactions on Industrial Electronics*, vol. 61, no. 1, pp. 107-114, 2014.

[16] W. C. Jinn and J. L. Hurng, "Novel Circuit Topology for Three-Phase Active Power Filter," *IEEE Transactions on Power Delivery*, vol. 22, no. 1, pp. 444-449, 2007.

[17] M. Aredes, J. Hafner and K. Heuma, "Three-Phase Four-Wire Shunt Active Filter Control Strategies," *IEEE Transactions on Power Electronics,* vol. 12, no. 2, pp. 311-318, 1997.

[18] V. Khadkikar, A. Chandra and B. N. Singh, "Generalised single phase p-q theory for active power filtering: simulation and DSP-based experimental investigation," *IET Power Electronics,* vol. 2, no. 1, pp. 67-78, 2008.

[19] X. Yuan, W. Merk and H. Stemmler, "Stationary-frame generalized integrators for current control of active power filters with zero steady state error for current harmonics of concern under unbalanced and distorted operating conditions," *IEEE Transactions on Industry Applications*, vol. 38, no. 2, pp. 523-532, 2002.

[20] V. Soares, P. Verdelho and G. D. Marques, "An Instantaneous Active and Reactive Current Component Method for Active Filters," *IEEE Transactions on Power Electronics*, vol. 15, no. 4, pp. 660-669, 2000.

[21] V. M. Moreno, A. P. Lopez and R. D. Garcias, , "Reference Current Estimation Under Distorted Line Voltage for Control of Shunt Active Power Filters", *IEEE Transactions on Power Electronics*, vol. 19, no. 4, pp. 988-994, 2004.

[22] R. Chudamani, K. Vasudevan and C. S. Ramalingam, " Non-linear least-squares-based harmonic estimation algorithm for a shunt active power filter," *IET Power Electronics*, vol. 2, no. 2, pp.134-146, 2009.

[23] J. M. Kanieski, R. Cardoso and H. A. Grundling , "Kalman filter based control system for power quality conditioning devices", *IEEE Transactions on Industrial Electronics*, vol. 60, no. 11, pp. 5214 - 5227, 2013.

[24] S. Saad and L. Zellouma, " Fuzzy logic controller for three-level shunt active filter compensating harmonics and reactive power," *Electric Power Systems Research*, vol. 79, no. 10, pp. 1337-1341, 2009.

[25] R. N. Ray, D. Chatterjee, S. K. Goswami, "Harmonics elimination in a multilevel inverter using the particle swarm optimization technique", *IET Power Electronics*, vol. 2, no. 6, pp. 646-652, 2009.

[26] C. N. Bhende, S. Mishra, S. K. Jain, "TS-fuzzy-controlled active power filter for load compensation", *IEEE Transactions on Power Delivery*, vol. 21, no. 3, pp. 1459-1465, 2006.

[27] L. H. Tey, P. L. So and Y. C. Chu, "Improvement of power quality using adaptive shunt active filter", *IEEE Transactions on Power Delivery*, vol. 20, no. 2, pp. 1558-1568, 2005.

[28] S. R. Arya and B. Singh, "Neural Network Based Conductance Estimation Control Algorithm for Shunt Compensation", *IEEE Transactions on Industrial Informatics*, vol. 10, no. 1, pp. 569-576, 2014.

[29] B. Singh and J. Solanki, "An implementation of an adaptive control algorithm for a three phase shunt active power filter", *IEEE Transactions on Industrial Electronics,* vol. 56, no. 8, pp. 2811-2820, 2009.

[30] P. Kanjiya and V. Khadkikar, "Artificial-Neural-Network-Based Phase-Locking Scheme for Active Power Filters", *IEEE Transactions on Industrial Electronics,* vol. 61, no. 8, pp. 3857 - 3866, 2014.

[31] K. K. Shyu, M. J. Yang, Y. M. Chen and Y. F. Lin, "Model reference adaptive control design for a shunt active power filter system", *IEEE Transactions on Industrial Electronics,* vol. 55, no. 1, pp. 97-106, 2008.

[32] A. Bhattacharya and C. Chakraborty, "A shunt active power filter with enhanced performance using ANN based predictive and adaptive controllers", *IEEE Transactions on Industrial Electronics,* vol. 58, no. 2, pp. 421-428, 2011.

[33] R. L. A. Ribeiro, C. C. Azevedo and R. M. Sousa, "A Robust Adaptive Control Strategy of Active Power Filters for Power-Factor Correction, Harmonic Compensation, and Balancing of Nonlinear Loads", *IEEE Transactions on Power Electronics,* vol. 27, no. 2, pp. 718-730, 2012.

[34] B. Singh and S. R. Arya, "Adaptive Theory-Based Improved Linear Sinusoidal Tracer Control Algorithm for DSTATCOM", *IEEE Transactions on Power Electronics,* vol. 28, no. 8, pp. 3768-3778, 2013.

[35] B. Singh, S. R. Arya, A. Chandra and K. A. Haddad, "Implementation of Adaptive Filter in Distribution Static Compensator", *IEEE Transactions on Industry Applications,* vol. 50, no. 5, pp. 3026-3033, 2014.

[36] S. R. Arya and B. Singh, "Performance of DSTATCOM using Leaky LMS Control Algorithm", *IEEE journal of Emerging and selected topics in Power Electronics,* vol. 1, no. 2, pp. 104-113, 2013.

[37] B. Singh and S. R. Arya, "Back-propagation control algorithm for power quality improvement using DSTATCOM", *IEEE Transactions on Industrial Electronics*, vol. 61, no. 3, pp. 1204-1212, 2014.

[38] B. Singh and S. R. Arya, "Composite observer-based control algorithm for distribution static compensator in four-wire supply system", *IET Power electronics*, vol. 6, no. 2, pp. 251–260, 2013.

[39] S. Rahmani, N. Mendalek and K. Haddad, "Experimental design of a nonlinear control technique for three phase shunt active power filter", *IEEE Transactions on Industrial Electronics*, vol. 57, no. 10, pp. 3364-3375, 2010.

[40] S. G. Jorge, C. A. Busada and J. Solsona, "Reduced order generalized integrator-based current controller applied to shunt active power filters", *IET Power Electronics,* vol. 7, no. 5, pp. 1083-1091, 2014.

[41] P. Kanjiya, V. Khadkikar and H. H. Zeineldin, "A noniterative optimized algorithm for shunt active power filter under distorted and unbalanced supply voltages", *IEEE Transactions on Industrial Electronics*, vol. 60, no. 12, pp. 5376 – 5390, 2013.

[42] Q. N. Trinh and H. H. Lee, "An advanced current control strategy for three-phase shunt active power filters", *IEEE Transactions on Industrial Electronics*, vol. 60, no. 12, pp. 5400-5410, 2013.

[43] H. Yi, F. Zhuo and Y. Zhang, "A source current detected shunt active power filter control scheme based on vector resonant controller", *IEEE Transactions on Industry Applications*, vol. 50, no. 3, pp. 1953-1965, 2014.

[44] W. Lenwari, M. Sumner and P. Zanchetta, "The use of genetic algorithms for the design of resonant compensators for active filters", *IEEE Transactions on Industrial Electronics*, vol. 56, no. 8, pp. 2852-2861, 2009.

[45] R. L. A. Ribeiro, T. O. A. Rocha and R. M. Sousa, "A Robust DC-Link Voltage Control Strategy to Enhance the Performance of Shunt Active Power Filters Without Harmonic Detection Schemes", *IEEE Transactions on Industrial Electronics*, vol. 62, no. 2, pp. 803-813, 2015.

[46] J. Matas, L. G. Vicuna, J. Miret and J. M. Guerrero, "Feedback Linearization of a Single-Phase Active Power Filter via Sliding Mode Control", *IEEE Transactions on Power Electronics*, vol. 23, no. 1, pp. 116-125, 2008.

[47] M. Odavic, V. Biagini and P. Zanchetta, "One-sample-period-ahead predictive current control for high performance active shunt power filters", *IET Power Electronics,* vol. 4, no. 4, pp. 414-423, 2011.

[48] P. Acuna, L. Moran and M. Rivera, "Improved active power filter performance for renewable power generation systems", *IEEE Transactions on Power Electronics*, vol. 29, no. 2, pp. 687-694, 2014.

[49] A. F. Zobaa, S. Aleem, "A new approach for harmonic distortion minimization in power systems supplying nonlinear loads", *IEEE Transactions on Industrial Informatics*, vol. 10, no. 2, pp. 1401-1412, 2014.

[50] R. Aghazadeh, H. Lesani and M. S. Pasand, "New technique for frequency and amplitude estimation of power system signals", *IEE Proceedings. Generation, Transmission and Distribution*, vol. 152, no. 3, pp. 435-440, 2005.

[51] R. A. Zadeh, A. Ghosh and G. Ledwich, "Combination of Kalman Filter and Least-Error Square Techniques in Power System", *IEEE Transactions on Power Delivery*, vol. 25, no. 4, pp. 2868- 2880, 2010.

[52] A. Routray, A. K. Padhan and K. P. Rao, "Novel Kalman Filter for Frequency Estimation of Distorted Signals in Power Systems", *IEEE Transactions on Instrumentation and Measurement*, vol. 51, no. 3, pp. 469- 479, 2002.

[53] P. K. Dash, R. K. Jena, G. Panda and A. Routray, "An Extended Complex Kalman Filter for Frequency Measurement of Distorted Signals", *IEEE Transactions on Instrumentation and Measurement*, vol. 49, no. 4, pp. 746- 753, 2000.

[54] C. H. Huang, C. H. Lee and K. J. Shih, "Frequency Estimation of Distorted Power System Signals Using a Robust Algorithm", *IEEE Transactions on Power Delivery*, vol. 23, no. 1, pp. 41- 50, 2008.

[55] M. Mojiri, D. Yazdani and A. Bakhshai, "Robust Adaptive Frequency Estimation of Three-Phase Power Systems", *IEEE Transactions on Instrumentation and Measurement,* vol. 59, no.7, pp. 1793-1802, 2010.

[56] E. Lavopa, P. Zanchetta and M. Sumner, "Real-Time Estimation of Fundamental Frequency and Harmonics for Active Shunt Power Filters in Aircraft Electrical Systems", *IEEE Transactions on Industrial Electronics*, vol. 56, no. 8, pp. 2875- 2884, 2009.

[57] R. Chudamani, K. Vasudevan and C. S. Ramalingam, "Real-Time Estimation of Power System Frequency Using Nonlinear Least Squares", *IEEE Transactions on Power Delivery*, vol. 24, no. 3, pp. 1021- 1028, 2009.

[58] D. P. Marcetic, J. J. Tomic and M. D. Kusljevic, "Unbalanced three-phase distribution system frequency estimation using least mean squares method and positive voltage sequence", *IET Science, Measurement and Technology*, vol. 8, no. 1, pp. 30- 38, 2014.

[59] M. D. Kusljevic, J. J. Tomi and L. D. Jovanovic, "Frequency Estimation of Three-Phase Power System Using Weighted-Least-Square Algorithm and Adaptive FIR Filtering", *IEEE Transactions on Instrumentation and Measurement*, vol. 59, no. 2, pp. 322-329, 2010.

[60] B. Subudhi, P. K. Ray and S. Ghosh, "Variable leaky least mean-square algorithm-based power system frequency estimation", *IET Science, Measurement and Technology*, vol. 6, no. 4, pp. 288-297, 2012.

[61] L. A. Moran, J. W. Dixon and R. R. Wallace, "A three-phase active power filter operating with fixed switching frequency for reactive and current harmonic

compensation," *IEEE Transactions on Industrial Electronics*, vol. 42, no. 4, pp. 402–408, 1995.

[62] T. Lobos and J. Rezmer, "Real-time determination of power system frequency," *IEEE Transactions on Power Delivery*, vol. 46, no. 4, pp. 877-881, 1997.

[63] N. Gupta, S. P. Singh and R. C. Bansal, "A digital signal processor based performance evaluation of three-phase four wire shunt active filter for harmonic elimination, reactive power compensation and balancing of non-linear loads under non-ideal mains voltages," *Electric Power Component and Systems*, vol. 40, no. 10, pp. 1119–1148, 2012.

[64] A. K. Pradhan, A. Routray and A. Basak, "Power system frequency estimation using least mean square technique," *IEEE Transactions on Power Delivery*, vol. 20, no. 3, pp. 1812–1816, 2005.

[65] T. S. Sidhu and M. S. Sachdev, "An iterative technique for fast and accurate measurement of power system frequency," *IEEE Transactions on Power Delivery*, vol. 13, no. 1, pp. 109–115, 1998.

[66] G. G. Rigatos, "A derivative free Kalman filtering approach to state estimation based control of nonlinear systems," *IEEE Transactions on Industrial Electronics*, vol. 59, no. 10, pp. 3987–3997, 2012.

[67] P. K. Ray and B. Subudhi, "Ensemble Kalman filtering algorithm applied to power system harmonics estimation," *IEEE Transactions on Instrumentation and Measurement*, vol. 61, no. 12, pp. 3216–3224, 2012.

[68] J. Barros and E. Perez, "Automatic Detection and Analysis of Voltage Events in Power Systems," *IEEE Transactions on Instrumentation and Measurement*, vol. 55, no. 5, pp. 1487 - 1493, 2006.

[69] R. A. Wiltshire, G. Ledwich and P. Oshea, "A Kalman Filtering Approach to Rapidly Detecting Modal Changes in Power Systems," *IEEE Transactions on Power System*, vol. 22, no. 4, pp. 1698 - 1706 , 2007.

[70] Z. Jinghe, G. Welch and G. Bishop, "A Two-Stage Kalman Filter Approach for Robust and Real-Time Power System State Estimation," *IEEE Transactions on Sustainable Energy*, vol. 5, no. 2, pp. 629 – 636, 2014.

[71] R. K. Mehra, "On the identification of variances and adaptive Kalman filtering", *IEEE Transactions on Automatic Control*, vol. AC-15, no. 2, pp. 175-184, 1970.

[72] V. V. Terzija, N. B. Djuric and B. D. Kovacevic, "Voltage phasor and local system frequency estimation using Newton type algorithm," *IEEE Transactions on Power Delivery*, vol. 9, no. 3, pp. 1368–1374, 1994.

[73] P. Xiao and K. A. Corzine, "Seven-level shunt active power filter for high-power drive systems," *IEEE Transactions on Power Electronics*, vol. 24, no. 1, pp. 6–13, 2009.

[74] RT-Lab Professional. Available at http://www.opal-rt.com/product/rtlab-Professional

[75] M. A. Rahman, T. S. Radwan, A. M. Osheiba and A. Lashine, "Analysis of current controllers for voltage-source inverter," *IEEE Transactions on Industrial Electronics*, vol. 44, no. 4, pp. 477-485, 1997.

[76] S. Buso, L. Malesani and P. Mattavelli, "Comparison of current control techniques for active filter applications," *IEEE Transactions on Industrial Electronics*, vol. 45, no. 5, pp. 722–729, 1998.

[77] S. Saetieo, R. Devaraj and D. A. Torrey, "The design and implementation of a three phase active power filter based on sliding mode control," *IEEE Transactions on Industry Applications*, vol. 31, no. 5, pp. 993–1000, 1995.

[78] B. Singh, K. Haddad and A. Chandra, "Active power filter with sliding mode control," *IEE Proceedings Generation, Transmission and Distribution*, vol. 144, no. 6, pp. 564 - 568, 1997.

[79] K. M. Tsang, W. L. Chan and X. Tang, "Multi-level shunt active power filter using modular cascade H-bridge and delay firing," *Electric Power Components and Systems*, vol. 41, no. 6, pp. 605–618, 2013.

[80] R. D. Patidar and S. P. Singh, "Digital signal processor based shunt active filter controller for customer-generated harmonics and reactive power compensation," *Electric Power Components and Systems*, vol. 38, no. 8, pp. 937–959, 2010.

[81] D. Casini, M. Marchesoni and L. Puglisi, "Sliding Mode Multilevel Control for Improved Performances in Power Conditioning Systems," *IEEE Transactions on Power Electronics*, vol. 10, no. 4, pp. 453 - 463, 1995.

[82] A. Sabanovic, "Variable Structure Systems with Sliding Modes in Motion Control—A Survey," *IEEE Transactions on Industrial Informatics*, vol. 7, no. 2, pp. 212 - 223, 2011.

[83] M. P. Kazmierkowski, R. Krishnan and F. Blaabjerg, "Control in Power Electronics". Academic Press, San Diego, CA, 2002.

[84] N. Mohan, T. M. Undeland and W. P. Robbins, "Power Electronics: Converters, Applications and Design," 3rd ed., Hoboken, NJ: John Wiley & Sons, 2003.

[85] E. Wiebe, J. L. Duran and P. R. Acosta, "Integral sliding mode active filter control for harmonic distortion compensation," *Electric Power Components and Systems*, vol. 39, no. 9, pp. 833–849, 2011.

[86] A. Luo, Z. Shuai, W. Zhu, R. Fan and C. Tu, "Development of Hybrid Active Power Filter Based on the Adaptive Fuzzy Dividing Frequency-Control Method," *IEEE Transactions on Power Delivery*, vol. 24, no. 1, pp. 424-432, 2009.

[87] P. Cortes, M. P. Kazmierkowski and R. M. Kennel, "Predictive Control in Power Electronics and Drives," *IEEE Transactions on Industrial Electronics*, vol. 55, no. 12, pp. 4312–4324, 2008.

[88] S. Buso, L. Malesani, P. Mattavelli and R. Veronese, "Design and Fully Digital Control of Parallel Active Filters for Thyristor Rectifiers to comply with IEC-1000-3-2 Standards ," *IEEE Transactions on Industry Applications*, vol. 34, no. 3, pp. 508 - 517, 1998.

[89] Y. A. R. I. Mohamed and E. F. Saadany, "An Improved Deadbeat Current Control Scheme With a Novel Adaptive Self-Tuning Load Model for a Three-Phase PWM Voltage-Source Inverter," *IEEE Transactions on Industrial Electronics*, vol. 54, no. 2, pp. 747 - 759, 2007.

[90] Y. Han, L. Xu, M. M. Khan and C. Chen, "Robust Deadbeat Control Scheme for a Hybrid APF With Resetting Filter and ADALINE-Based Harmonic Estimation Algorithm," *IEEE Transactions on Industrial Electronics*, vol. 58, no. 9, pp. 3893 - 3904, 2011.

[91] P. Cortes, G. Ortiz, J. I. Yuz and J. Rodríguez, "Model Predictive Control of an Inverter With Output LC Filter for UPS Applications," *IEEE Transactions on Industrial Electronics*, vol. 56, no. 6, pp. 1875 - 1883, 2009.

[92] S. Kouro, P. Cortes, R. Vargas, U. Ammann and J. Rodríguez, "Model Predictive Control—A Simple and Powerful Method to Control Power Converters," *IEEE Transactions on Industrial Electronics*, vol. 56, no. 6, pp. 1826-1838, 2009.

[93] J. Rodriguez, M. P. Kazmierkowski, J. R. Espinoza and P. Zanchetta, "State of the Art of Finite Control Set Model Predictive Control in Power Electronics," *IEEE Transactions on Industrial Informatics,* vol. 9, no. 2, pp. 1003 - 1016, 2013.

[94] V. Yaramasu, M. Rivera, B. Wu and J. Rodriguez, "Model Predictive Current Control of Two-Level Four-Leg Inverters-Part I: Concept, Algorithm, and Simulation Analysis," *IEEE Transactions on Power Electronics*, vol. 28, no. 7, pp. 3459-3468, 2013.

[95] M. Rivera, V. Yaramasu, J. Rodriguez and B. Wu, "Model Predictive Current Control of Two-Level Four-Leg Inverters-Part II: Experimental Implementation and Validation," *IEEE Transactions on Power Electronics*, vol. 28, no. 7, pp. 3469-3478, 2013.

[96] J. F. Petit, G. Robles and H. Amaris, "Current reference control for shunt active power filters under non sinusoidal voltage conditions," *IEEE Transactions on Power Delivery*, vol. 22, no. 4, pp. 2254-2261, 2007.

[97] C. L. Phillips and H. T. Nagle, *Digital Control System analysis and Design*, Prentice-Hall, 1995.

[98] B. D. O. Anderson and J. B. Moore, *Optimal Control*, Prentice Hall, Englewood Cliffs, New Jersy, 1989.

[99] M. Athans, P. Falb, *Optimal Control: An Introduction to the Theory and Its Applications,* McGraw Hill Book Company, New York, NY, 1966.

[100] F. L. Lewis, *Optimal Control*, John Wiley & Sons, New York, NY, 1986.

[101] S. Fukuda, "LQ control of sinusoidal current PWM rectifiers," *IEE Proceedings on Electric Power Applications*, vol. 114, no. 2, pp. 95–100, 1999.

[102] S. Fukuda, Y. Matsumoto, and A. Sagawa, "Optimal-regulator-based control of NPC boost rectifiers for unity power factor and reduced neutral point- potential variations," *IEEE Transactions on Industrial Electronics*, vol. 46, no. 3, pp. 527–534, 1999.

[103] K. Izumi, M. Tsuji, E. Yamada and J. Oyama, "Active power filter with optimal servo controller," *in 23rd IEEE International Conference on Industrial Electronics, Control and Instrumentation (IEEE-IECON)*, 1999, pp. 816–821.

[104] R. Grino and R. Costa-Castello, "Digital repetitive plug-in controller for odd-harmonic periodic references and disturbances," *Automatica*, vol. 41, no. 1, pp. 153–157, 2005.

[105] S. Alepuz, J. S. B. Monge and J. Bordonau, "Interfacing renewable energy sources to the utility grid using a three-level inverter," *IEEE Transactions on Industrial Electronics*, vol. 53, no. 5, pp. 1504–1511, 2006.

[106] T. Thomas and K. Haddad, "Design and performance of active power filters," *IEEE Industry Applications Magazine*, vol. 4, no. 5, pp. 38–46, 1998.

[107] B. Kedjar and K. Haddad, "DSP-based implementation of an LQR with integral action for a three-phase three-wire shunt active power filter," *IEEE Transactions on Industrial Electronics*, vol. 56, no. 8, pp. 2821-2828, 2009.

[108] A. Ghosh, R. Krishnan and B. Subudhi, "Robust PID Compensation of an Inverted Cart-Pendulum System: An Experimental Study," *IET Control Theory & Applications*, vol. 6, no. 8, pp. 1145-1152, 2012.

[109] M. I. M. Montero, E.R. Cadaval and F.B. Gonzalez, "Comparison of Control Strategies for Shunt Active Power Filters in Three-Phase Four-Wire Systems," *IEEE Transactions on Power Electronics*, vol. 22, no. 1, pp. 229 - 236, 2007.

[110] L. B. G. Campanhol, S. A. O. Silva and A. Goedtel, "Application of shunt active power filter for harmonic reduction and reactive power compensation," *IET Power Electronics*, vol. 7, no. 11, pp. 2825-2836, 2014.

[111] C. C. Che and Y. Y. Hsu, "A novel approach to the design of a shunt active filter for an unbalanced three-phase four-wire system under non sinusoidal conditions," *IEEE Transactions on Power Delivery*, vol. 15, no. 4, pp. 1258 - 1264 , 2000.

[112] F. Huerta, D. Pizarro, S. Cobreces, F. J. Rodriguez, C. Giron and A. Rodriguez, "LQG Servo Controller for the Current Control of LCL Grid-Connected Voltage-Source Converters," *IEEE Transactions on Industrial Electronics*, vol. 59, no. 11, pp. 4272-4284, 2012.

[113] K. H. Kwan, P. L. So and Y. C. Chu, "An output regulation-based unified power quality conditioner with Kalman filters," *IEEE Transactions on Industrial Electronics*, vol. 59, no. 11, pp. 4248-4262, 2012.

[114] L. Wu, F. Zhuo, P. Zhang, H. Li and Z. Wang, "Study on the Influence of Supply-Voltage Fluctuation on Shunt Active Power Filter," *IEEE Transactions on Power Delivery*, vol. 22, no. 3, pp. 1743 - 1749 , 2007.

[115] S. K. Jain, P. Agrawal and H. O. Gupta, "Fuzzy logic controlled shunt active power filter for power quality improvement," *IEE Proceedings on Electric Power Applications*, vol. 149, no. 5, pp. 317-328, 2002.

[116] Z. Zeng, J. Yang and N. Yu, "Research on PI and repetitive control strategy for Shunt Active Power Filter with LCL-filter," *in 7th IEEE International Conference on Power Electronics and Motion Control (IEEE-IPEMC)*, 2012, pp. 2833 - 2837.

[117] V. G. Kinhal, P. Agarwal and H. O. Gupta, "A Kalman Filtering Approach to Rapidly Detecting Modal Changes in Power Systems," *IEEE Transactions on Power System*, vol. 22, no. 4, pp. 1698 - 1706 , 2007.

[118] A. A. Girgis and W. L. Peterson, "Adaptive estimation of power system frequency deviation and its rate of change for calculating sudden power system overloads," *IEEE Transactions on Power Delivery*, vol. 5, no. 2, pp. 585 - 594, 1990.

[119] G. Fusco and M. Russo, "Self-tuning regulator design for nodal voltage waveform control in electrical power systems," *IEEE Transactions on Control Systems Technology*, vol. 11, no. 2, pp. 258 - 266, 2003.

[120] LEM, \Voltage Transducer LV 25-P," Datasheet.

[121] LEM, \Current Transducer LA 55-P," Datasheet.

[122] M. K. Mishra, K. Karthikeyan, G. Vincent and S. Sasitharan, "A DSP based integrated hardware set up for a DSTATCOM; Design, development and implementation issues," *IETE Journal of Research*, vol. 56, no. 1, pp. 11-21, 2010.

[123] Motorola Semiconductor Datasheet: SN74LS123, Motorola Semiconductor Products Inc., Phoenix, AZ, 1989.

[124] Fairchild Datasheet: HCPL 2601, Fairchild semiconductor Corporation, USA, 2001.

[125] Y. W. Li, D. M. Vilathgamuwa and F. Blaabjerg, "A robust control scheme for medium voltage level DVR implementation," *IEEE Transactions on Industrial Electronics*, vol. 54, no. 4, pp. 2249-2260, 2007.

[126] Y. W. Li, F. Blaabjerg and D. M. Vilathgamuwa, "Design and comparison of high performance stationary frame controllers for DVR implementation," *IEEE Transactions on Power Electronics*, vol. 22, no. 2, pp. 602-612, 2007.

[127] K. H. Kwan, Y. C. Chu and P. L. So, "Model based H∞ control of a unified power quality conditioner," *IEEE Transactions on Industrial Electronics*, vol. 56, no. 7, pp. 2493-2504, 2009.

[128] T. Hornik, and Q. C. Zhong, "A current control strategy for voltage source inverters in microgrids based on H_∞ and repetitive control," *IEEE Transactions on Power Electronics*, vol. 26, no. 3, pp. 943-952, 2011.

[129] G. Weiss, Q. C. Zhong, T. C. Green and J. Liang, "H_∞ Repetitive Control of DC-AC Converters in Microgrids," *IEEE Transactions on Power Electronics*, vol. 19, no. 1, pp. 219-230, 2004.

[130] R. Naim, G. Weiss, and S. Ben-Yaakov, "H_∞ control applied to boost power converters," *IEEE Transactions on Power Electronics*, vol. 12, no. 4, pp. 677-683, 1997.

[131] T. S. Lee, S. J. Chiang, and J. M. Chang, "H_∞ loop shaping controller designs for the single phase UPS inverters," *IEEE Transactions on Power Electronics*, vol. 16, no. 4, pp. 473-481, 2001.

[132] K. Zhou and J. C. Doyle, *Essentials of Robust control*, Prentice Hall; 1st edition, Louisiana, 1997.

[133] V. Khadkikar, "Enhancing Electric Power Quality Using UPQC: A Comprehensive Overview," *IEEE Transactions on Power Electronics*, vol. 27, no. 5, pp. 2284-2297, 2012.

[134] L. Chang, B. Hu, A. Li and F. Qin, "Unscented type Kalman filter: limitation and combination," *IET Signal Processing*, vol. 7, no. 1, pp. 167–176, 2013.

[135] S. Saha and F. Gustafsson, "Particle Filtering With Dependent Noise Processes," *IET Signal Processing*, vol. 60, no. 9, pp. 4497 - 4508, 2012.

[136] L. Ping, J. Lam and S. Zhan, "H_∞ Positive Filtering for Positive Linear Discrete-Time Systems: An Augmentation Approach," *IEEE Transactions on Automatic Control*, vol. 55, no. 10, pp. 2337 - 2342, 2010.

[137] G. Cheng and P. Shuangxia, "Nonlinear Adaptive Robust Control of Single-Rod Electro-Hydraulic Actuator with Unknown Nonlinear Parameters," *IEEE Transactions on Control Systems Technology*, vol. 16, no. 3, pp. 434 - 445, 2008.

Rakhee Panigrahi

Date of Birth: 7th August, 1980

Email: rpanigrahi99@gmail.com

Qualification

Ph.D. (Continuing)
NIT Rourkela

Mtech (Power Electronics and Drives)
NIT Rourkela [First Division]

B.E (Electrical Engineering)
U. C. E, Burla, Sambalpur University [First Division]

+2 (Science)
Council of Higher Secondary Education, Odisha [First Division]

10th
Board of Secondary Education, Odisha [First Division]

Publications

04 Journal Papers
05 Conference Papers

Permanent Address

Beheramal Chowk
At/Po/Dist: Jharsuguda-768203, Odisha, India